JOINT INSTITUTE FOR AERONAUTICS AND ACOUSTICS

National Aeronautics and Space Administration

Ames Research Center

JIAA TR - 75

Stanford University

TWO BLOWING CONCEPTS FOR ROLL AND LATERAL CONTROL OF AIRCRAFT

BY

D. A. Tavella, N. J. Wood, C. S. Lee and L. Roberts

Stanford University
Department of Aeronautics and Astronautics
Stanford, CA 94305

OCTOBER 1986

JIAA TR - 75

TWO BLOWING CONCEPTS FOR ROLL AND LATERAL CONTROL OF AIRCRAFT

BY

D. A. Tavella, N. J. Wood, C. S. Lee and L. Roberts

The work here presented has been supported by NASA Grant NCC 2-271.

ABSTRACT

Two schemes to modulate aerodynamic forces for roll and lateral control of aircraft have been investigated. The first scheme, called the lateral blowing concept, consists of thin jets of air exiting spanwise, or at a small angle with the spanwise direction, from slots at the tips of straight wings. For this scheme, in addition to experimental measurements, a theory was developed showing the analytical relationship between aerodynamic forces and jet and wing parameters. Experimental results confirmed the theoretically derived scaling laws. The second scheme, which was studied experimentally, is called the jet spoiler concept and consists of thin jets exiting normally to the wing surface from slots aligned with the spanwise direction.

NOMENCLATURE

a, a'	parameters defined in Eqs. (2.8) and (2.37).
A	wing aspect ratio, as a variable.
A_o	wing aspect ratio, as a reference.
b	wing semispan, as a variable.
b_o	wing semispan, as a reference.
Δb	semispan perturbation due to lateral blowing.
c	wing chord.
c_j	jet spoiler slot length.
C_{Di}	induced drag coefficient.
ΔC_d	increment of local drag coefficient.
ΔC_{Di}	change in induced drag coefficient due to lateral blowing.
C_p	pressure coefficient.
ΔC_{PT}	change in total pressure coefficient in jet wake.
C_ℓ	rolling moment coefficient.
$\tilde{C}_\ell$	measure of the rolling moment coefficient.
C_L	lift coefficient.
C_{Lo}	reference lift coefficient.
C_L'	lift slope.
C_{Lo}'	reference lift slope.
$\Delta C_L'$	change in lift slope due to lateral blowing.
C_l	local lift distribution.
C_{lo}	$C_l(y = 0)$.
C_l^o	reference local lift coefficient.
C_{lo}^o	$C_l^o(y = 0)$.
C_l^1	local lift coefficient for one-sided lateral blowing.
C_n	yawing moment coefficient.
C_μ	jet momentum coefficient.
e	wing efficiency factor.
$f(A)$	function in C_L' definition.
$F(A)$	function in relative lift gain expression.
$k, k_1,$ k_2, k_3	constants of order one.
p_T	local total pressure.

$p_{T\infty}$	free-stream total pressure.
Δp	difference between total jet pressure and discharge pressure.
R	jet radius of curvature.
S	wing surface area.
U_∞	free-stream velocity.
v,w	y,z velocity components.
v_j	jet discharge velocity.
x,y,z	reference axis coordinates.
α	angle of attack.
δ_j	jet slot thickness.
δ_e	equivalent aileron deflection.
ϵ	non-dimensional wing semispan perturbation due to lateral blowing.
γ	local circulation.
Γ	vortex intensity.
η	non-dimensional integration variable.
ζ	transformation variable and vorticity component in free-stream direction.
θ	tip jet local angle with respect to the spanwise direction.
θ_o	ejection angle of the tip jet with respect to the spanwise direction.
ρ_j	jet fluid density.
ρ_∞	free-stream fluid density.

CONTENTS

1. INTRODUCTION

The need to explore ways to achieve aerodynamic control forces without the intervention of deflecting solid surfaces has arisen in recent years. Among the techniques to produce aerodynamic forces such that no deflecting surfaces are involved are a variety of jet or blowing schemes. The better known ones are circulation control and jet flaps, which achieve lift modulation by introducing supercirculation. A variety of direct thrust jet arrangements has also been considered, where the controlling forces result from direct thrust vectoring. The two, less-studied concepts presented in this report are the lateral blowing scheme, which modulates lift by changing the wing downwash, and the jet spoiler scheme, where lift modulation results from surface flow separation. The first scheme was considered mainly as a roll and lift control device, while the second was intended primarily for yaw control.

The work reported here summarizes the studies on these two concepts carried out over the last two years. During this time individual aspects of the research were made available in the literature[1,2,3,4,5,6].

Regarding the lateral blowing scheme, jets in the form of thin sheets exiting in the spanwise direction from the tips of a straight wing, as shown in Fig. 1, can be used to modulate the aerodynamic forces acting on the wing. This modulation originates in aerodynamic interference, and exists in addition to any reaction forces attributable to the momentum of the jet. This property of such an arrangement of jets suggests the possibility of using this scheme in place of conventional ailerons or flaps to alter the aerodynamic forces acting on an aircraft.

This concept differs from ailerons or flaps in that no deflecting surfaces are involved, and in that the additional load arising from the activation of the jets distributes itself on the wing in a different way.

The application of this type of blowing scheme to lift modulation was first reported by Ayers and Wilde[7], who performed measurements on a swept wing of aspect ratio 1.39 and 50° sweep and observed significant gains in lift as well as a beneficial effect on stall. Carafoli[8] formulated a theory and conducted experiments with a straight wing of aspect ratio 2. He correctly observed that the underlying reason for lift gain is an effective

enlargement, brought about by the jet, of the wing span. His theoretical approach was an extension of Prandtl's lifting line theory and succeeded in representing fairly well the experimentally observed trends for moderate blowing intensities, but failed to establish analytical relationships between the wing, jet parameters, and the loads caused by blowing.

Later, Carafoli and Camaracescu[9] reported measurements on small aspect ratio wings, observing that lift augmentation is more intense for smaller aspect ratios, further confirming that the basic mechanism for lift increment is an effective enlargement of the wing span. Further experimental work on lateral blowing was reported by White[10], who noticed some beneficial effects on drag under certain conditions. Briggs and Schwind[11] considered the lateral blowing concept as a lift augmentation device for STOL aircraft. Their experiments suggest that a net gain in STOL capabilities is possible. Hickey[12] tested swept wings of aspect ratio 1.9 and 2.5, observing that the efficiency of the lateral blowing concept is greater for weaker blowing intensity. Wu et al[13,14] looked at a tip blowing arrangement with several thin jets exiting from the wing tips, and inferred similarities with the winglet concept.

All of these studies stressed relatively high blowing intensities such as would apply if the main objective of the concept were lift enhancement in an STOL environment. In the present study relatively weak load modulation is emphasized as is called for in lateral and roll control of aircraft in cruise. In such a case the desired effect is achieved with relatively weak blowing intensity. The study is done both theoretically and experimentally. On the theoretical side the analysis exploits the low blowing intensity in a perturbation sense, allowing for the derivation of scaling laws relating wing load to wing and jet parameters. The experimental study is done on a rectangular wing whose aspect ratio can be varied between 3.14 and 0.4, obtaining aerodynamic loads and conducting flow surveys over a wide range of wing and jet parameters. A comparison is then made between theoretical and experimental results.

As originally pointed out by Carafoli[8], the effect of lateral blowing on a straight wing can be visualized by thinking of the lateral jet as a fluid extension of the wing itself. Although the precise way in which this fluid extension affects the aerodynamics of the wing is one of great complexity,

the phenomenon can be characterized by three main facts: the outward displacement the tip vortices by the jet, the rolling up of the jet sheet, and the turbulent entrainment into the jet. The outward displacement of the tip vortices taken in isolation would cause the wing to react as if it had undergone an increment of its span. The jet roll-up is caused by the pressure difference between the upper and lower surfaces of the jet. The rolled-up jet eventually coalesces with the tip vortex. Viscous entrainment into the jet affects the pressure distribution on the wing surface and contributes to the complexity of the roll-up process.

The jet spoiler concept, shown in Fig. 2, consists of thin, high velocity jets that exit normally to the wing surface from slots arranged parallel to the spanwise direction. The jets interfere the surrounding stream, causing localized separation. The aerodynamic forces result from the presence of such separation and from the three-dimensionality of the flow field. The jet spoiler concept has been explored in the past in the context of missile aerodynamics as a means of generating rolling moments[15,16,17], in primarily supersonic regimes. In those cases the yawing moment produced by the jet spoiler was considerably smaller than the rolling moment. The different emphasis of this scheme in the present investigation, where yawing forces are the primary objective, leads to a different arrangement of the jet spoiler. In the work concerning missiles the jet was located very near the trailing edge of the rocket fins in order to enhance the forces normal to the fin plane. The source of high pressure air was to be provided by the ambient flow through ram inlets at the fin tips. In the present case, were the resultant normal force is to be minimized, the jet slot is located near the maximum thickness station and an external pressure source is used. A concept of identical nature to the one studied here was conceived by Cyrus, Kadlec and Klimas[18]. Two jets, symmetrically positioned at either side of a Darrieus-type wind turbine blade were proposed as a means of stalling the flow field about the blade. The resulting drag modulation could be used to control the wind turbine setting.

2. THE LATERAL BLOWING CONCEPT

2.1 Theoretical Analysis

The theoretical approach is based on two main assumptions:

- The most important effect of weak lateral blowing is to produce an outward displacement of the tip vortices, equivalent to an effective enlargement of the wing aspect ratio.
- The change of aspect ratio is regarded as an inviscid phenomenon. In other words, the effect of entrainment on the penetration of the jet into the free stream is neglected.

Under these assumption a closed-form analysis is possible, whose validity is corroborated by experiments.

2.1.1 Span Perturbation Concept

The effect of blowing in altering the wing span is computed by perturbing the wing span by a small amount dependent on jet parameters and angle of attack. It is assumed that the wing is rectangular, that the tip slot extends over the entire chord, and that it is aligned with the zero-lift direction of the wing chord. The load of the wing is assumed to be locally elliptical near the tip, both before and after blowing. The lift produced by the wing with perturbed span is

$$C_L = (C'_{L_o} + \Delta C'_L)\alpha. \tag{1}$$

The lift slope is expressed as

$$C'_L = 2\pi f(A). \tag{2}$$

The increment of lift slope must be referred to the aspect ratio of the unperturbed wing. Defining the relative span change as

$$\epsilon = \frac{\Delta b}{b_o}, \tag{3}$$

it results

$$\Delta C_L' = 2\pi\{f[A_o(1+\epsilon)](1+\epsilon) - f(A_o)\}. \tag{4}$$

Expanding in series

$$\frac{\Delta C_L'}{C_L'} = \left[1 + A_o\frac{\dot{f}(A_o)}{f(A_o)}\right]\epsilon + O(\epsilon^2). \tag{5}$$

This expression also includes the lift acting on the fluid extension of the wing. That part of the lift doesn't contribute to lift augmentation, since it is supported by the jet itself. However, to first order in ϵ the lift given by Eq. (5) is the same as the lift acting on the solid part of the wing. To prove this, compare two wings of equal chord, set at the same angle of attack, with self-similar loading, with spans b_o and $b_o + \Delta b$, and circulation $\gamma(\eta)$ and $(1 + a\epsilon)\gamma(\eta)$ each, as shown in Fig. 3. The lift increment represented by the shaded region is

$$\Delta C_L \propto \int_{-b_o}^{b_o}\left[(1+a\epsilon)\gamma\left[\frac{y}{b_o(1+\epsilon)}\right] - \gamma\left[\frac{y}{b_o}\right]\right]\frac{dy}{b_o}. \tag{6}$$

Expanding the argument of the first term in the integrand in series

$$\Delta C_L \propto -\epsilon\int_{-1}^{1}\dot{\gamma}(\eta)\eta d\eta + a\epsilon\int_{-1}^{1}\gamma(\eta)d\eta + O(\epsilon^2). \tag{7}$$

Integrating the first term by parts

$$\frac{\Delta C_L}{C_L} = (1+a)\epsilon + O(\epsilon^2). \tag{8}$$

Identifying a with $A_o \dot{f}(A_o)/f(A_o)$ this indicates that the lift supported by the fluid extension of the wing is of order ϵ^2.

The effect of blowing on induced drag can be estimated in the same manner. Calling e the span efficiency factor, the induced drag is given by

$$C_{D_i} = \frac{C_L^2}{\pi e A}. \tag{9}$$

A change in induced drag has then the form

$$\Delta C_{D_i} = \frac{(C_L [A_o(1+\epsilon)])^2}{\pi e A_o (1+\epsilon)}(1+\epsilon) - \frac{C_L^2(A_o)}{\pi e A_o} \tag{10}$$

In this equation the lift coefficient is expressed as a function of aspect ratio. Expanding for small ϵ

$$\frac{\Delta C_{D_i}}{C_{D_i}} = 2A_o \frac{\dot{f}(A_o)}{f(A_o)}\epsilon + O(\epsilon^2). \tag{12}$$

As was the case with the lift, this expression contains the induced drag acting on the fluid extension of the wing. In a similar manner it is possible to prove that the drag acting on the fluid extension is of order ϵ^2. With the circulation distributions shown in Fig. 3 the induced drag increment is

$$\Delta C_{D_i} \propto \int_{-b_o}^{b_o} \left[(1+a\epsilon)^2 \gamma\left[\frac{y}{b_o(1+\epsilon)}\right] \frac{\gamma(0)}{A_o(1+\epsilon)} - \gamma\left[\frac{y}{b_o}\right]\frac{\gamma(0)}{A_o}\right]\frac{dy}{b_o} \tag{12}$$

Expanding the circulation for the perturbed span case and integrating by parts as before

$$\frac{\Delta C_{D_i}}{C_{D_i}} = 2a\epsilon + O(\epsilon^2). \tag{13}$$

This equation indicates that the contribution to induced drag by the fluid portion of the wing is of order ϵ^2.

2.1.2. Scaling Laws

To compute the relative change of span due to blowing the jet is idealized as an infinitely thin sheet containing finite momentum, subjected to the load represented by the unshaded area in Fig. 3. Under the effect of this load the jet sheet curls upwards. This load is a function of the chordwise coordinate, causing the jet to curl up sooner near the leading edge of the wing. Δb is identified with the characteristic length that the jet penetrates into the free stream. The jet deformation is analyzed by assuming that it curls up under the effect of the chordwise average of the local lift load. Under this assumption the balance of pressure and centrifugal force on a thin inviscid jet sheet is expressed by

$$\frac{1}{R(y)} = \frac{C_l(y)}{C_\mu} A_o , \tag{14}$$

where R is the local radius of curvature and C_l is the local lift coefficient, as illustrated in Fig. 4. The jet momentum coefficient is defined as follows

$$C_\mu = \frac{\rho_j v_j^2 \delta_j}{q_\infty c} . \tag{15}$$

In differential form Eq. (14) is

$$\frac{d^2 z}{dy^2} = \left[1 + \left(\frac{dz}{dy} \right)^2 \right]^{3/2} \frac{C_l}{C_\mu} A_o . \tag{16}$$

With the transformation $\sinh\zeta = dz/dy$ this equation becomes

$$\frac{d\zeta}{dy} = \cosh^2\zeta \frac{C_l}{C_\mu} A_o , \tag{17}$$

which can be integrated to give

$$\frac{\dot{z}}{\sqrt{1+\dot{z}^2}} = A_o \int_{b_o}^{y} \frac{C_l(\eta)}{C_\mu} d\eta + \left.\frac{\dot{z}}{\sqrt{1+\dot{z}^2}}\right|_{y=b_o} . \tag{18}$$

Introducing the jet slope $\tan\theta = dz/dy$, Eq. 18 becomes

$$\sin\theta = A_o \int_{b_o}^{y} \frac{C_l(\eta)}{C_\mu} d\eta + \sin\theta_o . \tag{19}$$

A characteristic length ratio for the jet curl-up position is obtained by setting $\theta=\pi/2$, corresponding to a jet orientation perpendicular to the wing plane. This leads to the following integral expression for ϵ

$$\int_1^{1+\epsilon} C_l(\eta) d\eta = \frac{C_\mu}{A_o b_o}(1 - \sin\theta_o), \tag{20}$$

where θ_o is the angle of the jet with the spanwise direction at exit. To solve this equation we assume that the lift distribution near the wing tip has the form

$$\frac{C_l^2}{C_{l_o}^2} + \frac{y^2}{b_o^2(1+\epsilon)^2} = 1, \tag{21}$$

which can be expanded as

$$C_l = \sqrt{2} C_{l_o} \sqrt{1 + \epsilon - \frac{y}{b_o}} + O(\epsilon^2) . \tag{22}$$

Substituting this expression in Eq. 20 and multiplying the result by a constant k_1 of order one to account for the approximate nature of the analysis, we obtain for the effective relative enlargement of the span

$$\epsilon = k_1 \frac{3^{2/3}}{2} \left[\frac{C_\mu [1 - \sin(\theta_o)]}{C_{1o} b_o A_o} \right]^{2/3} . \tag{23}$$

Introducing the following relationship, valid in the linear range, with k_2 a constant of order one,

$$C_{1o} = k_2 2\pi \frac{f(A_o)\alpha}{b_o} + O(\epsilon), \tag{24}$$

the following expression, valid for $\epsilon \to 0$, is obtained

$$\epsilon = k \left[\frac{C_\mu [1 - \sin(\theta_o)]}{2\pi f(A_o) A_o \alpha} \right]^{2/3} , \tag{25}$$

where k is a constant of order one. Only the case of blowing tangentially to the span, where $\theta_o = 0$, will be considered. In this case, substitution of ϵ in Eq. (5) gives

$$\frac{\Delta C_L}{C_L} = kF(A_o) \left[\frac{C_\mu}{\alpha} \right]^{2/3} , \tag{26}$$

where $F(A_o)$ is a universal function of aspect ratio given by

$$F(A) = \left[1 + A \frac{\dot{f}(A)}{f(A)} \right] \left[\frac{1}{2\pi f(A) A} \right]^{2/3} . \tag{27}$$

Eq. (26) reveals that the scaling law relating lift increment with blowing intensity and angle of attack is algebraic. It also becomes clear that it is

impossible to linearize the lift gain about weak blowing or small angle of attack. The dependence on aspect ratio is much more complex and can be known only approximately for an arbitrary aspect ratio. However, for very small and very large aspect ratio simplifications are possible leading to power laws. In the limit of infinitely small aspect ratio

$$\lim_{A \to 0} f(A) = \frac{A}{4} \tag{28}$$

leads to

$$\lim_{A \to 0} \Delta C_L \propto C_\mu^{2/3} \left[\frac{\alpha}{A}\right]^{1/3} . \tag{29}$$

For the case of very large aspect ratio,

$$\lim_{A \to \infty} f(A) = 1 - \frac{2}{A} \tag{30}$$

gives

$$\lim_{A \to \infty} \Delta C_L \propto \left[\frac{C_\mu}{A}\right]^{2/3} \alpha^{1/3} . \tag{31}$$

To find an expression for F(A) for an arbitrary aspect ratio, a formula for the lift slope valid for any aspect ratio is required. Such a formula has been determined by Germain[19]

$$f(A) = \left[1 + \frac{2}{A} + \frac{16}{(\pi A)^2} \log(1 + \pi e^{-9/8} A)\right]^{-1} \tag{32}$$

2.1.3 Rolling Moment

Lateral blowing will produce a rolling moment if there is a difference in the intensity of blowing between the two tips of the wing. The case to be analyzed here corresponds to blowing from one of the tips only. The rolling moment coefficient is defined as

$$C_\ell = \frac{\text{rolling moment}}{2q_\infty S b_o} \tag{33}$$

Calling C_l^o and C_l^1 the lift coefficients per unit of span before and after blowing respectively, the rolling moment can be expressed

$$C_\ell = \frac{b_o}{4}\int_{-1}^{1}(C_l^1 - C_l^o)\eta d\eta. \tag{34}$$

To evaluate this integral the assumption is introduced that the lift distributions are elliptical along the span

$$C_l^o = C_{l_o}^o\sqrt{1-\eta^2} \tag{35}$$

$$C_l^1 = C_{l_o}^o\sqrt{1-\frac{(\eta-\epsilon/2)^2}{(1+\epsilon/2)^2}} \tag{36}$$

To first order, the center values of these distributions are related to each other in the form

$$C_l^1 = C_{l_o}^o(1+a'\epsilon), \tag{37}$$

with a' a magnitude that depends on A and α. The rolling moment becomes

$$C_\ell = \frac{b_o}{4}C_{l_o}^o(1+a'\epsilon)\int_{-1}^{1}\sqrt{1-\frac{(\eta-\epsilon/2)^2}{(1+\epsilon/2)^2}}\eta d\eta. \tag{38}$$

Performing this integral and expanding for small ϵ,

$$C_\ell = \frac{b_o}{4} C^o_{l_o} (1 + a'\epsilon)\left[\frac{\pi}{4}\epsilon + O(\epsilon^{3/2})\right]. \tag{39}$$

The effect of blowing can be thought of as consisting of two parts; a lateral distortion of the lift distribution and a local increment of its magnitude. Eq. (39) indicates that the lateral distortion part is the more important of the two. Ignoring terms of higher order and substituting for C_{l_o}

$$C_\ell = k\left[\frac{\pi f(A_o)}{256 A_o^2}\right]^{1/3} C_\mu^{2/3} \alpha^{1/3} \tag{40}$$

This equation indicates that the rolling moment due to one sided blowing follows the same scaling as the lift increment as far a flowing intensity and angle of attack are concerned. The limiting forms for large and small aspect ratio also have the same algebraic form.

2.1.4 Rolling Moment from Half-span Models

Since lateral blowing affects the lift distribution over the entire span of the wing, special considerations are needed to interpret the tests with half-span models, which can only simulate simultaneous blowing from both tips. Denote by $\tilde{C}_l$ the lift per unit of length produced by a half-span model, and consider the quantity

$$\tilde{C}_\ell = \frac{b_o}{4}\int_0^1 [C_l(\eta) - C_l^o(\eta)]\eta d\eta, \tag{41}$$

where in this case C_l is given by

$$C_l = C^o_{l_o}(1 + a\epsilon)\sqrt{1 - \frac{\eta^2}{(1+\epsilon)^2}} \tag{42}$$

The quantity $\bar{C}_\ell$ can be measured from half-span model tests and can be considered to be an indication of rolling moment if its relationship with C_ℓ is known. Eq. (41) can now be written

$$\bar{C}_\ell = \frac{b_o}{12} C^o_{l_o} (2 + a)\epsilon + O(\epsilon^2). \tag{43}$$

The following relationship can be found

$$\bar{C}_\ell = \frac{4}{3\pi}\left[2 + A_o \frac{\hat{f}(A_o)}{f(A_o)}\right] C_\ell \tag{44}$$

The factor multiplying C_ℓ varies monotonically between 1.27 for $A_o = 0$ and 0.85 for $A_o \to \infty$. For an aspect ratio of about 5.5, $\bar{C}_\ell$ and C_ℓ are equal.

2.2 Experimental Investigation

2.2.1 Apparatus and Techniques

The low speed wind tunnel has a 45.72cm by 45.72cm test section. It is a continuous operation, closed-loop facility driven by a variable pitch fan. Pitch control is achieved by remote adjustment of the blade pitch. A maximum centerline free stream speed of 57 m/s is obtainable. Calibration and setting of the tunnel is by observation of a reference pressure difference across the contraction, the two reference locations being sufficiently removed from the test section to avoid model interference.

The requirements for the model were symmetry about the chordline, simplicity of construction, modest aspect ratio, and minimum jet interference with the wind tunnel walls. A NACA 0018 airfoil section with a chord of 15cm and a span, not including the tip piece, of 22.6cm was selected. The basic aspect ratio of the wing model was 3.14. This thick section was chosen to facilitate the incorporation of both a plenum duct and a large number of pressure tappings. A side view of the model is shown in Fig. 5. Initial scalings of the mass flow requirements and expected translations of the tip

vortex suggested that a slot width of 0.16cm would be suitable. Four removable tip pieces were built, as shown in Fig. 5: Tip (a) had a symmetrically located slot designed for ejection parallel to the wing span. Tip (b) had an offset slot and was tested with the slot location nearer the upper surface, which was the configuration for which gains were observed. Tip (c) had a symmetrically located slot with a slant angle of 20°, and the emphasis of the testing was on the downward oriented slant, a configuration for which significant gains were obtained. Tip (d) combined the slant and offset situations. However, due to manufacturing constraints it could only simulate the offset-down-slanted-down or offset-up-slanted-up combinations. These were not desirable combinations, since it was found that they tended to produce effects that counteract each other. In all three cases the slots extended over 73.33% of the wing chord, and the tip shapes were determined by a diameter distribution equal to the wing thickness distribution. The model was mounted on a 20.3cm diameter disk flush inserted into the tunnel floor and which could be rotated to provide incidence adjustment. A circular splitter plate which could slide along the span of the model enabled simulation of various aspect ratios.

A total of 192 surface pressure tappings, divided equally between 8 spanwise stations, were installed in the model. At each station the pressure tappings were divided equally between upper and lower surfaces. An additional tapping was provided in the plenum to assess blowing pressure.

A high pressure air supply capable of providing a maximum of 0.25Kg/s of mass flow was used for the tip jet blowing. The mass flow was measured using a Ventury type mass flow meter and correlated with estimates from measurements of the internal duct pressure.

2.2.2 Data Acquisition

The 192 pressure tappings in the wing were connected to a 4-barrel "J" series Scanivalve module with 48 ports per barrel. The Scanivalve was automatically stepped and the data acquired by a PDP 11/23 minicomputer, enabling a full spanwise load distribution to be recorded by a single pass of the Scanivalve. Each individual Scanivalve pressure was obtained as the average of 30 samples at a frequency of approximately 1KHz. The data was

reduced to pressure coefficients, sectional lift coefficients, and overall load coefficients.

In the tests the jet momentum coefficient was evaluated with the formula

$$C_\mu = \frac{2\delta_j \Delta p}{c q_\infty} \tag{45}$$

where Δp is the difference between the total pressure of the jet, as measured in the wing model plenum, and the pressure where the jet discharges.

Flow surveys in the near wake were conducted using a 0.3175cm diameter five-hole probe mounted on a 3-axis traversing gear. The measured data included total and static pressures, and three components of velocity. The wake surveys were carried out over a range of angles of attack (from 0° to 8°) and blowing ratios (C_μ from 0.02 to 1.0) at three measuring stations (from 13% chord to 140% chord of the airfoil trailing edge). Approximately 450 data points with spacing of 0.635cm were recorded in each wake survey. The measuring planes were perpendicular to the free-stream velocity. All of the vortices observed in the experiments were at least seven vortex radii from the wind tunnel wall, therefore it is believed wall interference would not change the overall flow structure. The facility was fully integrated with the PDP 11 minicomputer for on-line data reduction.

2.2.3 Flow Structure

a) Straight blowing

A typical velocity vector plot in the cross-flow plane for a case of weak blowing from the symmetrically located, straight-slot tip is shown in Fig. 6. The velocity vectors are plotted at the measuring station facing upstream. The dashed line represents the projection of the model contour on the measuring plane. A vector representing the free-stream velocity is also plotted to show the relative magnitudes of the cross-flow plane velocities. The coordinates are normalized by the half span b. A well-defined tip vortex can be observed in this case. The shear layer resulting from the spanwise load distribution can be noticed in the rapid change in velocity

direction near the lower surface. The wing was mounted vertically during the test, the coordinate axis being rotated by 90° to avoid confusion.

Fig. 7 shows a contour plot for the total pressure loss coefficient, defined as

$$\Delta C_{PT} = \frac{P_T - P_{T\infty}}{q_\infty}. \tag{46}$$

The streamwise component of vorticity can be obtained from the measured velocity components in the cross-flow plane by means of the following equation

$$\zeta = \frac{\partial w}{\partial y} - \frac{\partial v}{\partial z}. \tag{47}$$

Due to the relatively large spacing between measurement points, significant error will be introduced if the data points are used directly to evaluate this equation. Therefore, the numerical differentiation is preceded by a cubic spline fit to the measured cross-flow velocity components. A contour plot for the streamwise component of vorticity, for the same test case as before, is presented in Fig. 8. The residual vorticity from the wing indicates that the tip vortex is not yet fully developed at this location.

The vorticity contour is very similar to the total pressure loss contour shown in Fig. 7. The regions of high vorticity almost coincide with the regions of high pressure loss, with the vorticity contour better defined and exhibiting more symmetry near the core region. Due to the better definition of the core region shown by the vorticity contours, this contours were used to determine the location and size of the vortices in the following discussion.

Fig. 9 shows the vorticity contours at the same conditions without blowing. It is clear that the tip vortex undergoes changes with tip blowing. The tip vortex for the no-blowing case is compact, containing tightly packed vorticity near the core. Under the effect of blowing the vortex moves outward and becomes considerably more diffused.

A secondary vortex of opposite sign was observed at low angles of attack and high blowing ratios. Fig. 10 shows a typical cross-flow velocity vector plot for the straight blowing case, exhibiting the vortex pair. The secondary vortex is one of the two counterrotating vortices normally produced by a jet in a cross flow. This characteristic, when associated with jets of circular cross-section, has been known for a long time. The same phenomenon arises in connection with jets of slender cross-section. Wu et al[14] studied non-symmetrical jets issuing from a flat plate into a cross flow and observed a pair of vortices with the stronger one on the leeward side. When the jet sheet is parallel to the free stream the two counterrotating vortices are of the same intensity. When the jet sheet is at an angle of incidence the vortex on the leeward side is larger than the windward vortex, since the induced velocity on the outer edge of the leeward vortex aligns itself with the free stream, as shown in Fig. 11. As the incidence increases the difference in strengths also increases. The strengths of these vortices increases with blowing ratio, since more intense blowing is associated with more entrained mass. For this reason the secondary vortex is discernable at higher blowing rates and lower angles of attack. In Fig. 10 the jet vortex on the leeward side has coalesced with the wing tip vortex, which makes the primary vortex much stronger than the secondary vortex.

To further examine the effect of blowing on the wake, the size and strength of the vortex for different blowing ratio and angle of attack are plotted in Figs. 12 and 13. The size of the vortex was determined by assuming that its edge is were the equality $\zeta b/2U_\infty = 1$ is satisfied. As Fig. 8 shows, when blowing is present the sized of the vortex is significantly larger and weakly dependent on blowing intensity. Tip blowing appears to be an effective way to diffuse the tip vortices.

The strength of the vortex can be calculated by integrating the streamwise component of the vorticity in the vicinity of the vortex,

$$\Gamma = \iint \zeta dydz, \tag{48}$$

where the integration extends over the cross-sectional area of the vortex. The intensity of the primary vortex increases with angle of attack and

blowing intensity. The symbols under the abscissa $\Gamma = 0$ denote the counter-rotating secondary vortices. The strength of the secondary vortex also increases with blowing intensity but decreases rapidly with angle of attack. At $\alpha = 8°$ no secondary vortex was observed. The intensity of the tip vortex is seen to be a nonlinear function of both blowing intensity and angle of attack.

The locus of the primary vortex core at 13% chord downstream of the airfoil trailing edge, for varying angle of attack and blowing ratio, is plotted in Fig. 14. The wing tip contours at $\alpha = 2°$ and $8°$ are also plotted in this figure to show the relative magnitude of the vortex displacement.

b) Slanted and offset blowing

Fig. 15 shows typical lift distributions along the span for the three non-symmetrical slot arrangements. Significant gains are obtained for the slanted-down and offset-up configurations. When the jet is slanted up of offset down the lift augmentation is severely penalized and the lift distributions for these unfavorable cases are not shown.

The lift enhancement for the slanted-down case can be explained by a simple inviscid argument. When the jet is slanted downward it can penetrate farther into the free stream before it curls up and merges with the tip vortex. The effective aspect ratio is therefore larger than it would be with straight blowing. The concentrated lift increment near the wing tip for the offset-up configuration can be attributed to viscous entrainment into the jet. Due to the proximity of the jet to the airfoil upper surface, a favorable change in pressure distribution near the wing tip occurs. Apart from this gain, the lift increment extends over the whole span. This indicates that, as in the case of the slanted-down configuration, the offset-up configuration causes a greater tip vortex outward displacement than the straight blowing case.

Figs. 16 and 17 show the cross-flow plane velocity plots for the slanted-down and the slanted-up cases respectively. There is a well defined vortex pair for the slanted-down case, a pattern which appears significantly more complex for the slanted up configuration. After a detailed study of the vortex trajectory, it was found that the weaker counterrotating vortex pair near the wing tip in Fig. 17 originated from part of the jet near the

trailing edge. Due to the insufficient contraction length on the slot near the trailing edge, a small portion of the jet sheet separated from the main jet. However, the structure of the primary vortex pair can still be clearly observed in this figure. Integration of the vorticity of the vortex system showed that the strength of the primary vortex is about the same for these two configurations, but the secondary vortex in the slanted-down case is significantly stronger than the same vortex in the slanted-up case. From these observations a plausible explanation for the observed effects on lift can be given: The effective incidence of the jet relative to the free stream decreases when the jet is slanted down (it acquires a negative dihedral angle), and increases when the jet is slanted up. Therefore, the slanted-down blowing case produces a greater penetration into the free stream and a stronger secondary vortex. Such an effect adds up to the inviscid argument expounded above. In the slanted-up case the opposite effect predominates (shorter jet trajectory, weaker secondary vortex).

Figs. 18 and 19 show the cross-flow plane velocity vectors for the offset-up and the offset-down configurations, for the same angles of attack and blowing intensities. As it was the case with the slanted-down configuration, the vortex pair is more symmetric and better defined in the offset-up case. The secondary vortex pair for the offset-down case is due to the separation of the jet sheet in the same manner as in the slanted-up case. The tip vortices are of about the same strength in the cases of offset-up and offset-down, while the secondary vortex is stronger in the offset-up configuration.

The jet profiles for the offset-up configuration were measured in still air to check if the lateral displacement of the tip vortex for the offset-up and the slanted-down cases originated from the same mechanism. It was found that the jet does have a slant angle of 2° as shown in Fig. 20. However, this angle is too small to cause the lateral displacement of the tip vortex in the offset cases. Careful examination of the jet profile indicates that it is also skewed toward the upper side in the offset-up case. The ratio of the half width of the lower side, to that of the upper side is approximately 0.8. The precise mechanism which generated the skewed profiles has not been determined, although it may be associated with the asymmetric

contraction (required by model construction) the flow undergoes as it reaches the slot.

2.2.4 Aerodynamic forces

The case of straight blowing is considered first. The source of lift gain can be identified in greater detail by analyzing the isobar patterns shown in Figs. 21 to 24. Over most of the upper surface blowing causes a shift of the isobars towards the trailing edge, indicating increased suction, except for a small region near the corner of the trailing edge and the tip, where suction decreases. The increase in suction is more marked near the tip and on the rear two-thirds of the chord. The lower surface shows a less complex situation; there is a fairly uniform gain in the pressure excess.

Figs. 25 (a) and 25 (b) show how blowing affects the load distribution on the upper and lower surfaces. Over most of the upper surface the pressure changes by an almost uniform value, except near the tip, where three regions can be distinguished. Close to the leading edge suction is slightly decreased. This is probably due to the effective contouring imposed by the jet on the wing planform. A larger portion of the region near the tip is subjected to a significant increase in suction. This added suction denotes an acceleration of the fluid due to entrainment into the jet and the velocity induced by the rolled-up tip vortex, indicating the presence of both viscous and inviscid mechanisms. The decreased suction in the small region near the trailing edge is probably due to the removal, by blowing, of the tip vortex which had established itself above that area of the wing before blowing was applied. Examination of the load on the lower surface indicates that the increase in pressure is more pronounced near the tip. Since viscous entrainment into the jet is also expected to be present on the jet lower surface, and would tend to accelerate the flow, the observed decceleration suggests that the inviscid effect of span increase is more important than the effect of viscous entrainment for a symmetrical arrangement of the slot. The main source of lift is the redistribution of downwash along the span, causing a change in the effective angle of attack. With regard to the effect of aerodynamic twist imparted to the wing by the curled-up jet, it appears to be localized near the tip and of minor importance relative to the total lift coefficient. However, this phenomenon might be of some importance in

connection with the rolling moment, where the importance of pressure changes near the tip are amplified.

Figs. 26 and 27 reveal that the increment of lift due to lateral blowing is a non-linear function of angle of attack. A change in angle of attack at fixed blowing rate causes the wing aspect ratio to change, modifying the loading at the wing tip, which in turn affects the effective aspect ratio. The combined effects of these changes suggests that the lift slope will be singular about the value of angle of attack for zero lift.

Figs. 28 and 29 show a non-linear dependence of lift gain on blowing rate. This non-linearity can also be explained in terms of simultaneous changes affecting each other; an increment in the blowing rate causes a change in the loading of the wing near the tip, and this in its turn affects the length that the jet projects into the free stream. This explanation would suggest that the singular behavior occurs about $C_\mu = 0$.

The rolling moment due to one-sided lateral blowing is discussed in terms of the quantity $\bar{C}_\ell$, which is plotted in Fig. 30. This quantity, called "measure of the rolling moment coefficient", also exhibits non-linear dependence on blowing intensity and angle of attack. The considerable scatter shown in Fig. 30 is probably due to magnification of experimental uncertainties near the tip. In order to evaluate the potential of this concept as a means of generating rolling moment, the deflections of two different conventional aileron configurations required to produce the same rolling moment with lateral blowing (for this purpose it is assumed $\bar{C}_\ell = C_\ell$), are shown in Fig. 31. The ailerons are on wings of identical planform as that presently under consideration, cover 25% of the chord and extend over 25% and 50% of the span respectively[20] . The moments produced by the deflection of only one of the ailerons in the full-span wing were used to compute the deflection angles in Fig. 31.

The effect of aspect ratio on lift increment was also investigated. This was done for the case of straight blowing only. The effect of variable aspect ratio was studied by inserting the wing model through a sliding splitter plate, and simulating different wing spans by different plate positions. The results for selected angles of attack and blowing intensities are summarized in Fig. 32. There is a more intense lift increment at smaller aspect ratios. In fact, it is expected that the lift gain would

become unbounded for infinitely small aspect ratio. This is a consequence of a relative change in span, at constant blowing strength, becoming ever more significant as the aspect ratio decreases.

The effect of different tip configurations on lift distribution is shown in Figs. 33 and 34. It can be seen that the offset-up and the slant-down cases enhance the lift all along the wing span. The resultant lift changes are shown in Figs. 35 and 36. The combination offset-down and slant-up showed considerable deterioration in performance. A combination of the two favorable cases, slant-down and offset-up, would in principle be of great interest, but due to constraints in model manufacture, this configuration could not be tested.

2.2.5 Comparison between Theory and Experiment

The main assumptions and results of the analytical study can be checked against measurements of both the flow filed structure and the aerodynamic forces. The spacing between the tip vortices behind a wing is proportional to the wing span through a weak function of the wing planform. Then the effective change in wing span due to blowing should be proportional to the lateral migration of the tip vortex when blowing is applied. If the information in Fig. 14 is replotted in logarithmic form, the theoretically derived relationship between vortex outward displacement and blowing intensity, $\Delta b \sim C_\mu^{2/3}$, can be verified. As can be seen in Fig. 37, the horizontal migration of the tip vortex follows the 2/3 scaling law quite closely.

Further evidence of the change-of-span effect is obtained by examining the loci of the tip vortices as shown in Fig. 38. As expected, the jet penetrates farther into the free stream for the favorable cases, slant-down and offset-up. In the case of the slanted jet, the theoretical development predicts a dependence on jet slant of the form $\Delta b \sim (1 - \sin\theta_o)^{2/3}$. The jet profile of the slanted jet was measured in still air and the angle was found to be 18.5°, 7.5% off the design angle of 20°. The theoretical prediction in this case would indicate

$$\frac{\Delta b_{\theta_o}}{\Delta b_{\theta_o=0}} = (1 \pm \sin 18.5°)^{2/3} = 1.20,\ 0.78 \qquad (49)$$

The measured values are 1.40 and 0.54, which deviate from the predicted values by +17% and -31% respectively. This deviation is probably due to the dihedral effect, present in the experiment and ignored by the theory, and The intervention of viscous factors. As discussed above, the dihedral effect tends to alter the loading near the tip in a manner that jet penetration is enhanced in the slant-down case, and diminished in the slant-up case.

The scaling law given by Eq. (27) can also be checked by a logarithmic plot of the lift increment, as shown in Figs. 39 and 40. Data taken from other sources has also been added. It can be seen that the 2/3 power law is followed closely both for blowing intensity and angle of attack.

The theory predicts an algebraic dependence of lift increment on aspect ratio for very small and very large aspect ratios. An assessment of the power laws given by Eqs. (29) and (31) is shown in Fig. 41. The limits for very large and very small aspect ratio are difficult to visualize, but the trends appear to confirm them.

Figs. 42 through 45 demonstrate that the 2/3 power scaling law also holds for the offset and slanted configurations. This agreement is an indication that the basic mechanism for lift augmentation still operates through an enlargement of the aspect ratio in these cases. The differences in efficiency occur due to a more or less effective penetration of the tip jet into the free stream.

Better insight into the validity of the scaling law is inferred from the relative lift increments as shown in Figs. 46 and 47. If these results are replotted against $(C_\mu/\alpha)^{2/3}$, the data are expected to collapse on a straight line. As can be seen in Fig. 48, this is accomplished for all the data points, except for the ones corresponding to $\alpha = 2°$. The reason for this disagreement is to be found in the formation of a strong secondary vortex at this angle of attack. As explained before, this phenomenon occurs more strongly at small angles of attack and affects the tip vortex in a manner that a reduced lift increment is achieved. Although a detailed explanation of this interaction is not available, its presence can be credited with a negative influence on lift augmentation. In the unfavorable cases of slant-up and offset-down blowing configurations, similar vortex structures were observed.

Finally a general collapse of data points is presented in Fig. 49, where F(A) was evaluated f(A) as given by Eq. (32). The collapse is less marked at smaller aspect ratios, but in general it can be considered quite good. This also confirms the theoretical prediction of a singular behavior near A = 0. Sources of disagreement may be found in experimental error, a less clear assessment of the aspect ratio for small wing span, and also the effect of having a slot which didn't extend over the whole length of the chord. This last factor can become relevant for small aspect ratios and was not taken into account in the theory.

3. THE JET SPOILER CONCEPT

3.1 Apparatus and Techniques

The same wind tunnel and instrumentation were utilized as in the study of the tip blowing concept. The wing model was modified by drilling two jet slots, 5.715cm in length and 0.1575cm in width, on upper and lower surfaces, as shown in Fig. 50. The source of high pressure air for the jets was a centrifugal blower with a range of 0 to 2.5psi.

3.2 Data Acquisition

The same data acquisition procedures and systems as in the case of the tip blowing concept were used. In this case the following definition of C_μ was adopted

$$C_\mu = 2\frac{v_j^2 \delta_j c_j}{U_\infty^2 cb}. \tag{1}$$

3.3 Results and Discussion

Measurements with both one-sided and two-sided blowing were taken. For the one-sided blowing configuration the model was fitted with the upper surface slot only. For the two-sided blowing configuration the jets drew air from a common plenum.

Fig. 51 shows a three-dimensional view of the pressure distribution on the upper surface of the wing for the one-sided blowing case. This indicates a high pressure region ahead of the jet and a region of lowered pressure behind it. The high pressure region ahead of the jet is consistent with previous observations in two-dimensional inviscid calculations[21], and in two-dimensional experiments[22]. This increase in pressure is a response to the jet behaving as if it were a solid body, effectively displacing the fluid away from the wing surface. The origin of the reduced pressure region downstream of the jet can be understood by observing the difference between the one- and two-sided blowing cases illustrated in Figs. 52 and 53, which depict the chordwise pressure distribution at a point halfway between the two ends of the slot for the one-sided and the two-sided blowing cases. It can be seen that the two-sided blowing case produces significantly less

suction behind the jet slot. The present definition of the jet momentum coefficient requires the mass flow for the two-sided case be twice as much as the mass flow for the one-sided case for a fixed jet exit velocity. Fig. 54 illustrates the velocity distributions of the jets for wind-off conditions, measured along the spanwise centerline of the slots, at 4" from the wing surface. It can be noticed that the two-sided case, with its correspondingly higher mass flow, exhibits a more distorted velocity distribution. For each jet the three-dimensional flow field should consist of a pair of counterrotating vortices which interact with the single tip vortex. The more even velocity distribution of the one-sided blowing case leads to a better-defined pair of counterrotating vortices, causing more intense suction forces. This fact is clearly shown in the flow mappings of Figs. 55 and 56. The one-sided case exhibits two vortices, one can be identified with that arising from the inboard edge of the jet, while the other constitutes the tip vortex, which has engulfed the vortex originating from the outboard edge of the jet. In the two-sided blowing case, however, the inboard vortex appears to be absent, the wing tip vortex being the most dominant structure. The reason for the skewness of the two sided blowing case is the absence of stagnant conditions in the plenum, due to the higher demand for air in that case for the same jet exit velocity.

Experiments with a spoiler jet issuing from a flat plate with a high subsonic and supersonic free stream speeds[23] show the same type of chordwise pressure distribution. The pressure distribution is also qualitatively similar in the case of the solid spoiler.

The effect of the redistribution of surface pressure when blowing is applied is a change in the local drag coefficient, which leads to the yawing moment for which this concept is intended. If the jet slot were located near the airfoil maximum thickness, as was the case here, both the increase in pressure upstream, and the suction downstream of the slot would contribute to a local drag increase. This location also causes a modest cancellation of the components of force normal to the wing chord, thus having a very small impact on lift, as can be seen in Fig. 57. This counteraction also results in a reasonable rolling moment coupling, a feature quite desirable in this context. In the application of the jet spoiler to missile fins, where a

strong rolling moment was sought, the jet slots had to be located near the trailing edge in order for the concept to be effective.

The total drag distributions shown in Figs. 58 and 59 suggest that one-sided blowing is significantly more efficient when the jet exits from the upper surface than when it exits from the lower surface. This is expected, since decreasing the speed of the high velocity stream on the upper surface implies a higher induced pressure than a corresponding decrease on the lower surface. The more concentrated drag distribution in Fig. 60 seems to indicate that for negative angles of attack the wing tip vortex more effectively distorts the counterrotating vortex pair formed by the jet. The two peaks observed in Fig. 61 for intense blowing are an indication of the distancing of the wing tip vortex from the jet vortices, which are then less affected by the former. Comparing Figs. 60 and 59 it can be inferred that superposition of effects, for the configurations tested here, does not apply. This is likely to be due to the detrimental effect of jet momentum distortion for the two-sided case being fairly independent of blowing intensity.

Fig. 62 indicates that the yawing moment in the one sided case is a fairly weak function of angle of attack in the range $-2° < \alpha < 12°$. The yawing moment is defined as

$$C_n = \frac{b_o}{4}\int_0^1 \eta \Delta C_d d\eta \qquad (2)$$

Fig. 63 confirms that in this particular case this concept is less effective in the two-sided configuration, with the dependence on angle of attack also being stronger. In the latter case the yawing moment is of course symmetrical about $\alpha = 0°$.

Figs. 64 and 65 show that the rolling moment is comparable to the yawing moment, but exhibits a rather erratic dependency. The definition of rolling moment user here is given by Eq. (2.34).

Further insight into the behavior of this concept can be gained by analyzing the relationship between yawing moment and blowing intensity. By averaging the yawing moment produced by the one-sided case in the range $0° < \alpha < 12°$, where the dependence on α is rather weak, the logarithmic plot

shown in Fig. 66 was generated. The linear relationship shown in this plot indicates that a power dependence exists. A linear regression analysis gives

$$C_n = k_3 C_\mu^{0.85} \tag{3}$$

with k_3 a proportionality constant, presumably a function of airfoil thickness and jet location. The numerical value of the power affecting C_μ could also depend on airfoil thickness. The relevant feature is that this power is less than one, implying higher sensitivity of yawing moment to blowing at lower intensities.

A practical assessment of the potential of jet spoilers to effect yaw control is derived from a comparison with the performance of a typical solid spoiler. For this purpose measurements[24] on a straight wing of aspect ratio 4, with a 15% percent thick Clark Y airfoil cross-section, were used. The wing was fitted with a spoiler on the upper surface, placed at the maximum thickness location, and extending over 37.5% of the wing span. To compensate for the different aspect ratios of the two wings, the values of the yawing moments produced by the jet spoiler were multiplied by the ratio 4/3.14. The comparison is still rather approximate, since the two airfoils have different thickness, the Clark Y is not symmetrical, and the fraction of span covered by the solid spoiler is greater. In this comparison the thickness aspect would make the jet spoiler look more effective than it actually is - it is expected that thick airfoils will respond better to the concept than thin ones - while the span extension would make it look less effective. For these reasons this analysis is to be taken only as a rough indication of jet spoiler potential. The solid spoiler was deflected 60° with respect to the wing chord and the lift coefficient of the case used in this comparison was 0.36. The lift coefficient, which is unimportant in the one-sided jet spoiler, is quite important in the solid spoiler. In the case of the solid spoiler both rolling and yawing moments increase with angle of attack, the rolling moment significantly faster. Fig. 67 shows the vertical projection of the solid spoiler that would be required to equate the yawing and rolling moments produced by the one-sided jet spoiler for varying blowing

intensity. The lower values of vertical projection in roll than in yaw are an indication of the substantially smaller coupling between roll and yaw in the jet spoiler case.

4. CONCLUSIONS

Two blowing schemes for lateral and roll control of aircraft have been studied. The tip blowing concept, intended for roll control, was analyzed theoretically and experimentally. The jet spoiler concept, considered as a yaw-control device, was studied experimentally. Both concepts emphasize moderate blowing intensity.

The analysis of the wing tip blowing concept lead to the derivation of scaling laws relating aerodynamic forces to jet and wing parameters, which were then verified experimentally. It was found that the dependence on blowing intensity and angle of attack occurs through a 2/3 power law, while the dependence on aspect ratio is more complex. In the limits of small and large aspect ratios this complex dependence also reduces to power laws. The postulate that the basic mechanism responsible for lift augmentation is of inviscid nature has been confirmed. Such mechanism consists in an effective alteration of the wing aspect ratio as a result of the lateral jet, which behaves as an extension of the wing. Several jet slot arrangements were tested, from which it was inferred that tip configuration affects performance through two main mechanisms; a change in the effective penetration of the jet into the free stream depending on the initial orientation imparted to the jet by the slot, and a more or less drastic modification of the flow structure resulting from the interaction of the jet with the tip vortex. The first mechanism is accounted for theoretically, while the second, when present, tends to invalidate the theoretical results. The second mechanism is associated with the appearance of secondary vortices, in a manner similar as in the jet-in-cross-flow problem. The theoretical results are best confirmed when only one vortex, consisting of the tip vortex engulfing the jet, is present.

A comparison with the performance of conventional ailerons was carried out, indicating the intensity of blowing that would be required to produce a rolling moment comparable to the one produced by a standard aileron, for specified aileron deflection.

The tests done on the jet spoiler concept aimed at exploring its potential for generating yaw-control aerodynamic forces with little lift penalty and moderate roll coupling. Both one-sided blowing and two-sided blowing

configurations were tested. For the same jet momentum coefficient, which amounts to twice as much mass flow, the two-sided case showed less efficiency. This is attributed partly to the absence of stagnant conditions in the plenum.

In this concept the yawing moment arises from an increment of pressure upstream of the jet slot and a decrement downstream, which, when integrated over the vertical projection of the wing surface causes a local increment in drag. The larger the vertical projection of the area over which the pressure induced by the jet spoiler acts, the greater the efficiency is expected to be. Hence, thick airfoils should respond to this scheme better than thin ones. The optimal location of the jet spoiler appears to be the maximum thickness station of the airfoil section, since such a location would allow for positive drag to be generated by both the increased- and the decreased-pressure regions.

The yawing moment produced by the one-sided jet spoiler is fairly independent over a considerable range. In contrast, the yawing and rolling moments generated by solid spoilers exhibits a marked dependence on angle of attack. For the jet spoiler tested here a power law of the form $C_n \sim C_\mu^{0.85}$ was found.

Comparison with solid spoiler experiments indicates that for comparable yawing moments, the jet spoiler exhibits considerably less rolling moment coupling.

REFERENCES

1. Tavella, D., Wood, N. and Harrits, P. "Measurements on wing tip blowing," JIAA TR-64, Stanford University, 1985.

2. Tavella, D., Wood, N.J. "Influence of tip blowing on rectangular wings," AIAA paper 855001, 1985.

3. Tavella, D.A. and Roberts, L. "The concept of lateral blowing," AIAA paper 855000, 1985.

4. Tavella, D.A., Lee, C.S., and Wood, N.J. "Influence of wing tip configuration on lateral blowing efficiency," AIAA paper 860475, 1986.

5. Lee, C.S., Tavella, D., Wood, N.J., and Roberts, L. "Flow structure of lateral wing-tip blowing," paper 861810, proceedings AIAA 4th Applied Aerodynamics Conference, San Diego, CA 1986.

6. Tavella, D.A., Lee, C.S., Wood,N.J., and Roberts, L. "The jet spoiler as a yaw control device," paper 861806, proceedings AIAA 4th Applied Aerodynamics Conference, San Diego, CA 1986.

7. Ayers, R.F. and Wilde, M.R., "An experimental investigation of the aerodynamic characteristics of a low aspect ratio swept wing with blowing in a spanwise direction from the tips," The College of Aeronautics, Cranfield, UK, Note 57, 1956.

8. Carafoli, E., " The influence of lateral jets, simple or combined with longitudinal jets, upon the wing lifting characteristics," Proceedings ICAS Third Congress, 1962.

9. Carafoli, E. and Camarasescu, N., "New research on small span-chord ratio wings with lateral jets," Foreign Technology Division, Translation FTD-Hc-23-319, 1969.

10. White, H.E., "Wind tunnel investigation of the use of wing-tip blowing to reduce drag for take off and landing," The David W. Taylor Model Basin Aerodynamics Laboratory, AERO Report 1040, 1963.

11. Briggs, M.M. and Schwind, R.G., "Augmetation of fighter aircraft lift and STOL capability by blowing outboard from the wing tips," AIAA paper 830078, 1963.

12. Hickey, D.H., "Experiments with spanwise blowing from the tip," FHA Technical Memorandum 24, unpublished, 1983.

13. Wu, J.M., Vakili, A., and Chen, Z.L., "Wing-tip jets aerodynamic performance," ICAS 82-5.6.3, 1982.

14. Wu, J.M., Vakili, A.D., and Gilliam, F.T., "Aerodynamic interaction of wing tip flow with discrete wing tip jets," AIAA paper 842206, 1984.

15. Vogler, R.D. and Turner, T.R., "Wind tunnel investigation at transonic speeds of a jet control on a 35-degree swept wing - Transonic-Bump method," NACA RM L55K09, 1956.

16. Shutt, E.D., "Free-flight investigation at Mach numbers between 0.5 and 1.7 of the zero-lift rolling effectiveness and drag of various surface, spoilers, and jet controls on an 80-degree delta wing missile," NASA TN D205, 1960.

17. Blair, A.B., "An experimental wind tunnel investigation of a ram-air-spoiler roll control device on a forwar control missile at supersonic speeds," NASA TP 1353, 1978.

18. Cirus, J.D., Kadlec, E.G., and Klimas, P.C., "Jet spoiler arrangement for wind turbine," Patent US A6532430, 1983.

19. Germain, P. "Recent evolution in problems and methods in aerodynamics," J. Roy. Aeronaut. Soc. 71, 673-691, 1967.

20. Johnson, H.S. and Hagerman, R., "Wind-tunnel investigation of the low speed lateral control characteristics of an unsewpt, untapered semispan wing of aspect ratio 3.13 equipped with various 25-percent-chord plain ailerons," NACA TN 2199, 1951.

21. Tavella, D. and Karamcheti, K., "Aerodynamics of an airfoil with a jet issuing from its surface," AIAA paper 810220, 1981.

22. Leopold, D., Krothapalli, A., and Tavella, D., "Some observations on the aerodynamics of an airfoil with a jet exhausting from the lower surface," AIAA paper 830173, 1982.

23. Heyser, A., and Maurer, F., "Experimentelle Untersuchungen an festen Spoilern und Strahlspoilern bei Machschen Zahl von 0.6 bis 2.8," Zeitschrift fuer Flugwissenshaften, V. 10, 4/5, 1962.

24. Wenzinger, C.J. and Rogallo, F.M., "Wind tunnel investigation of spoiler deflector and slot lateral control devices on wings with full span split and slotted flaps," NACA R 706, 1941.

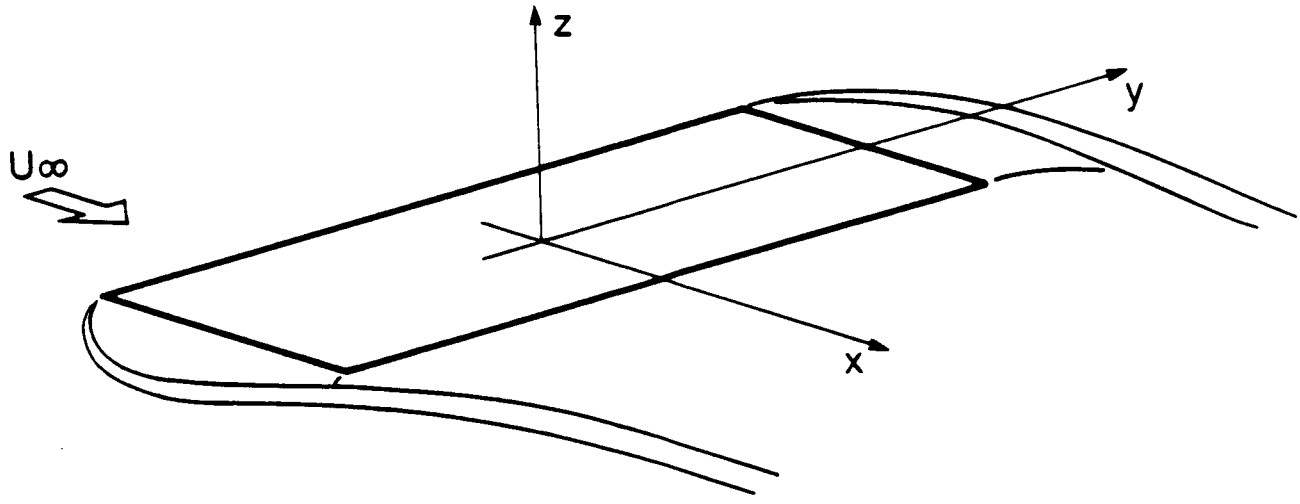

Fig. 1 The tip blowing concept.

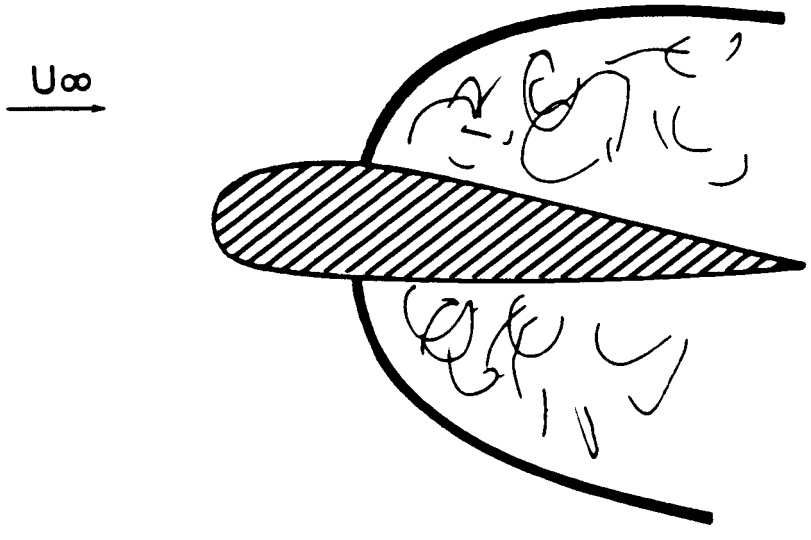

Fig. 2 The jet spoiler concept.

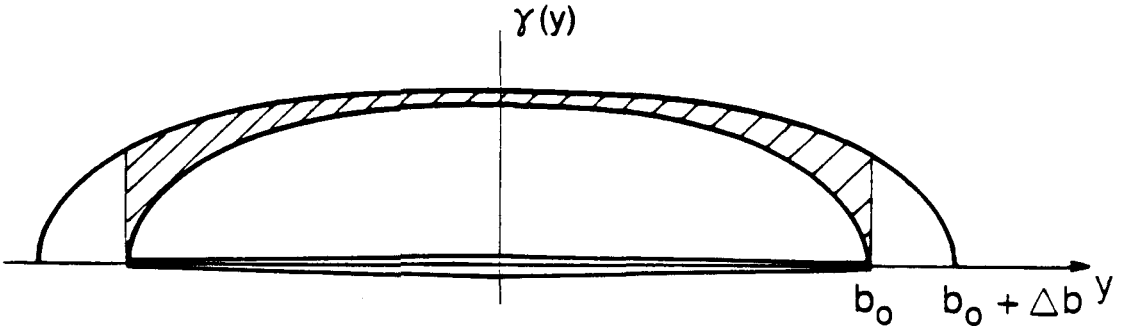

Fig. 3 Span perturbation.

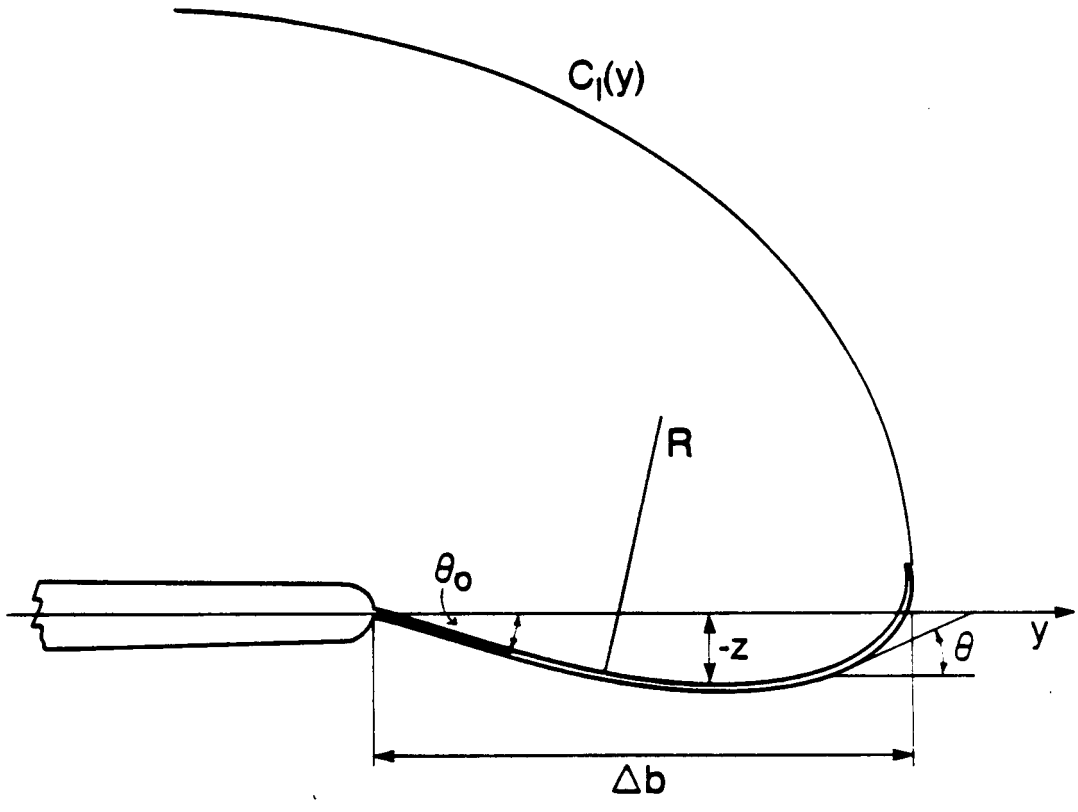

Fig. 4 Tip jet parameters.

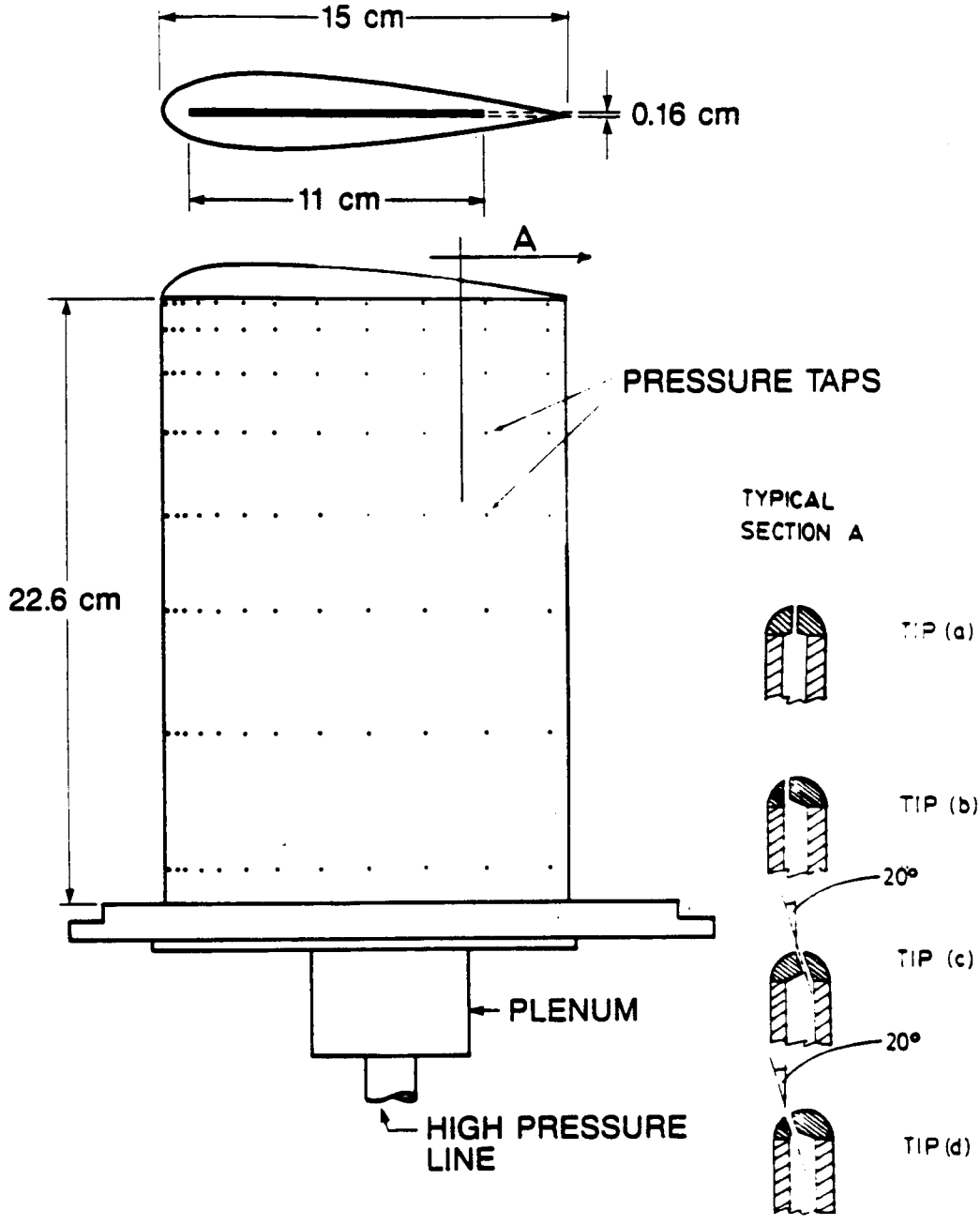

Fig. 5 Wind tunnel model for lateral blowing.

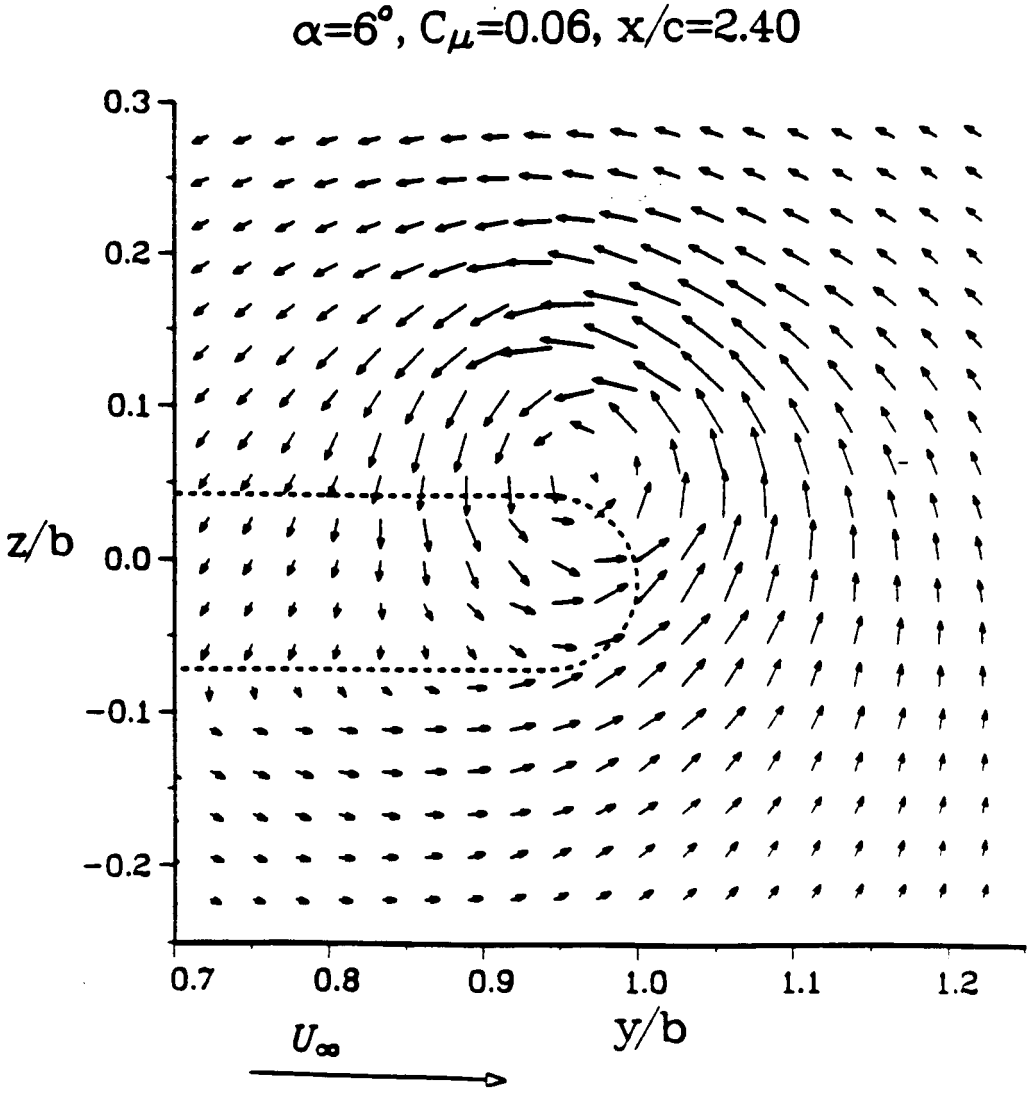

Fig. 6 Straight blowing: Single velocity plot.

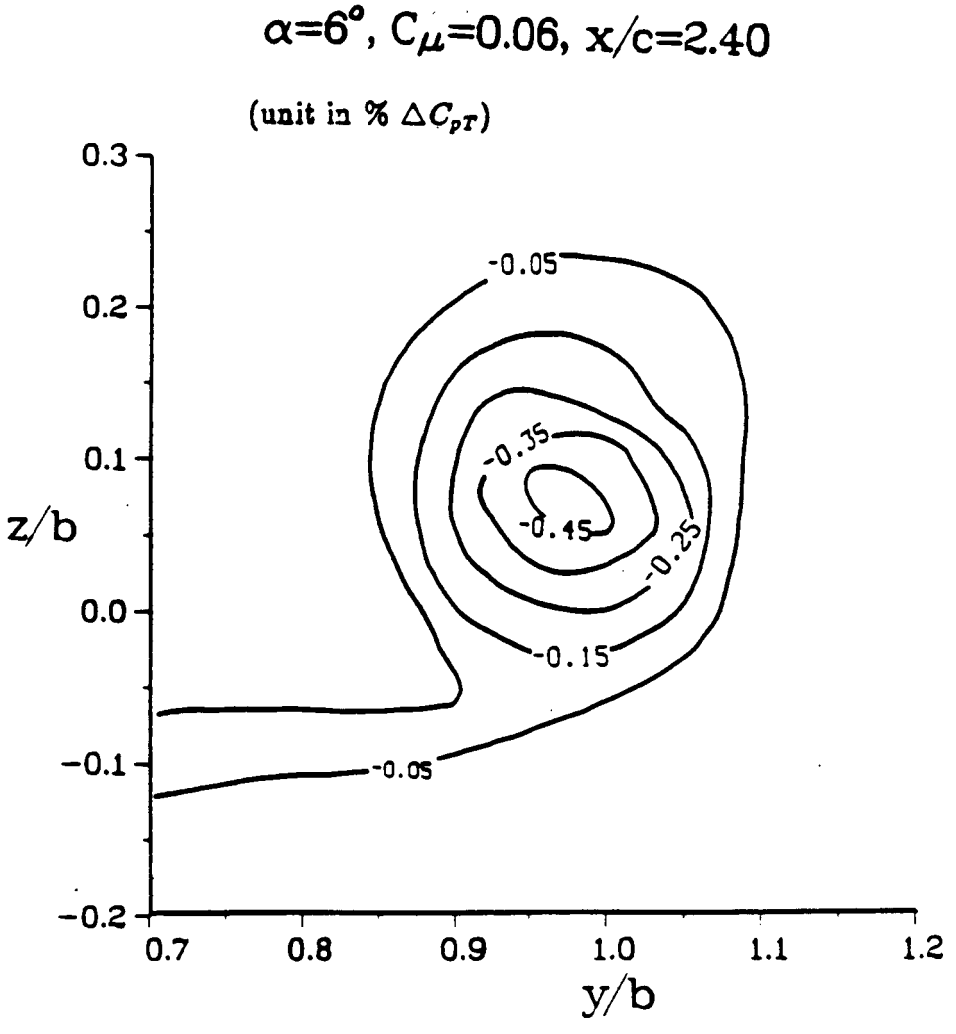

Fig. 7 Vortex total pressure contours.

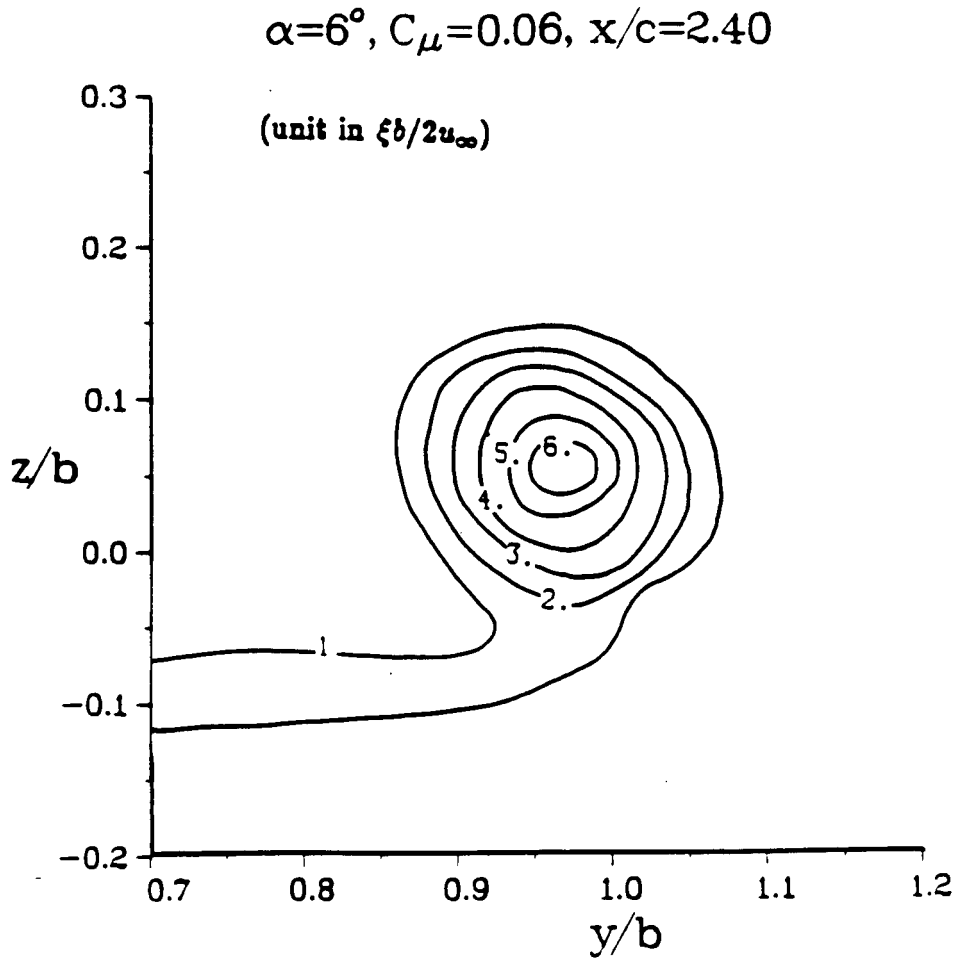

Fig. 8 Vorticity contours, with blowing.

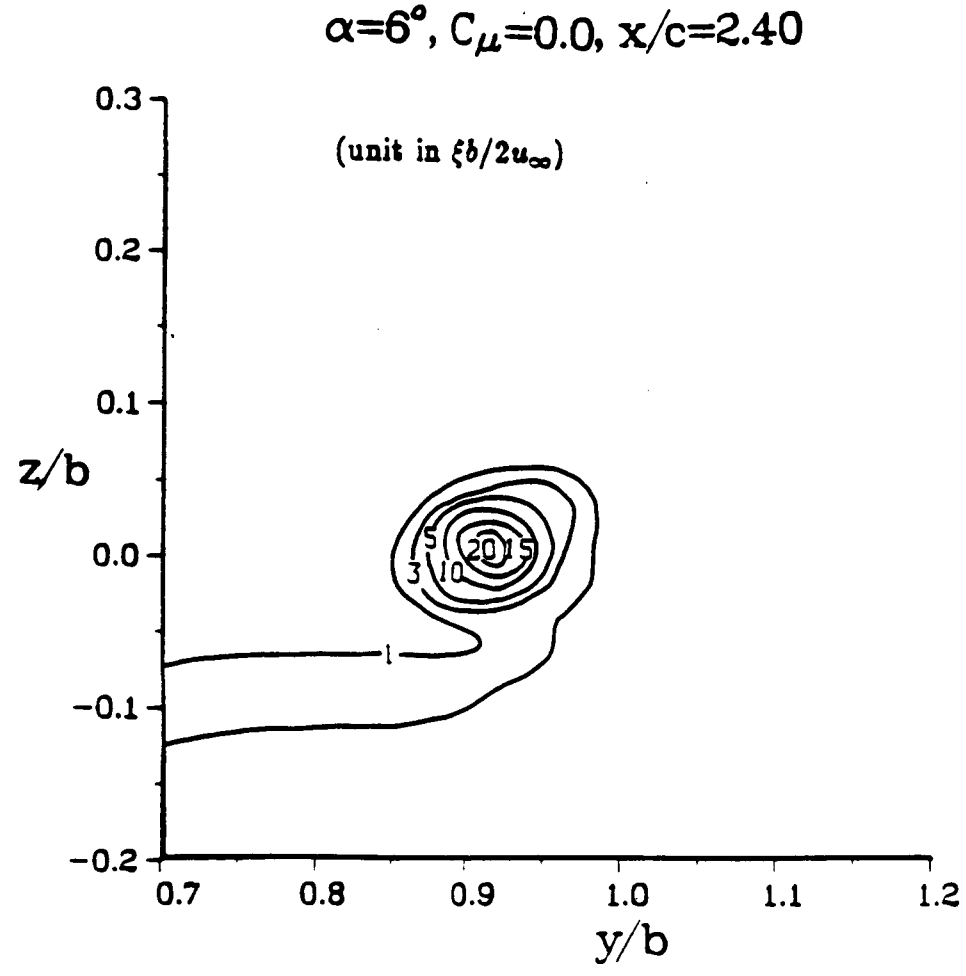

Fig. 9 Vorticity contours, no-blowing.

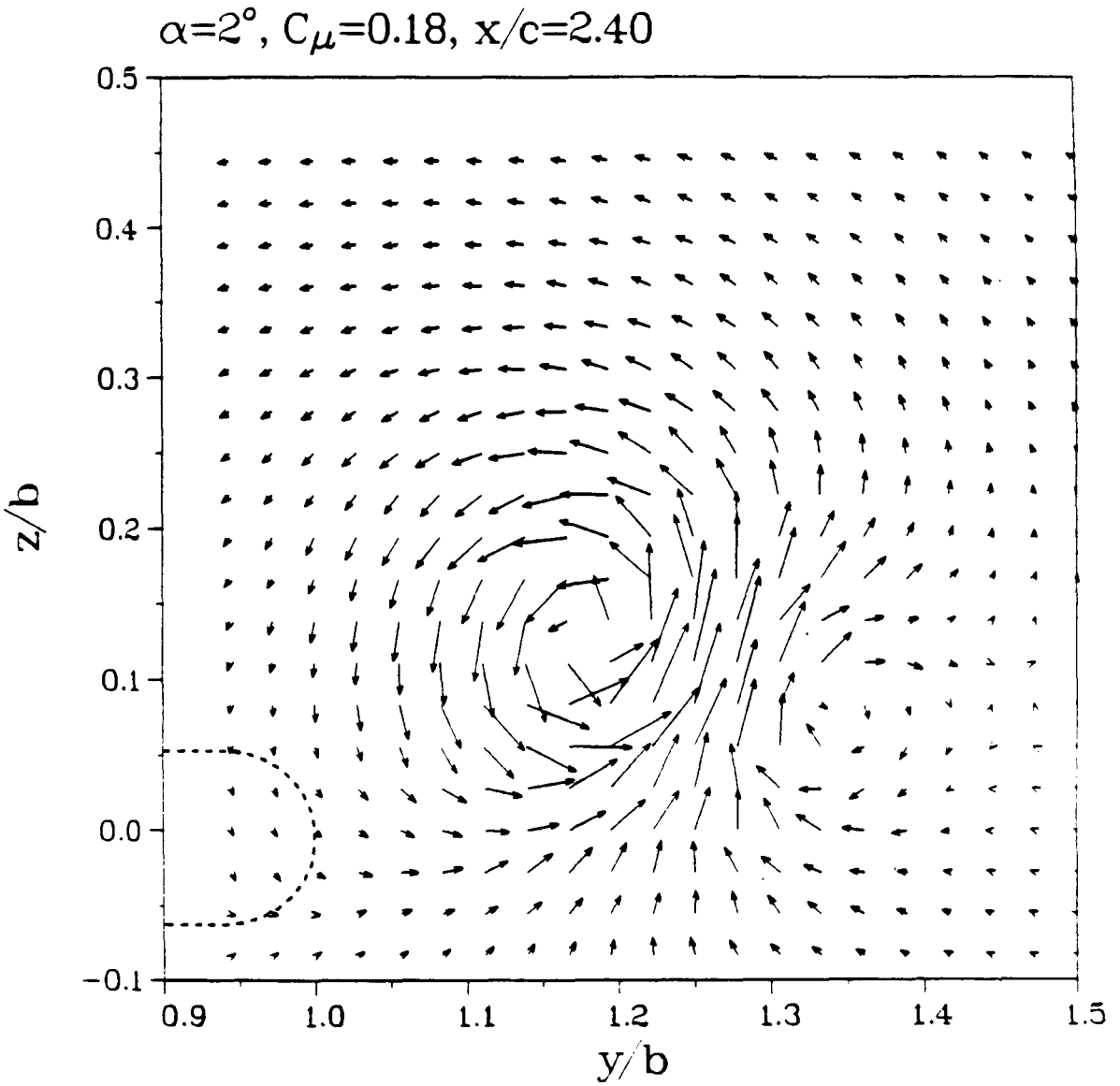

Fig. 10 Primary and secondary vortices, straight blowing.

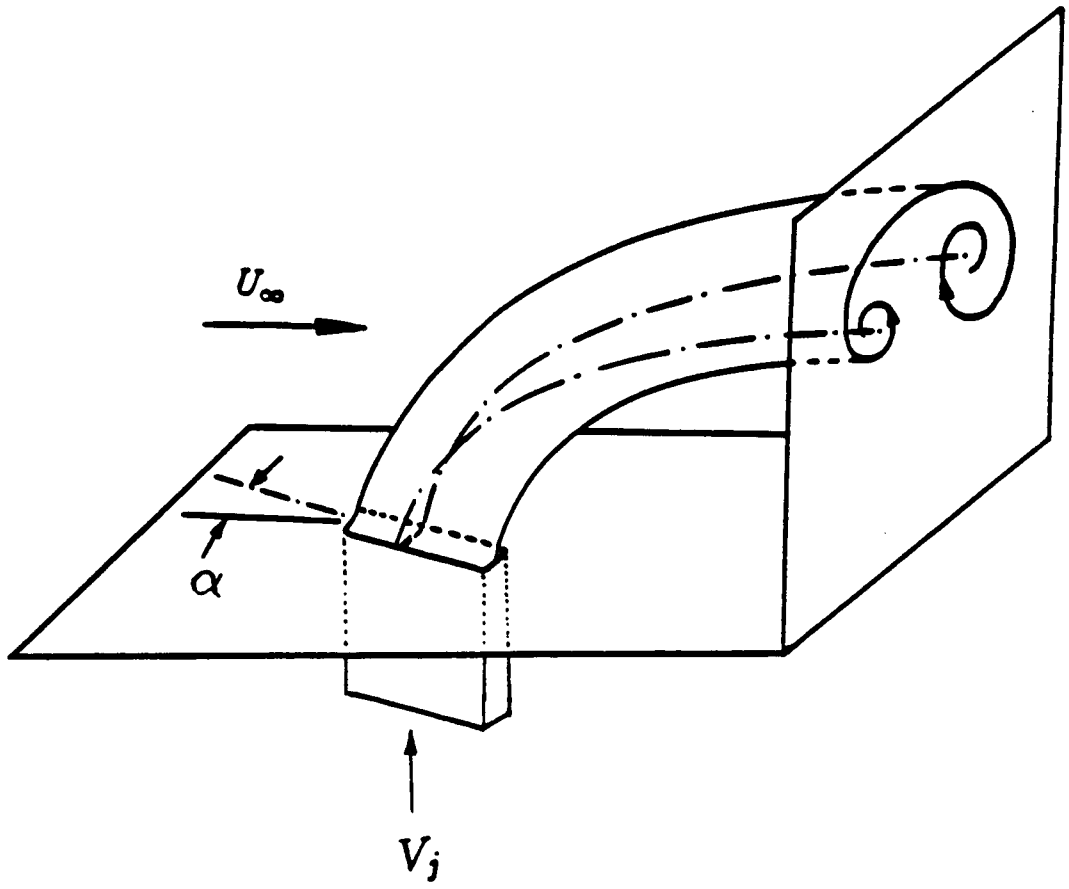

Fig. 11 Jet sheet at incidence, taken from Ref. (14).

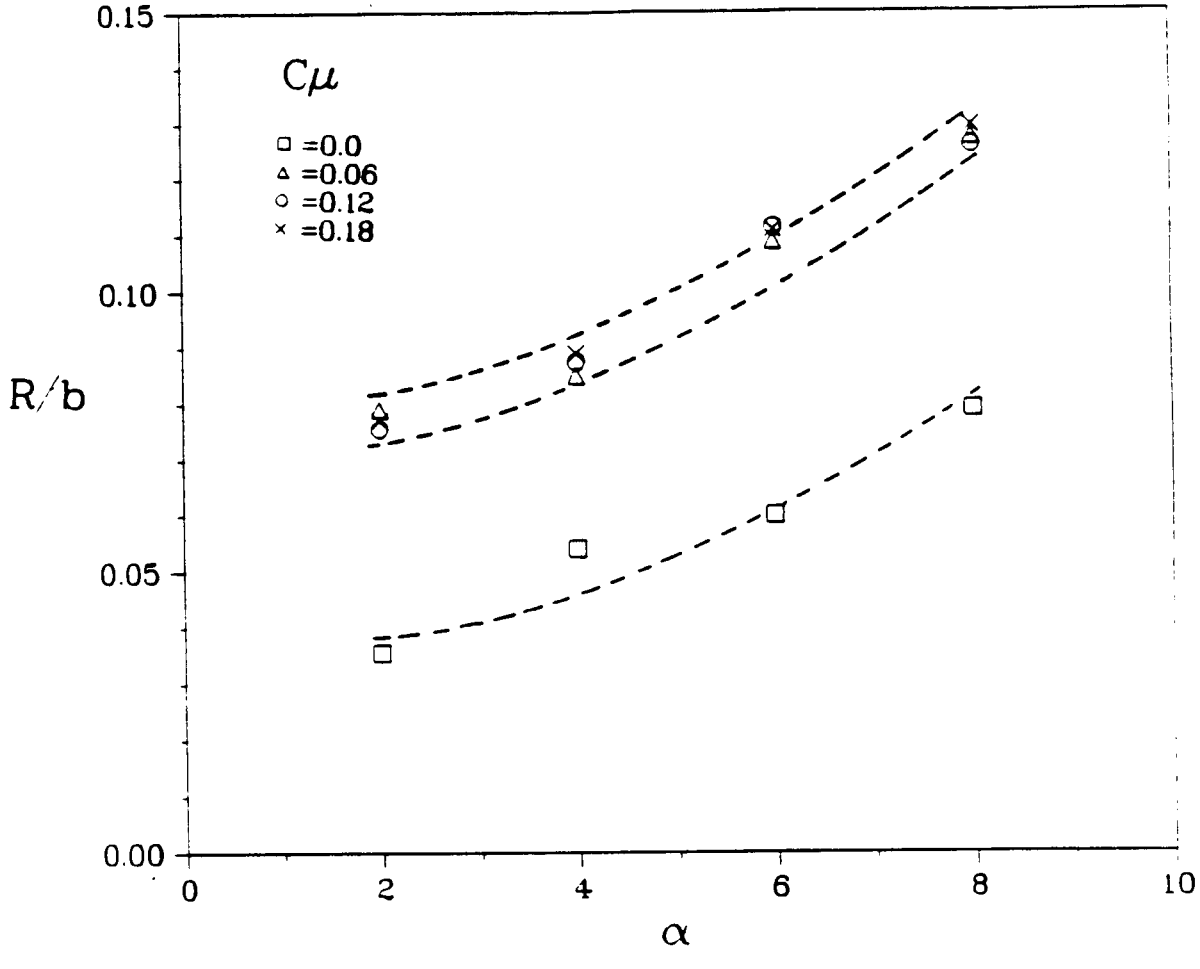

Fig. 12 Size of primary vortex, straight blowing.

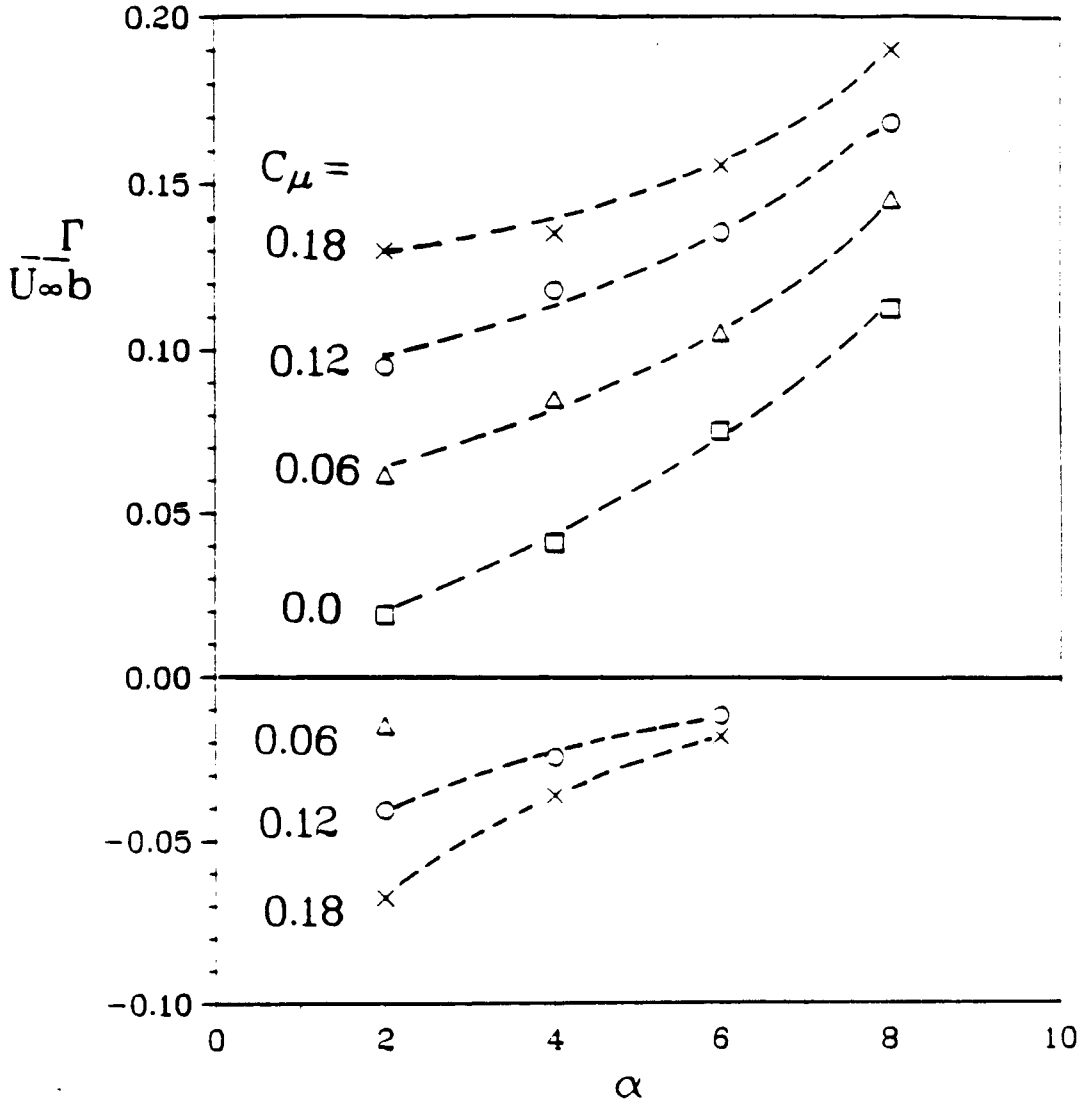

Fig. 13 Strength of primary and secondary vortices, straight blowing.

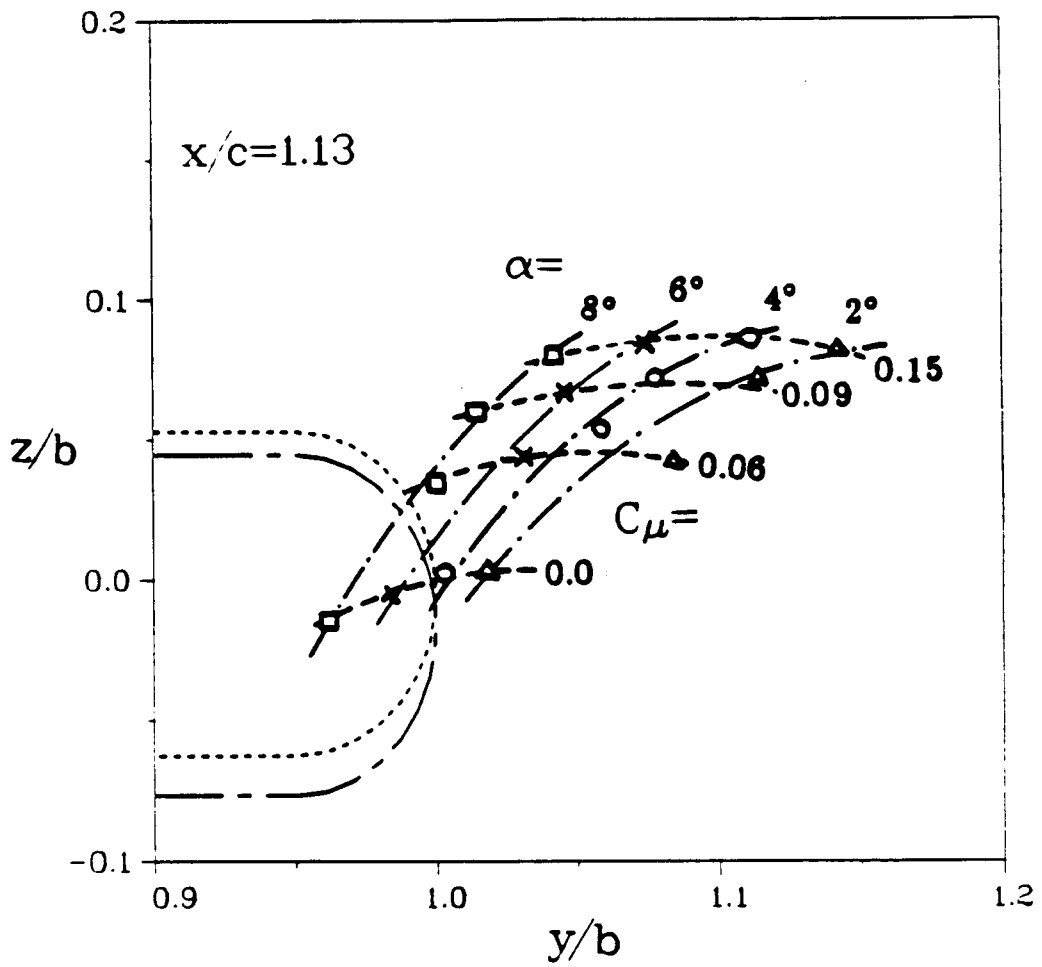

Fig. 14 Vortex migration, straight blowing.

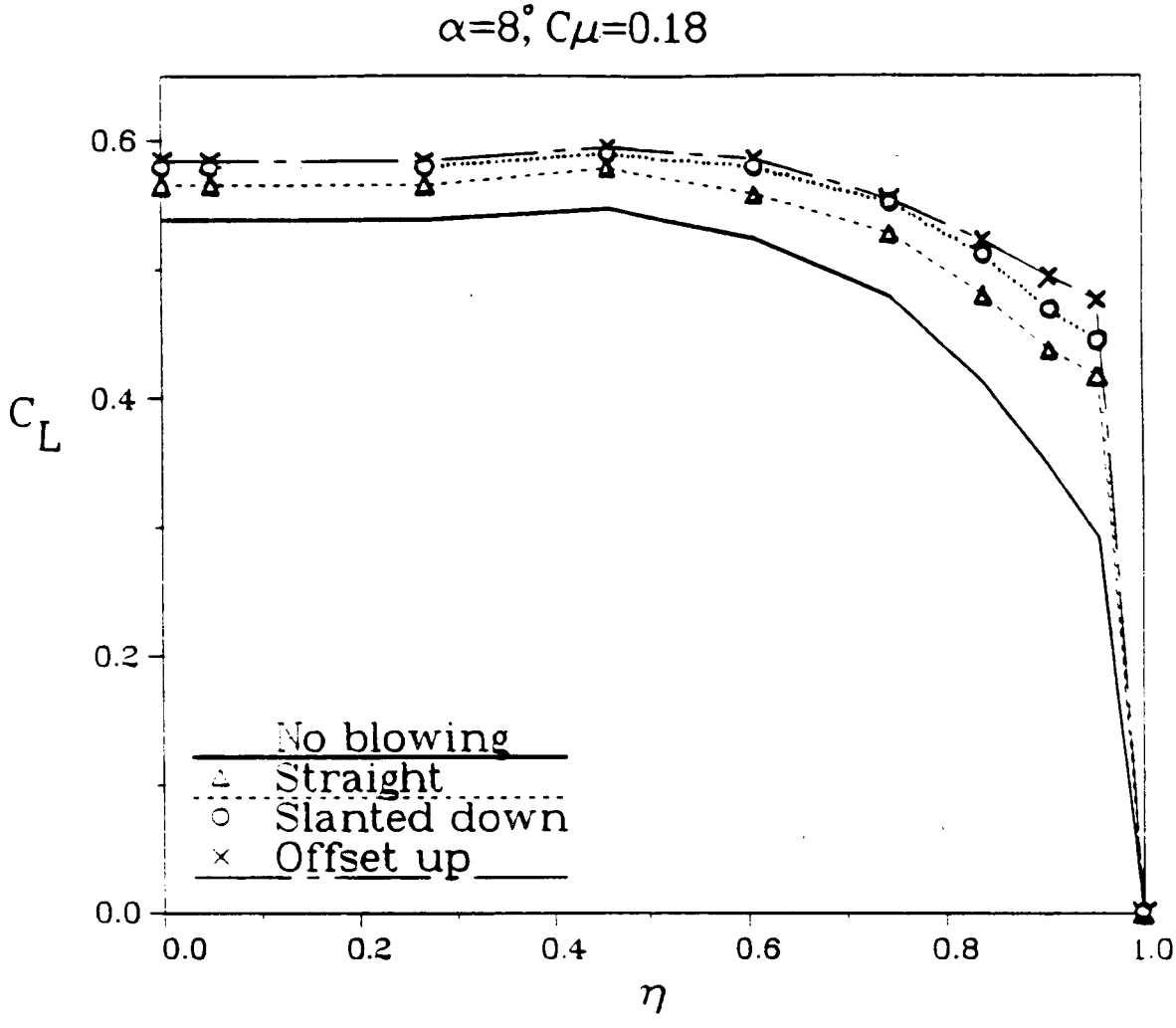

Fig. 15 Spanwise lift distribution for favorable configurations.

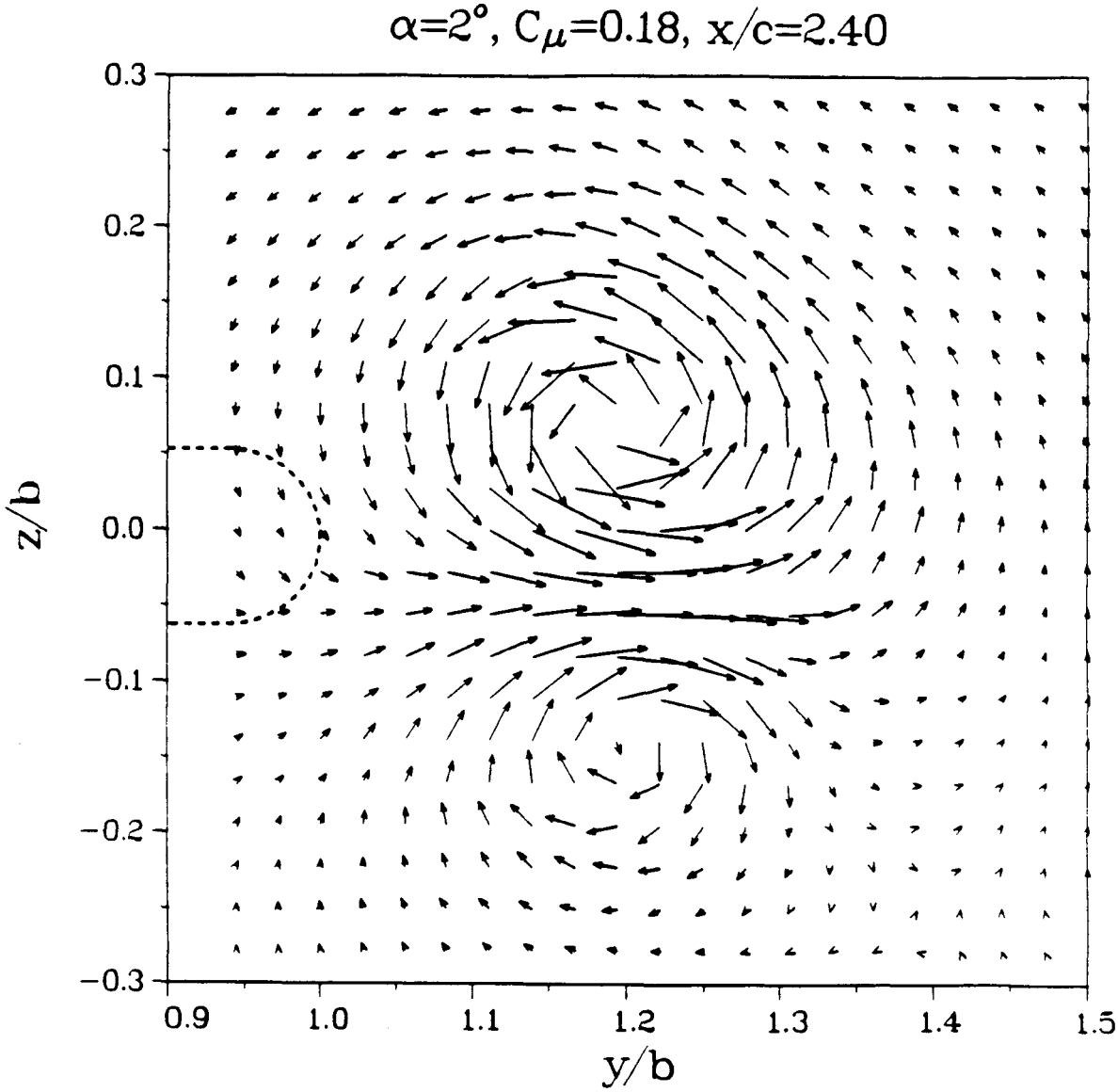

Fig. 16 Cross-flow plane velocity, slanted-down.

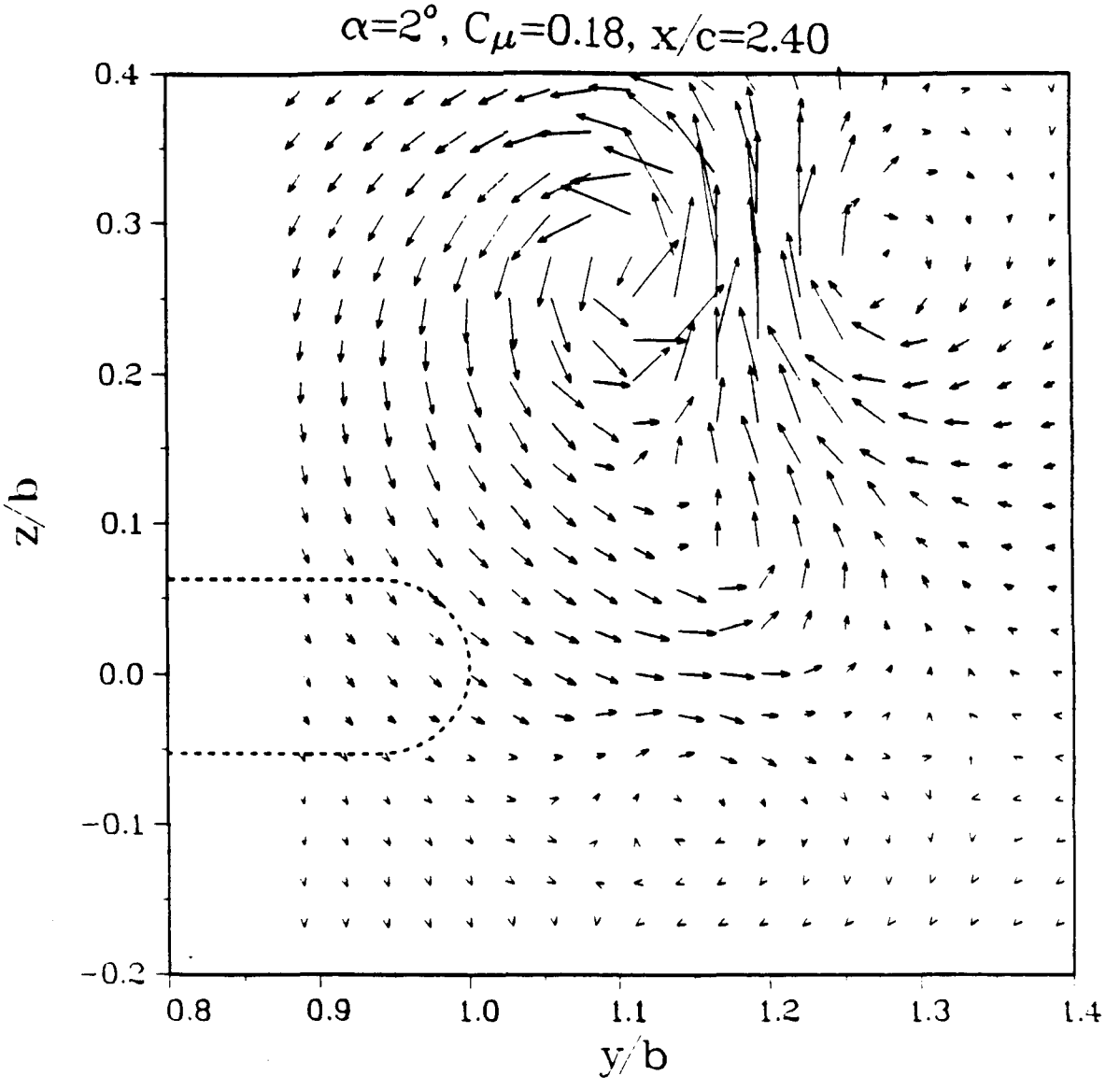

Fig. 17 Cross-flow plane velocity, slanted-up.

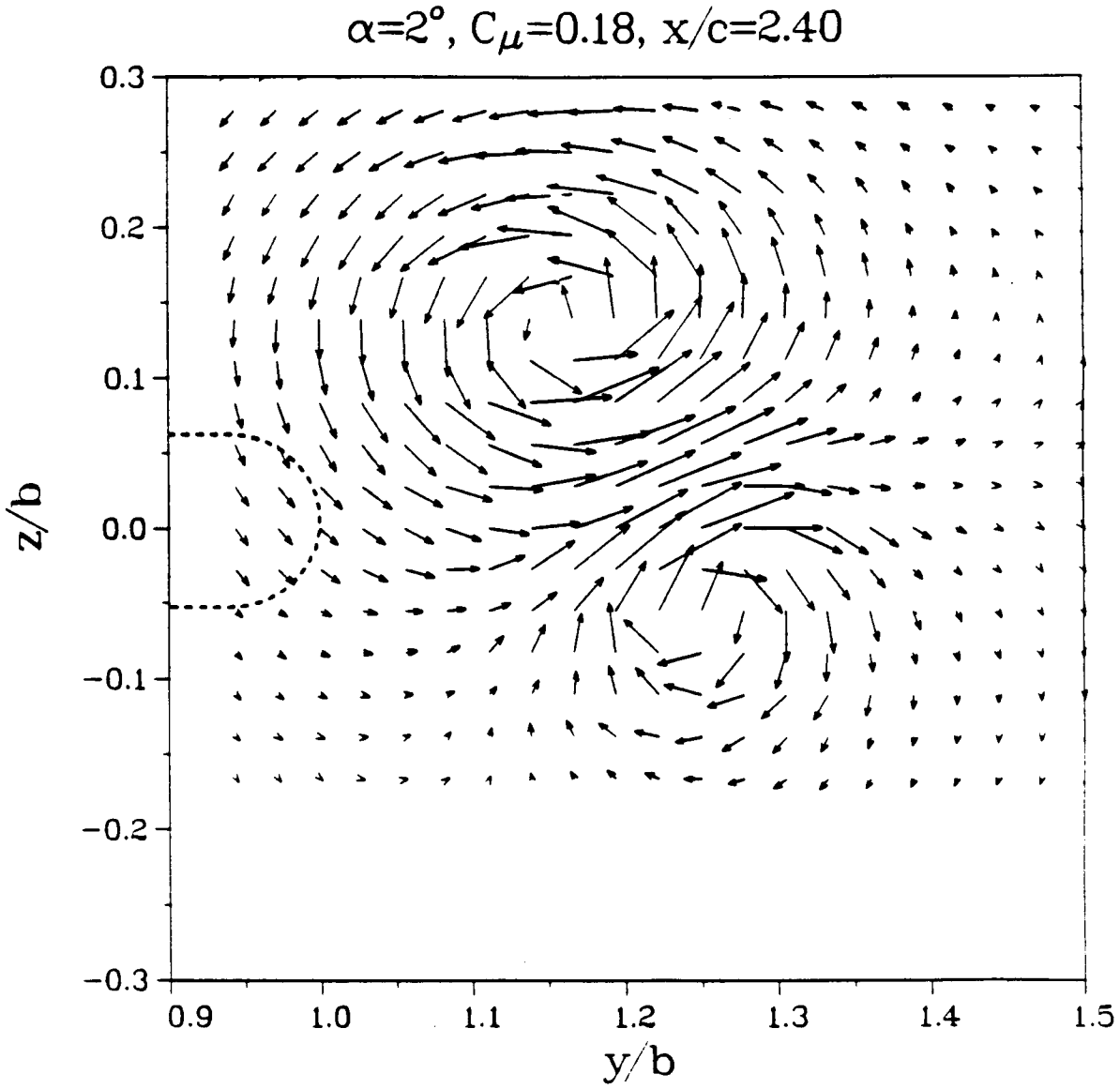

Fig. 18 Cross-flow plane velocity, offset-up.

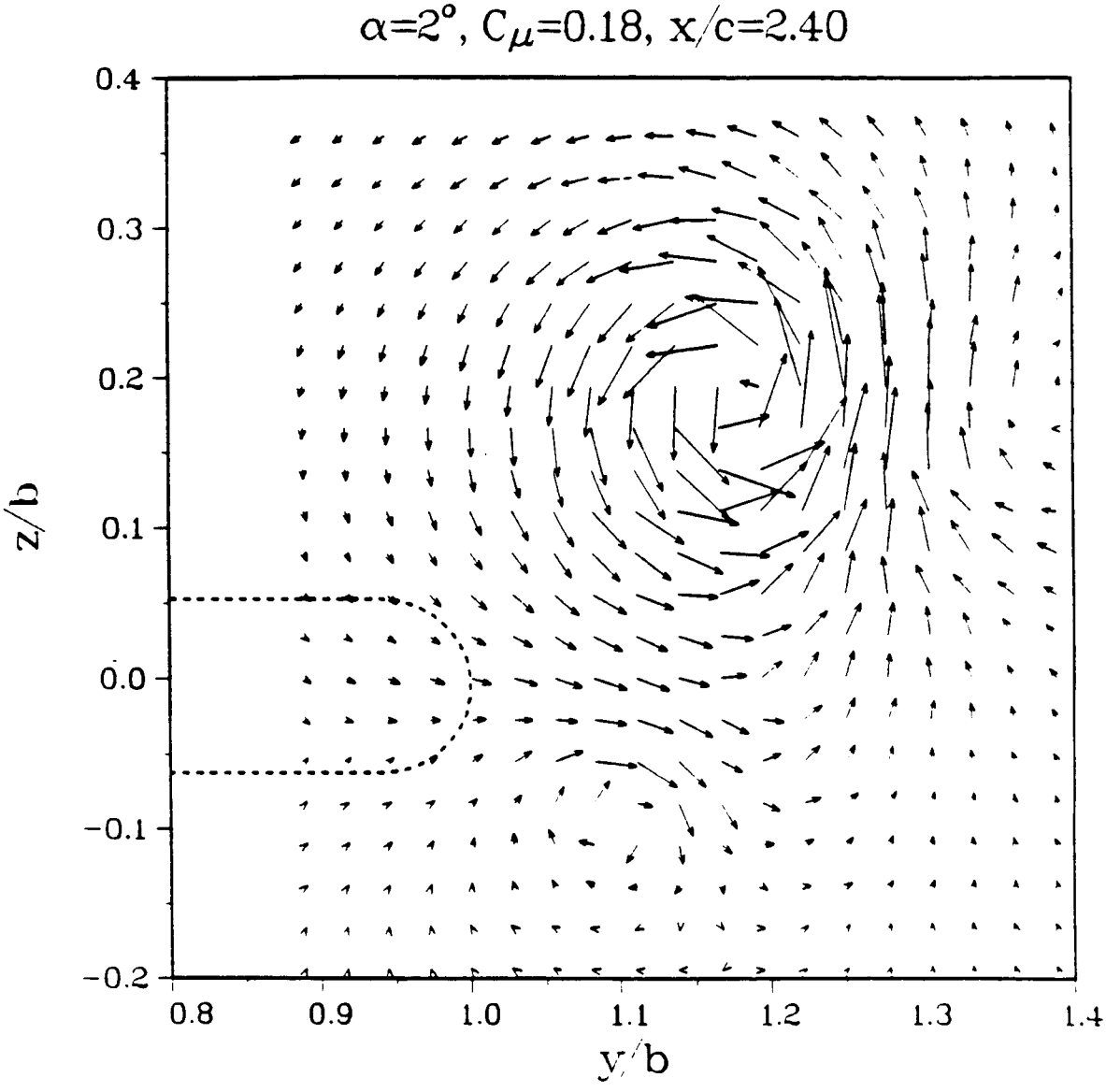

Fig. 19 Cross-flow plane velocity, offset-down.

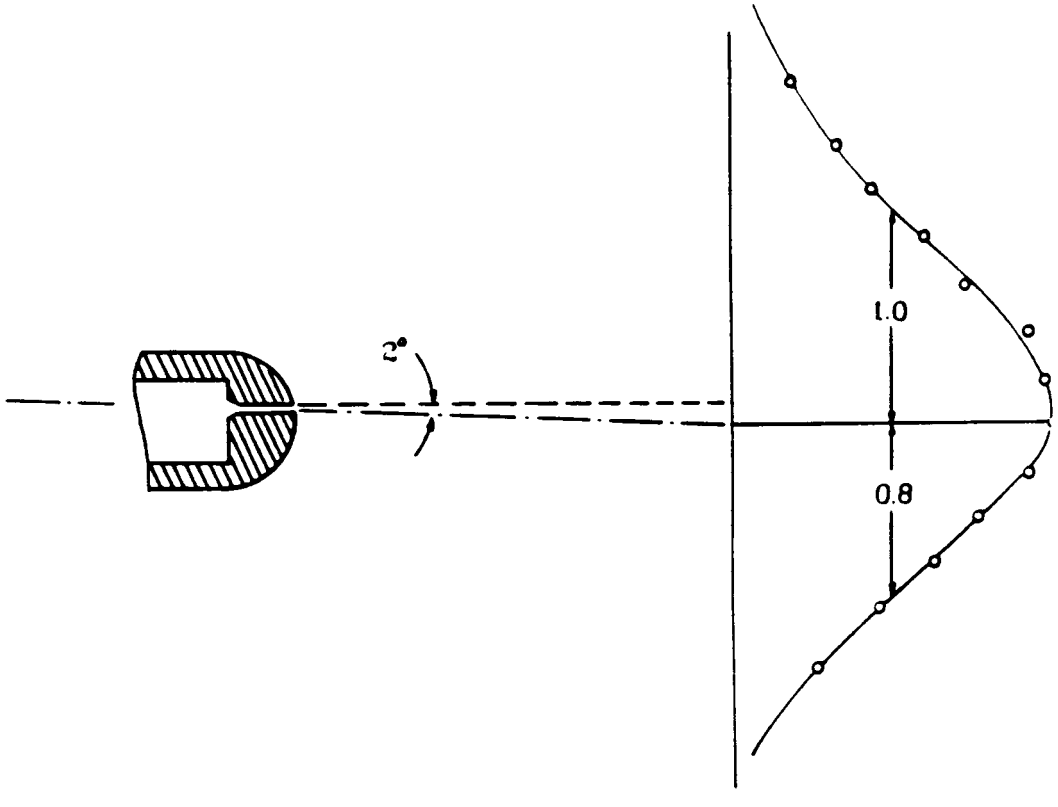

Fig. 20 Jet profile, offset slot.

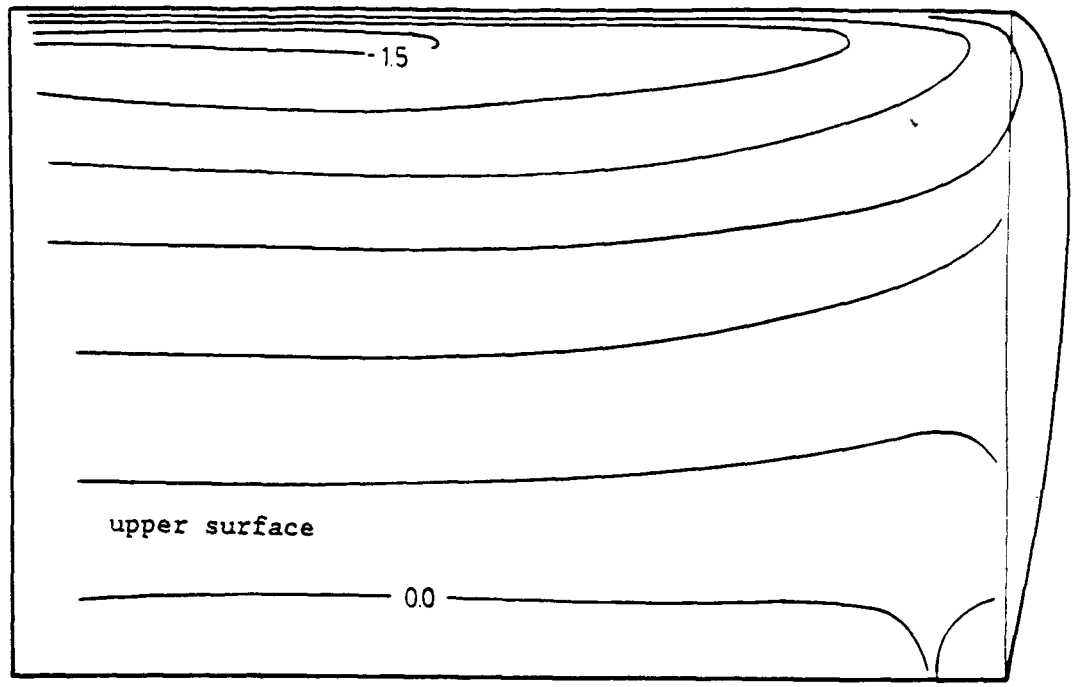

$\Delta C_p = 0.25$; $\alpha = 6°$; $C_\mu = 0.0$

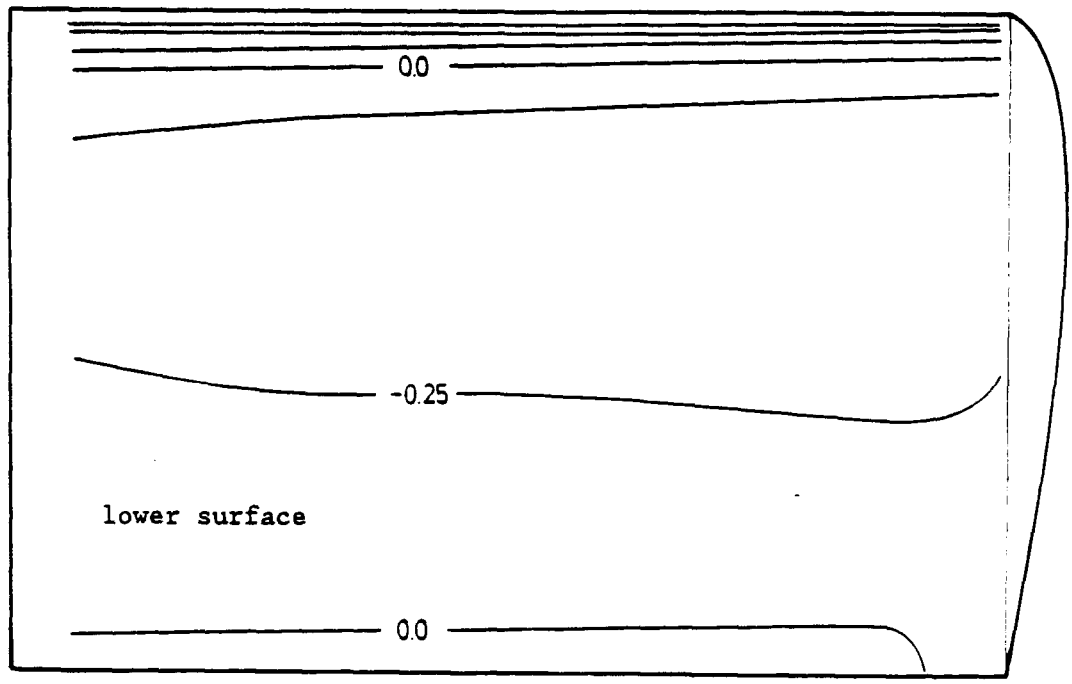

Fig. 21 Isobar contours.

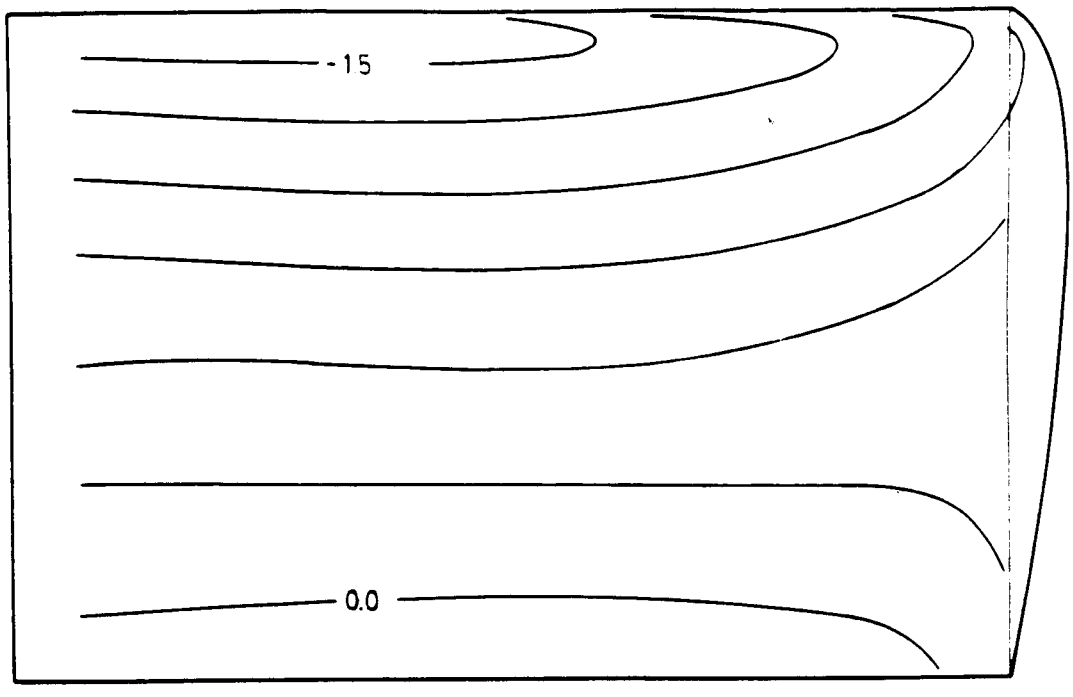

$\alpha = 6°$; $C_\mu = 0.04$

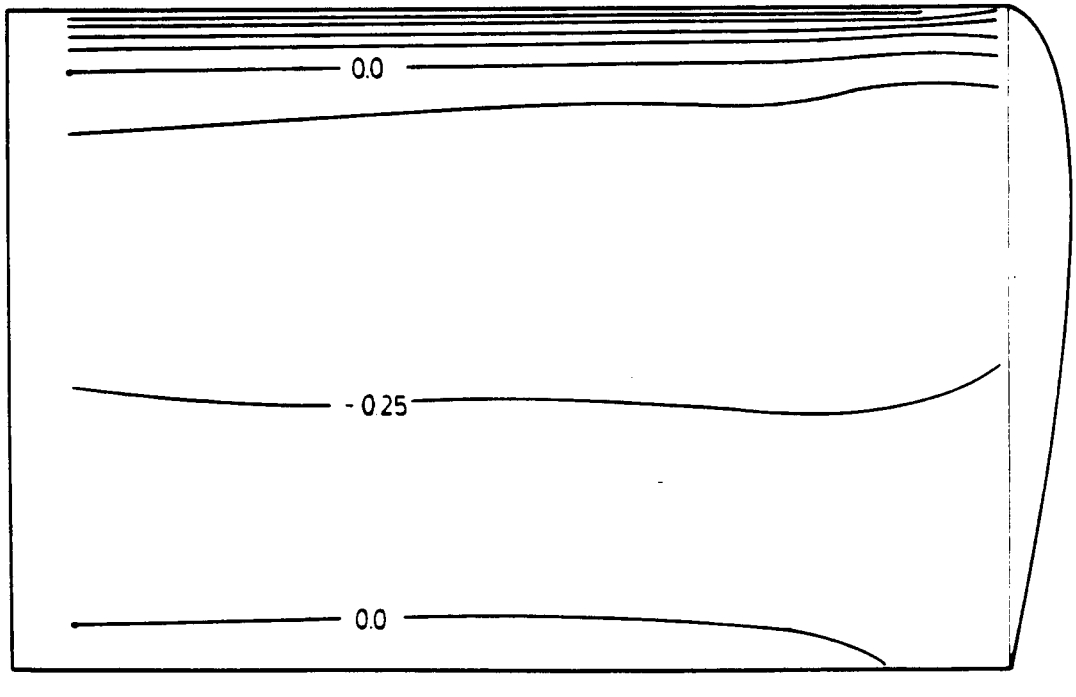

Fig. 22 Isobar contours.

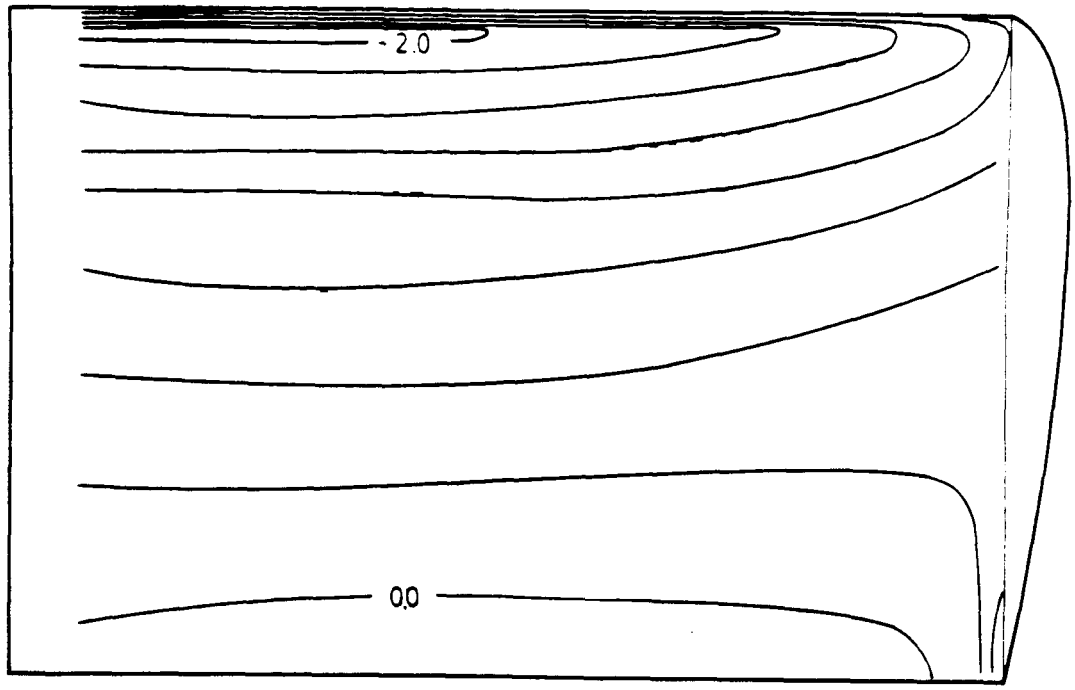

$\alpha = 8°$; $C_\mu = 0.0$

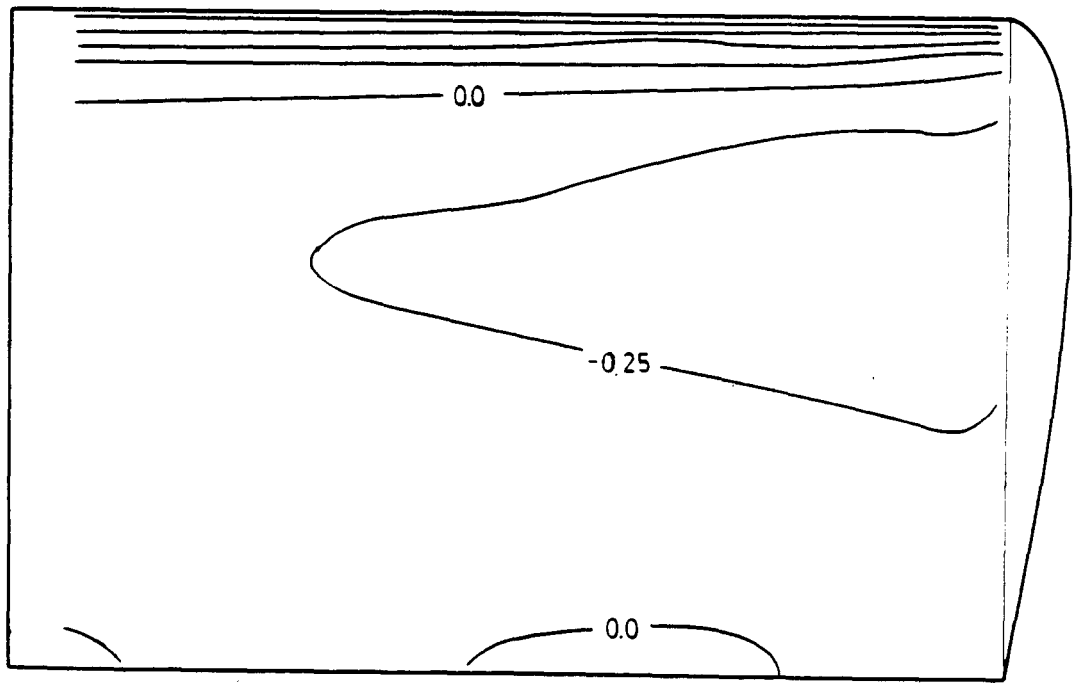

Fig. 23 Isobar contours.

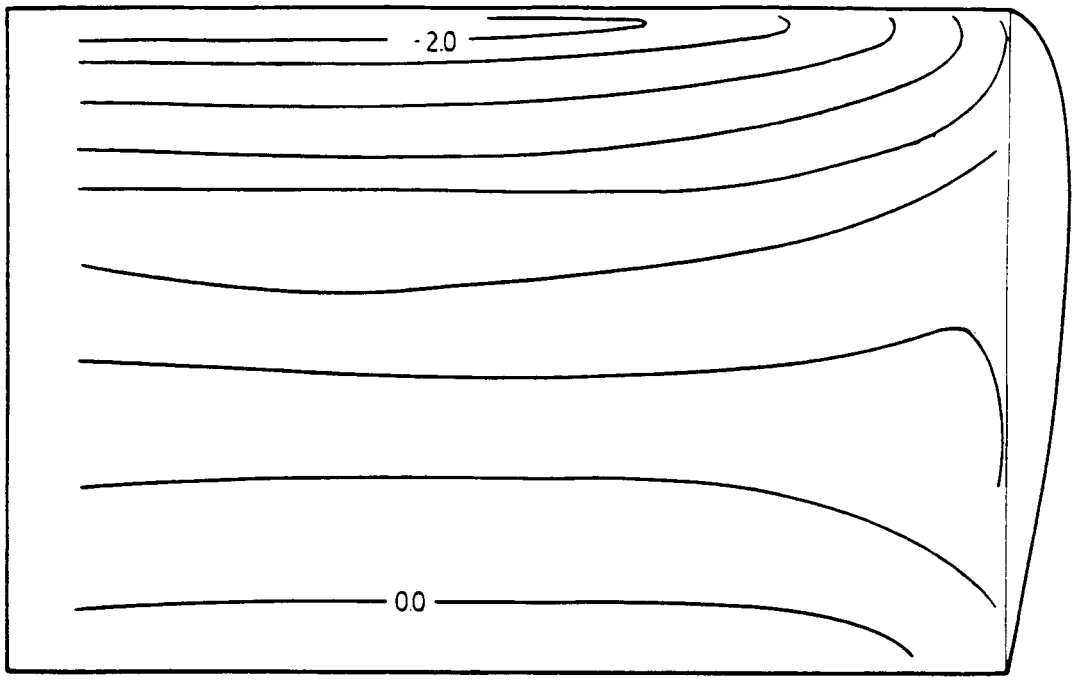

$\alpha = 8°$; $C_\mu = 0.1$

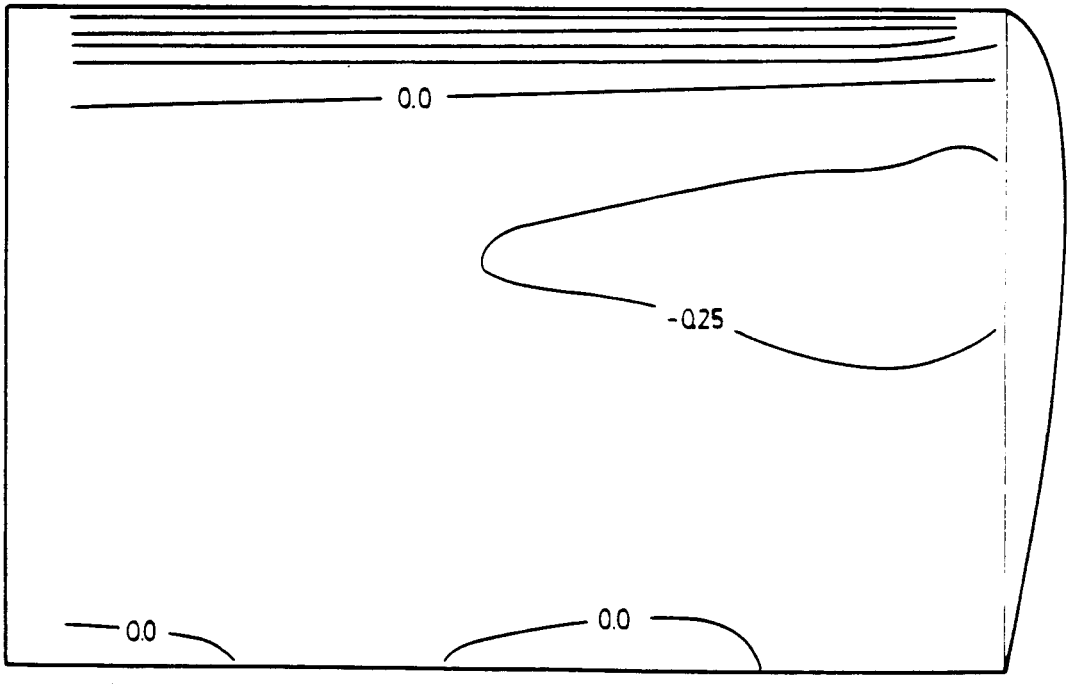

Fig. 24 Isobar contours.

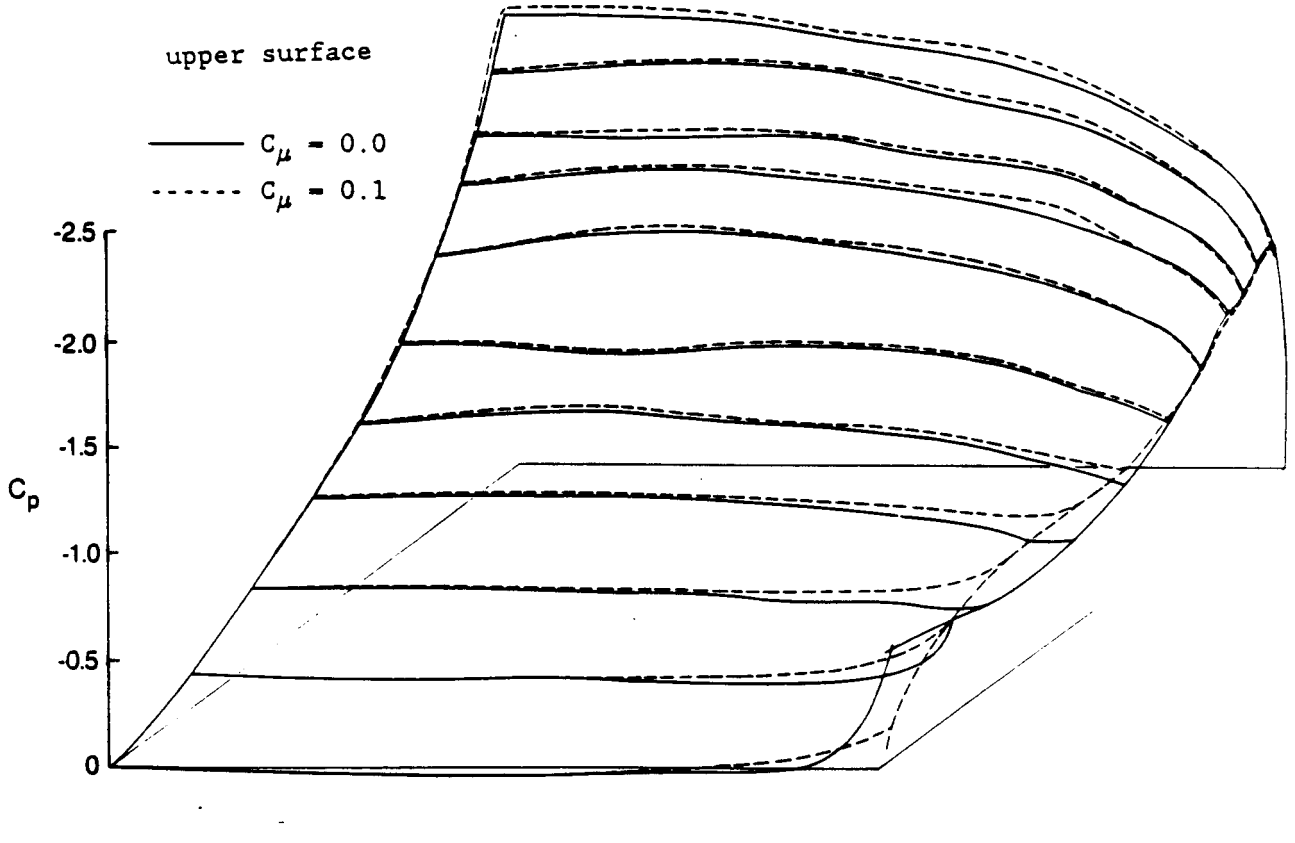

Fig. 25 (a) Upper surface load distribution.

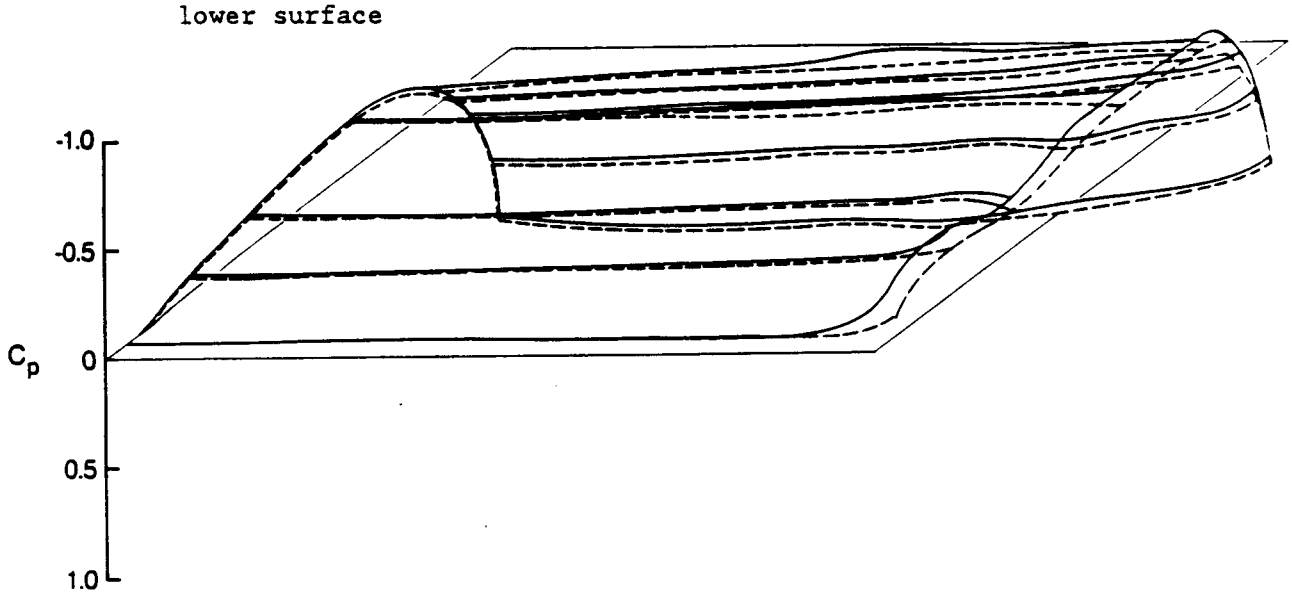

Fig. 25 (b) Lower surface load distribution.

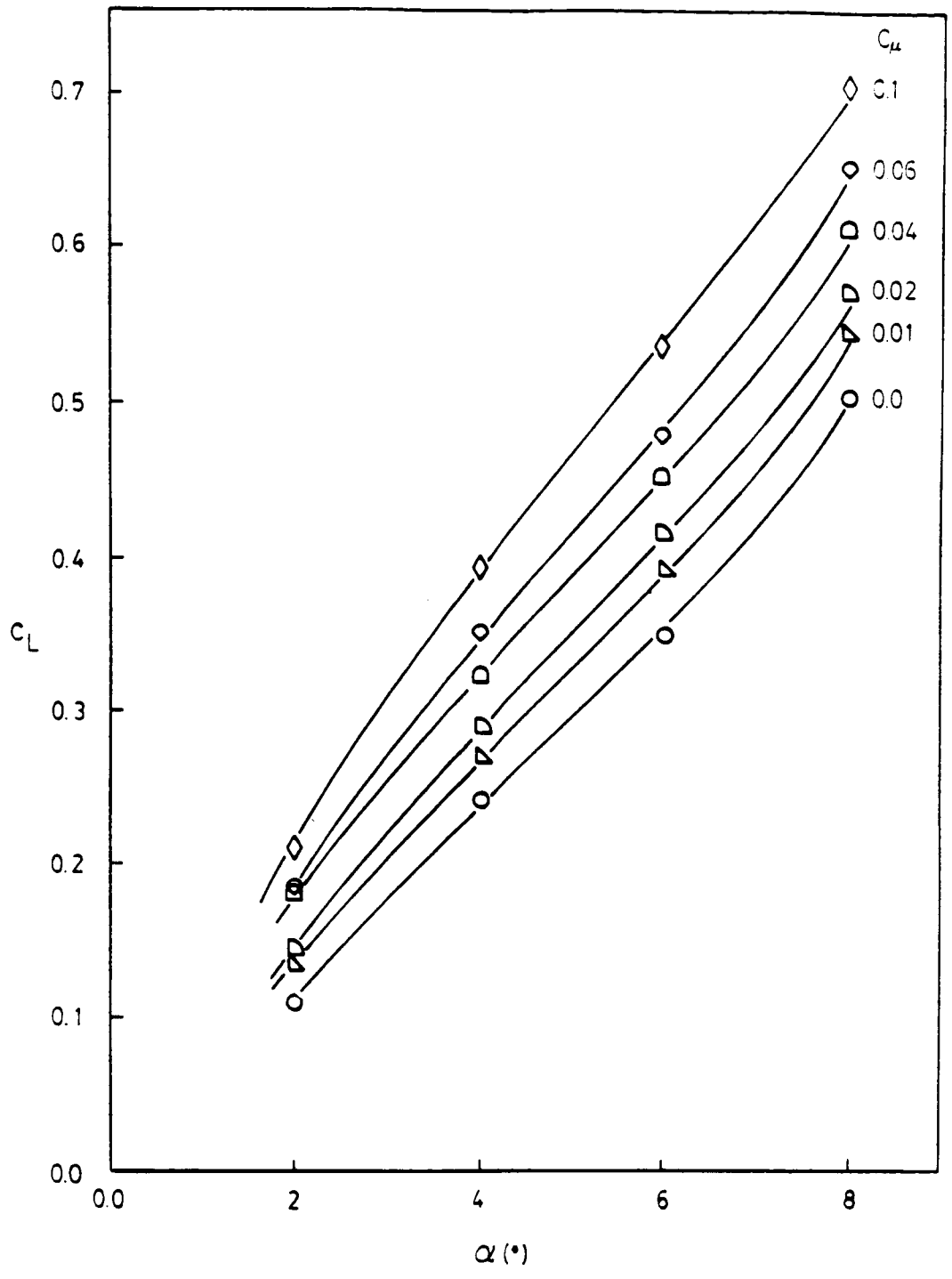

Fig. 26 Effect of angle of attack on lift coefficient.

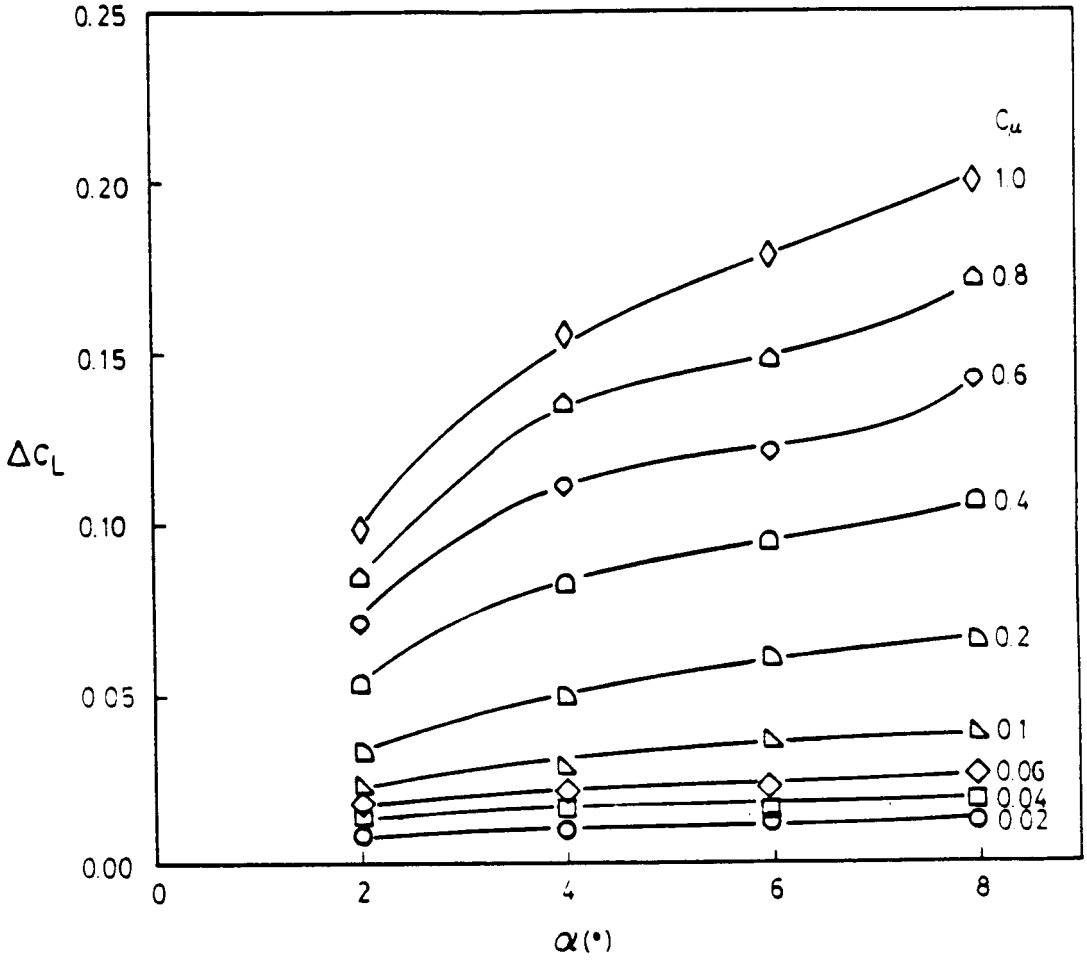

Fig. 27 Lift coefficient increment as function of angle of attack.

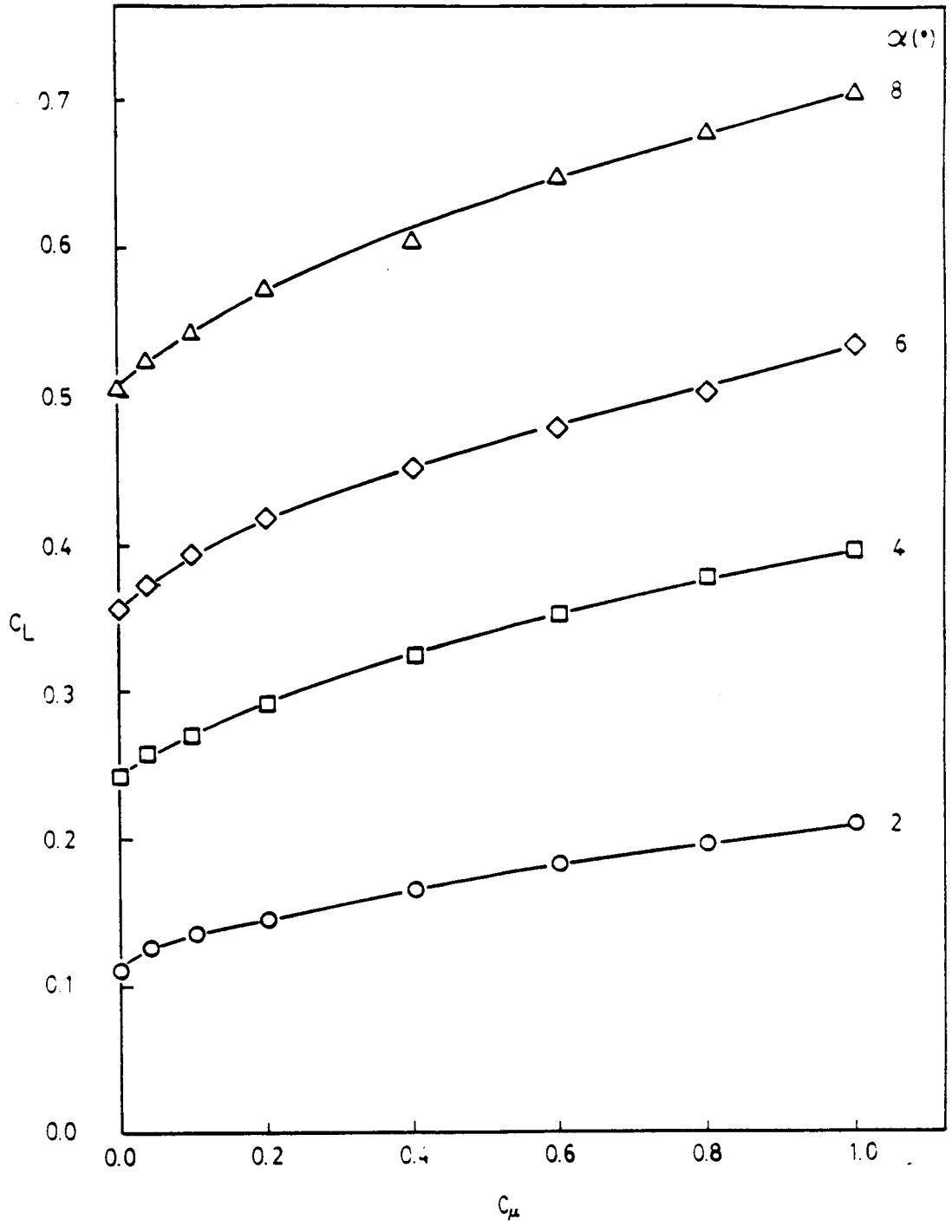

Fig. 28 Effect of blowing on lift coefficient.

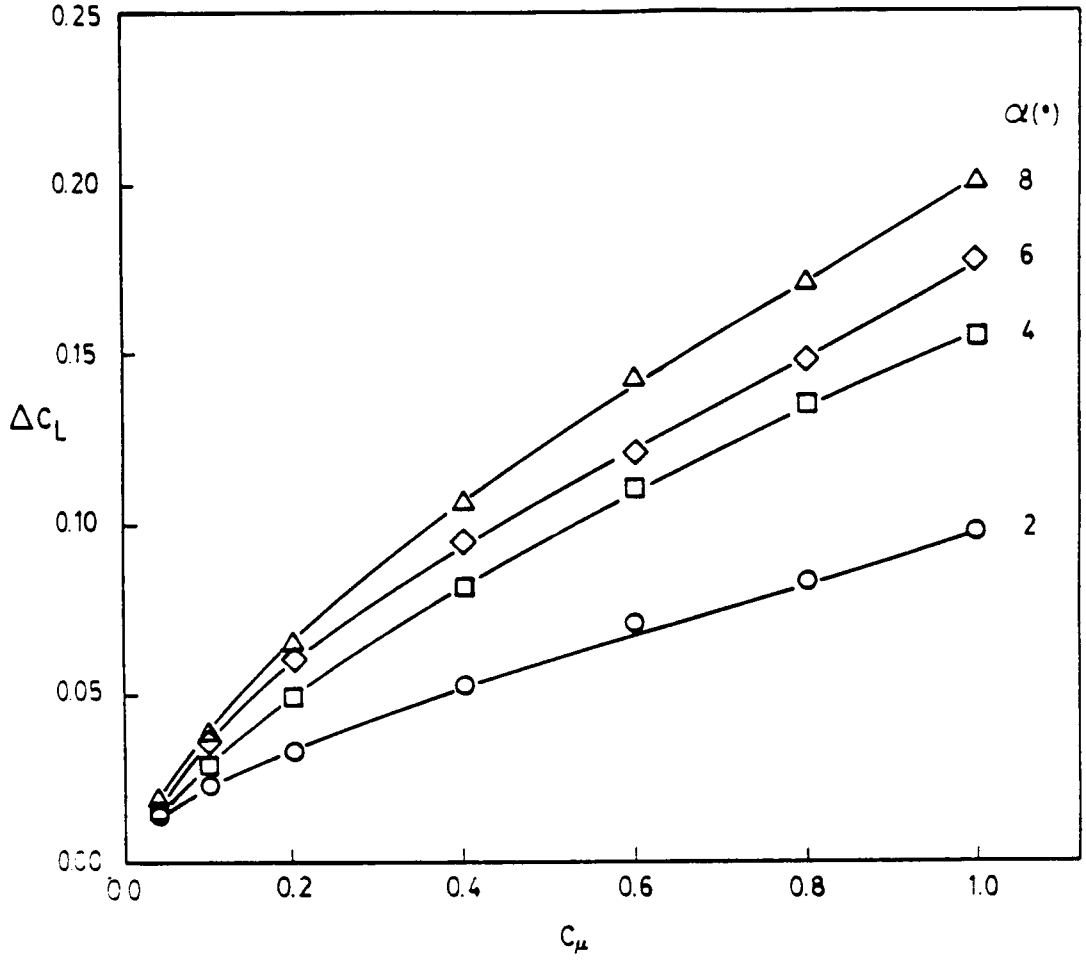

Fig. 29 Lift coefficient increment as a function of blowing intensity.

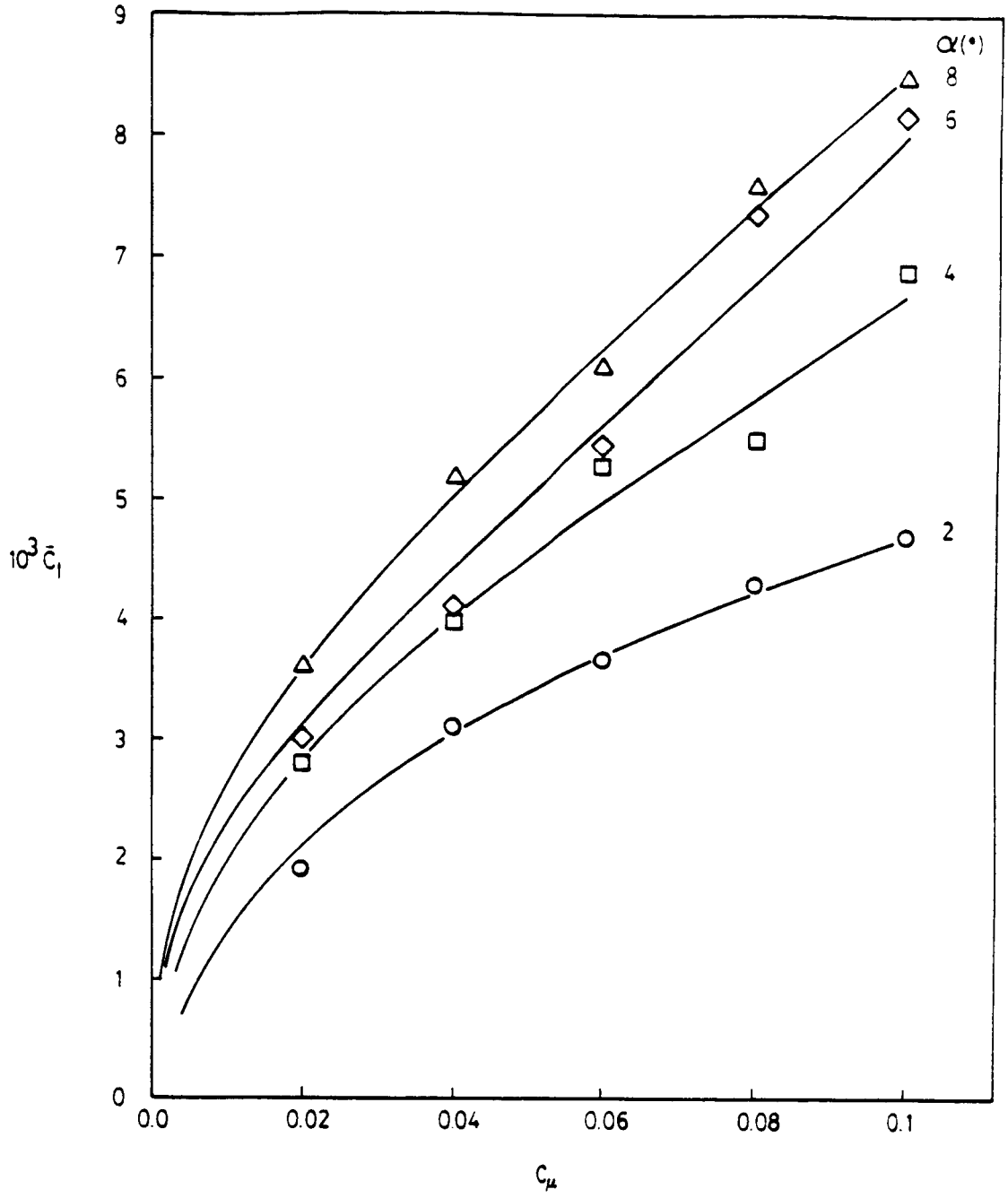

Fig. 30 Measure of the rolling moment coefficient.

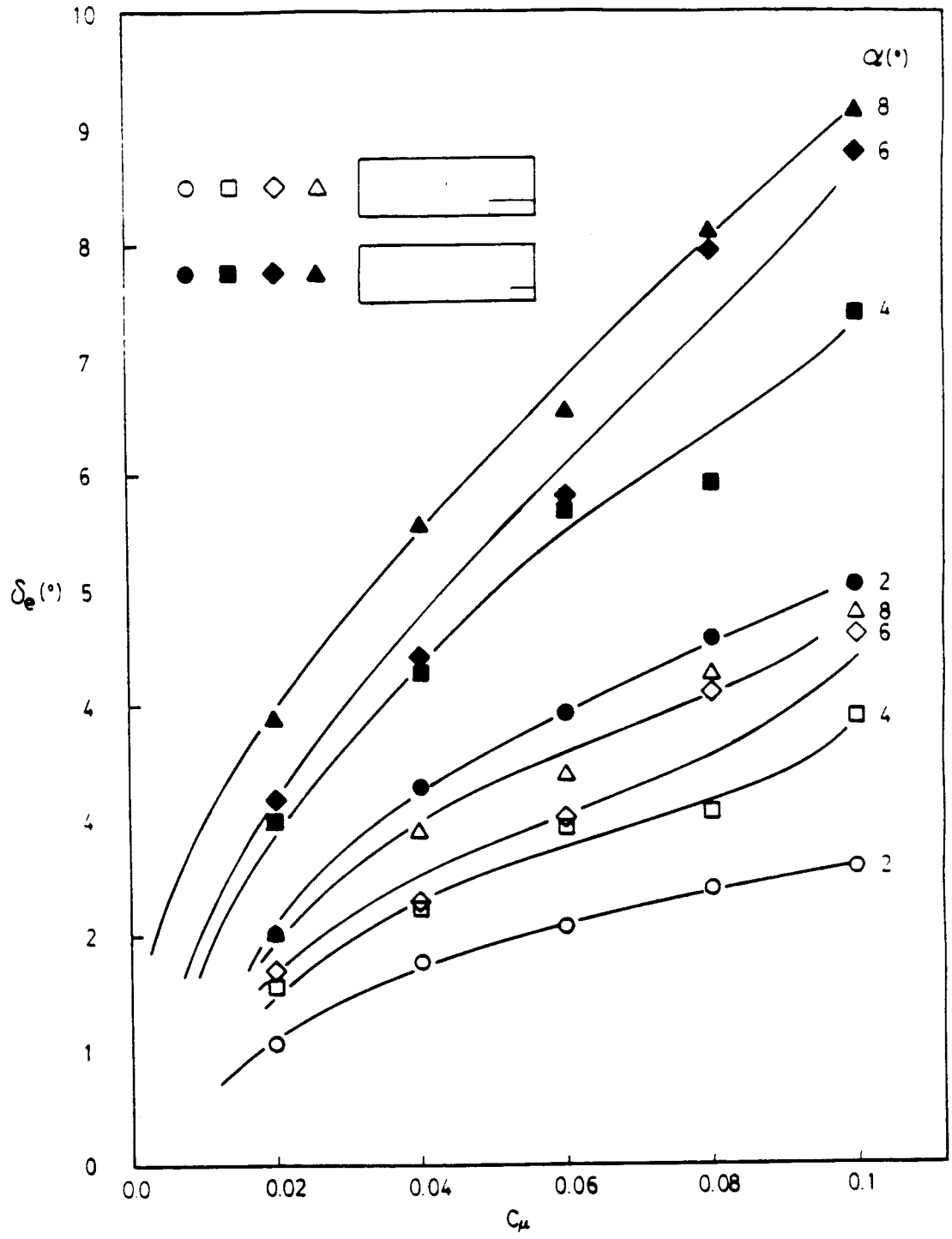

Fig. 31 Equivalent aileron deflection.

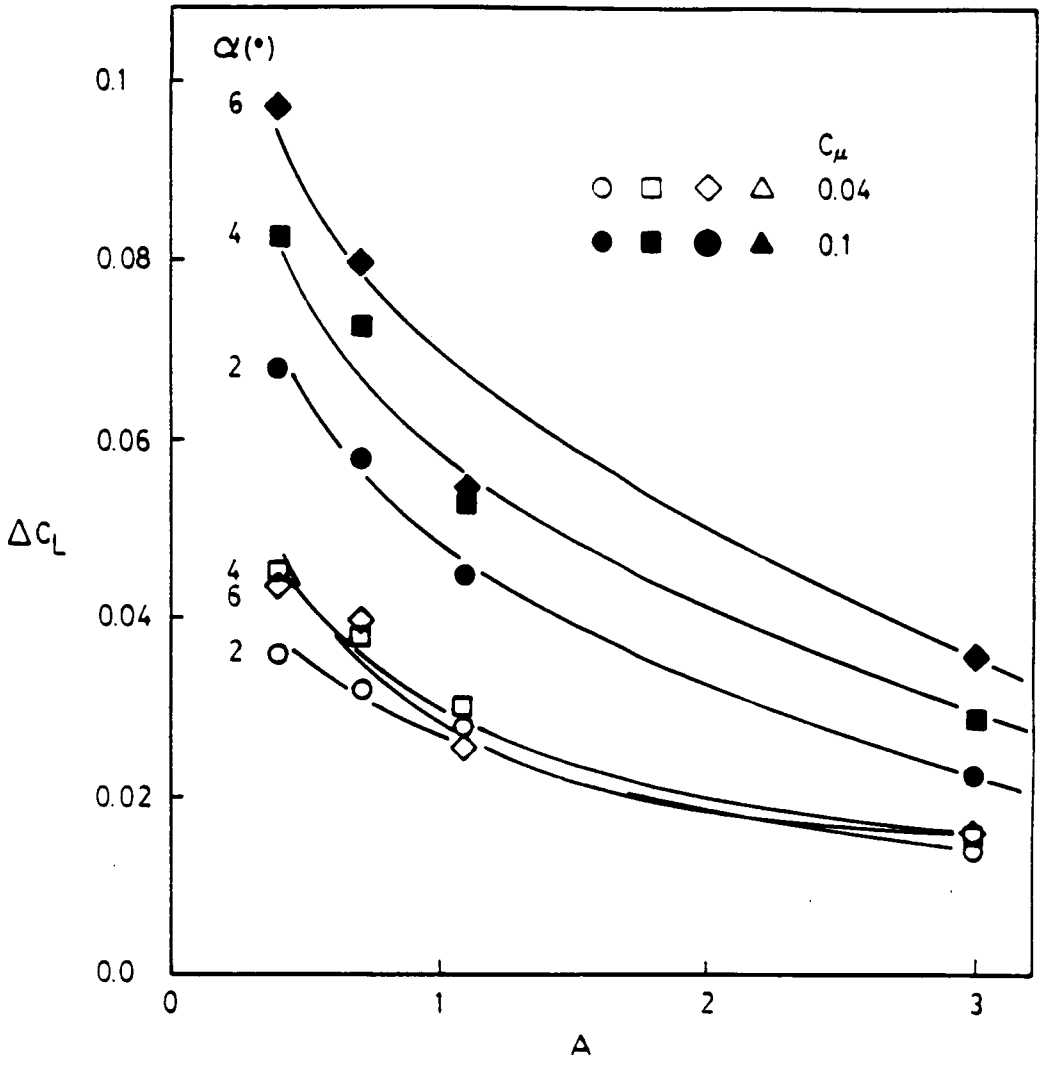

Fig. 32 Effect of wing aspect ratio on lift increment.

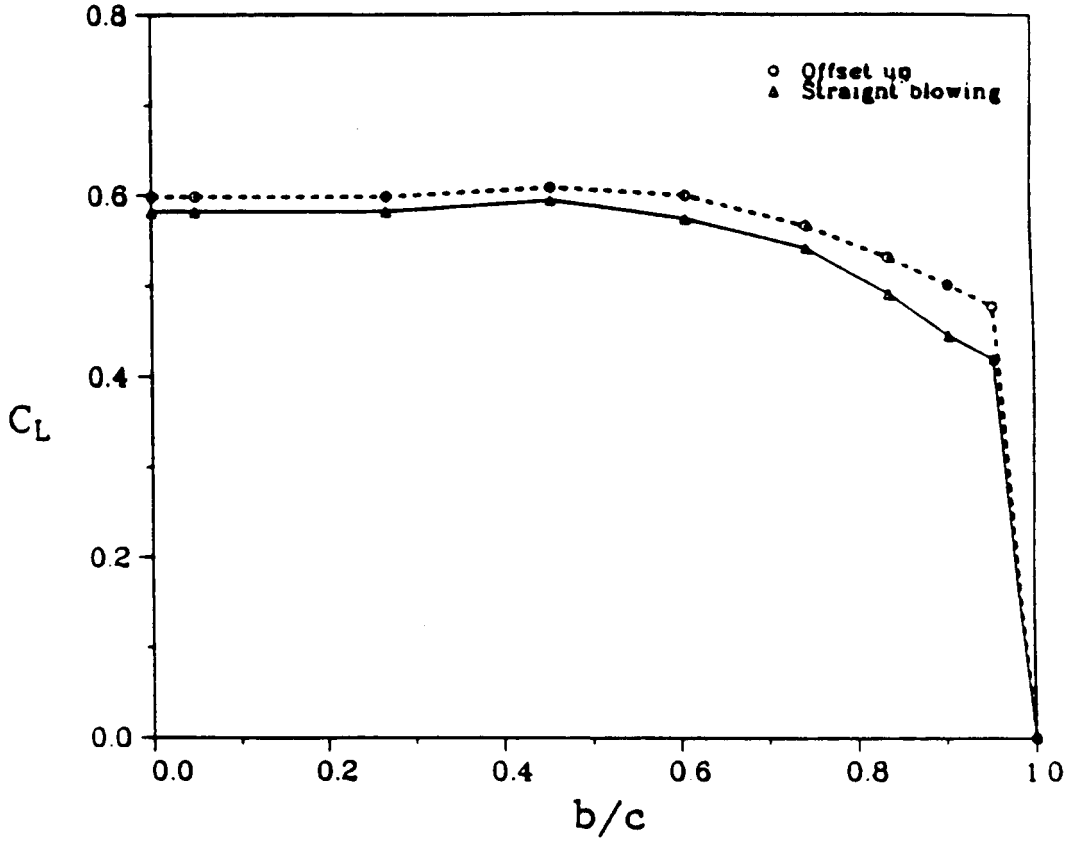

Fig. 33 Spanwise lift distribution, offset-up.

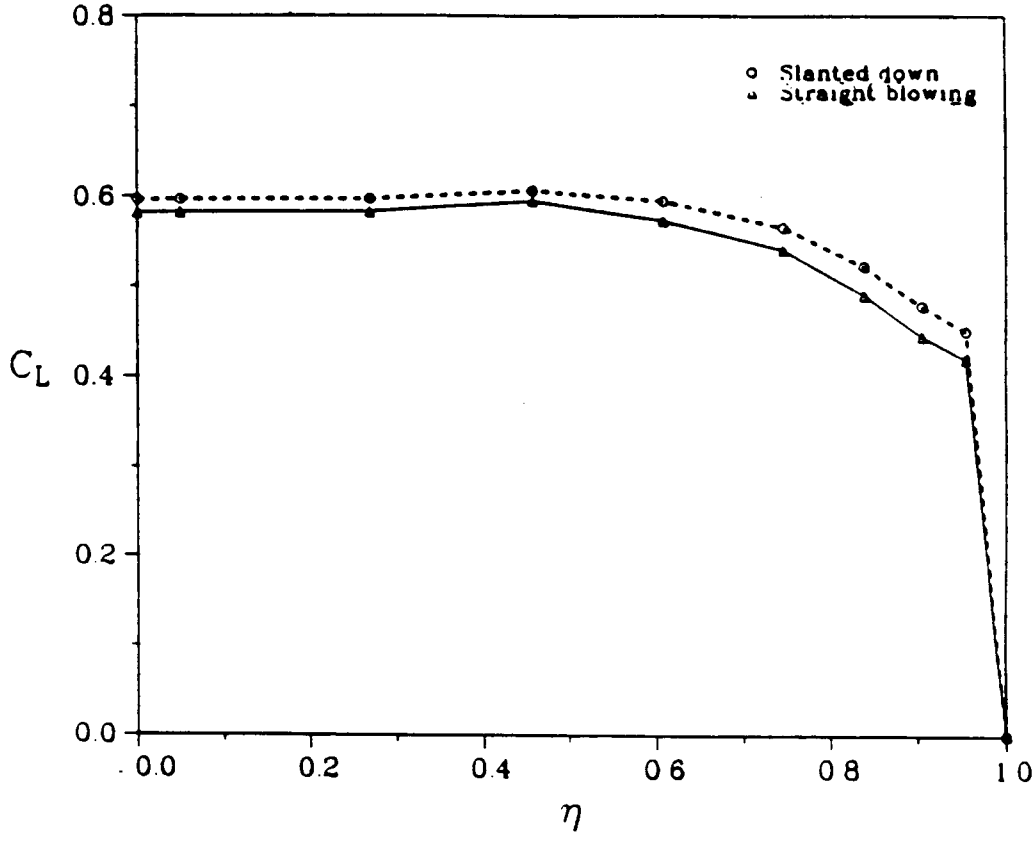

Fig. 34 Spanwise lift distribution, slanted-down.

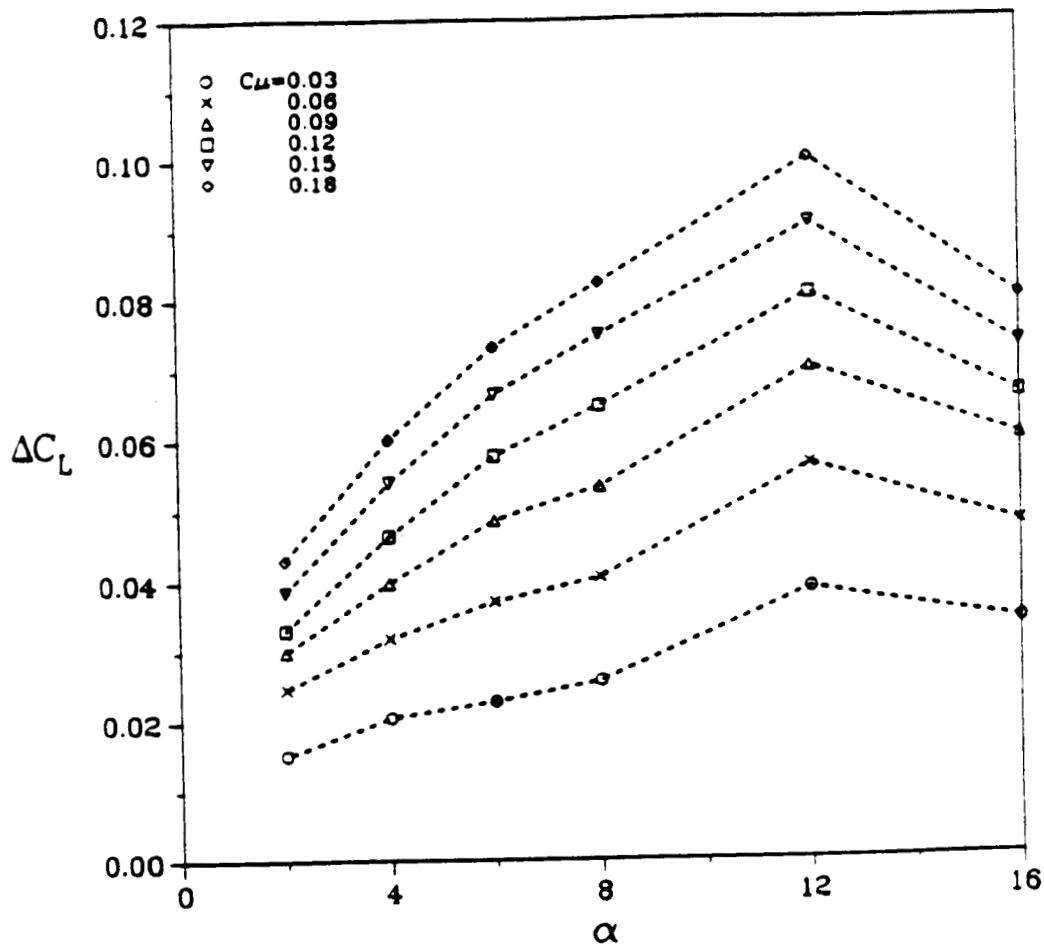

Fig. 35 Lift coefficient increment, offset-up.

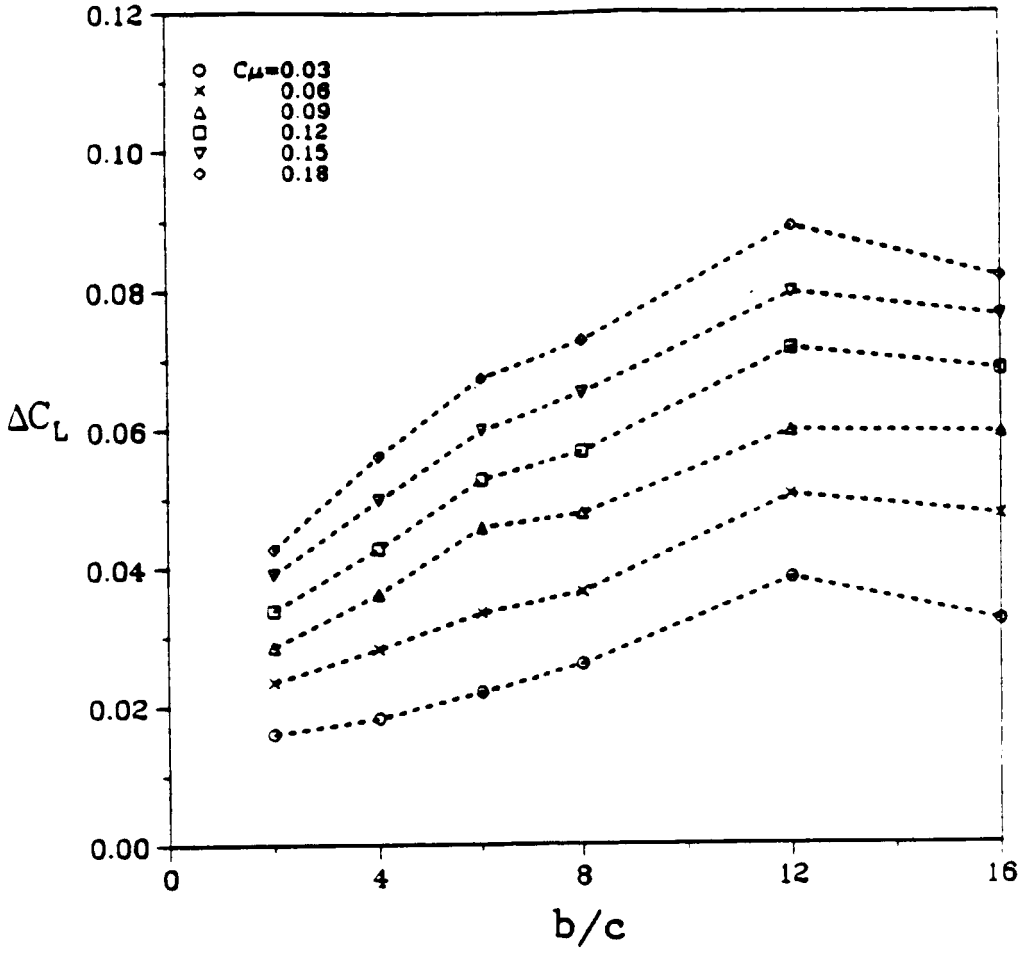

Fig. 36 Lift coefficient increment, slanted-down.

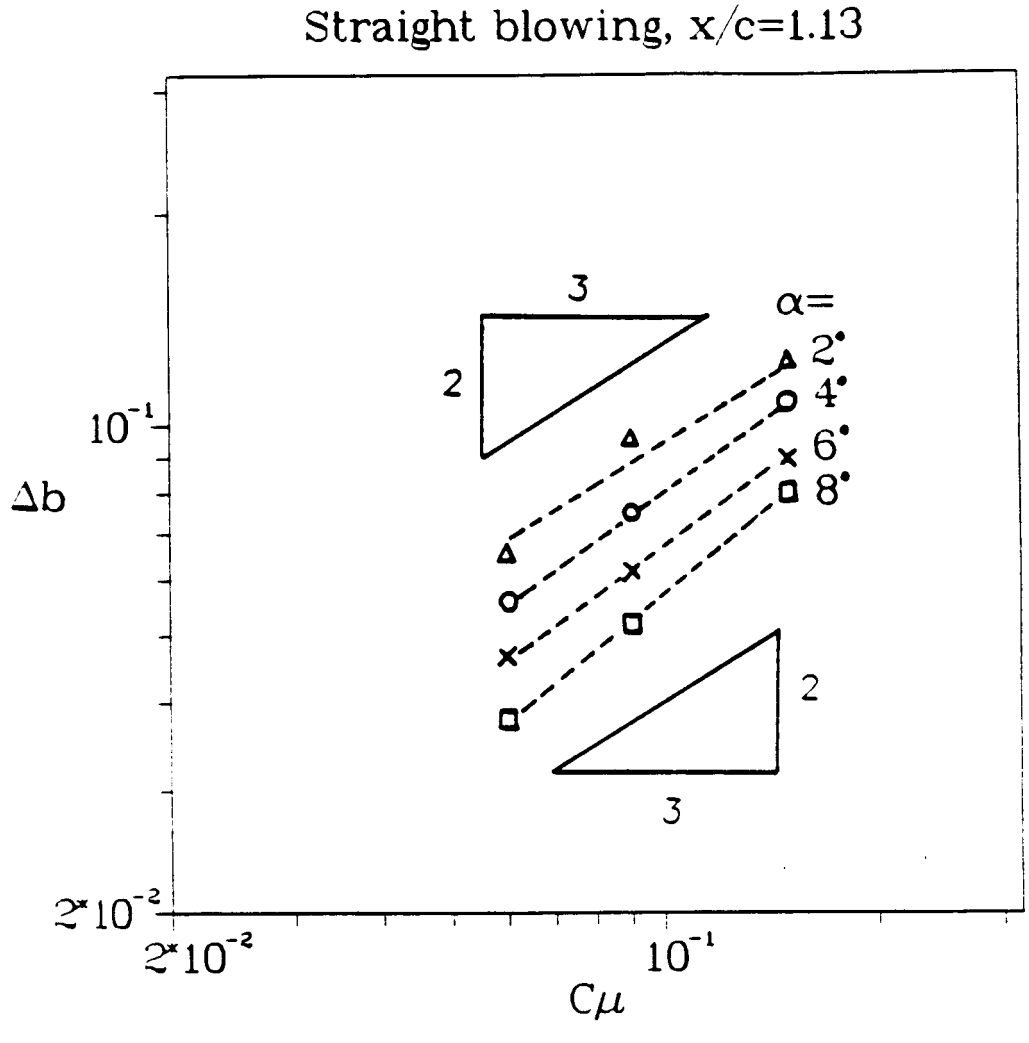

Fig. 37 Log-log plot of lateral vortex displacement.

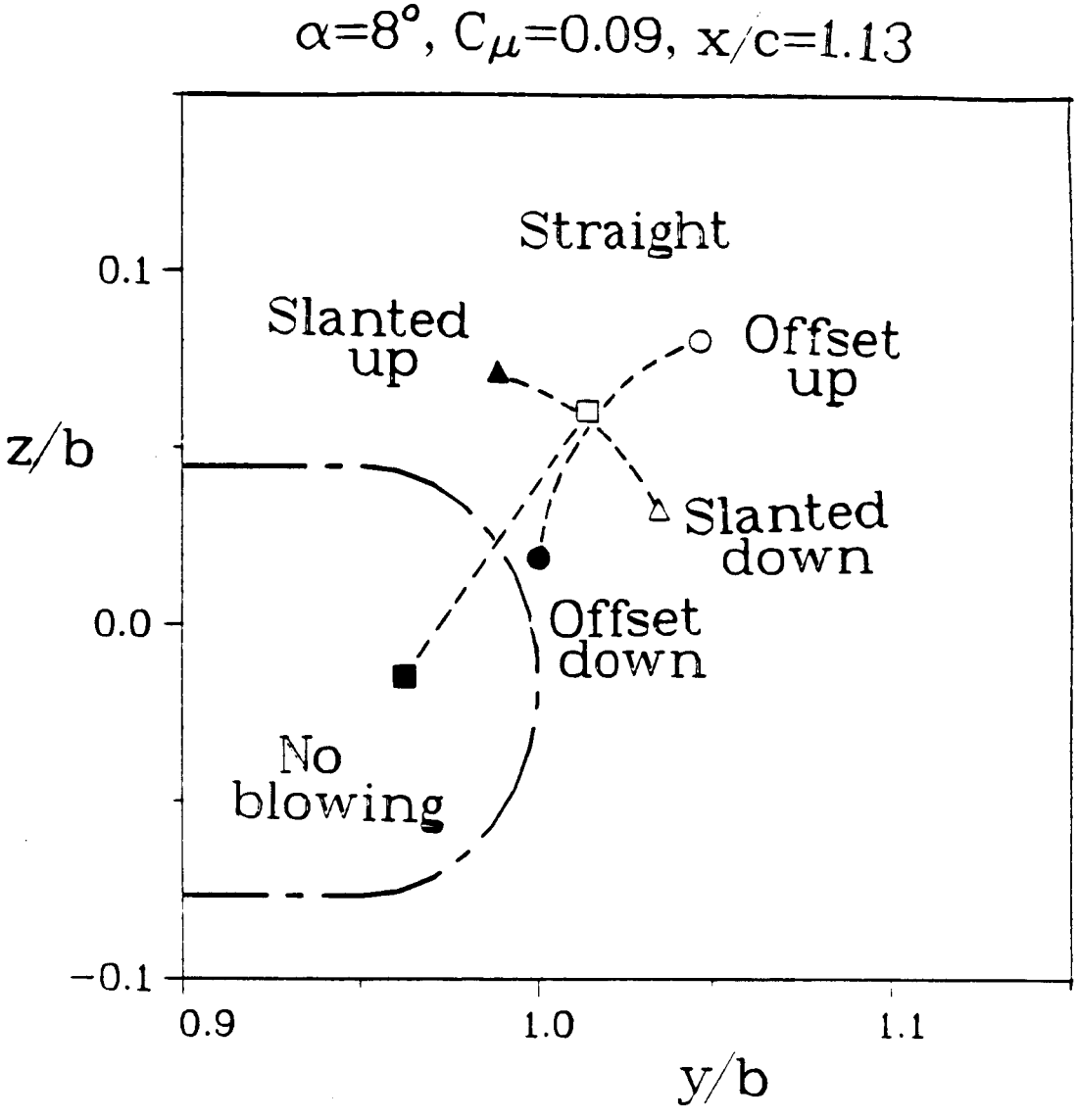

Fig. 38 Tip vortex migration for different tip configurations.

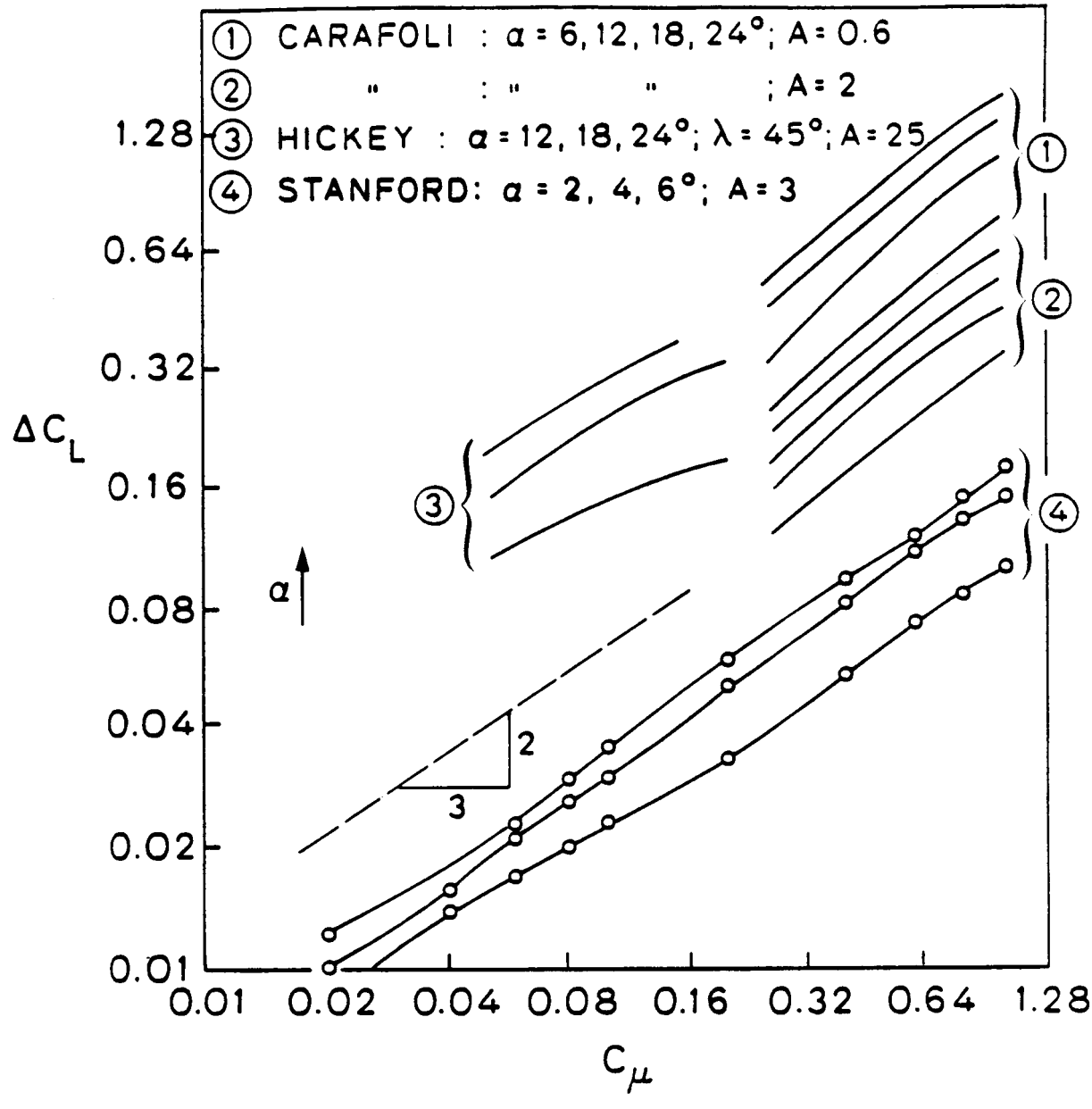

Fig. 39 Log-log plot of lift increment vs. jet intensity, straight blowing.

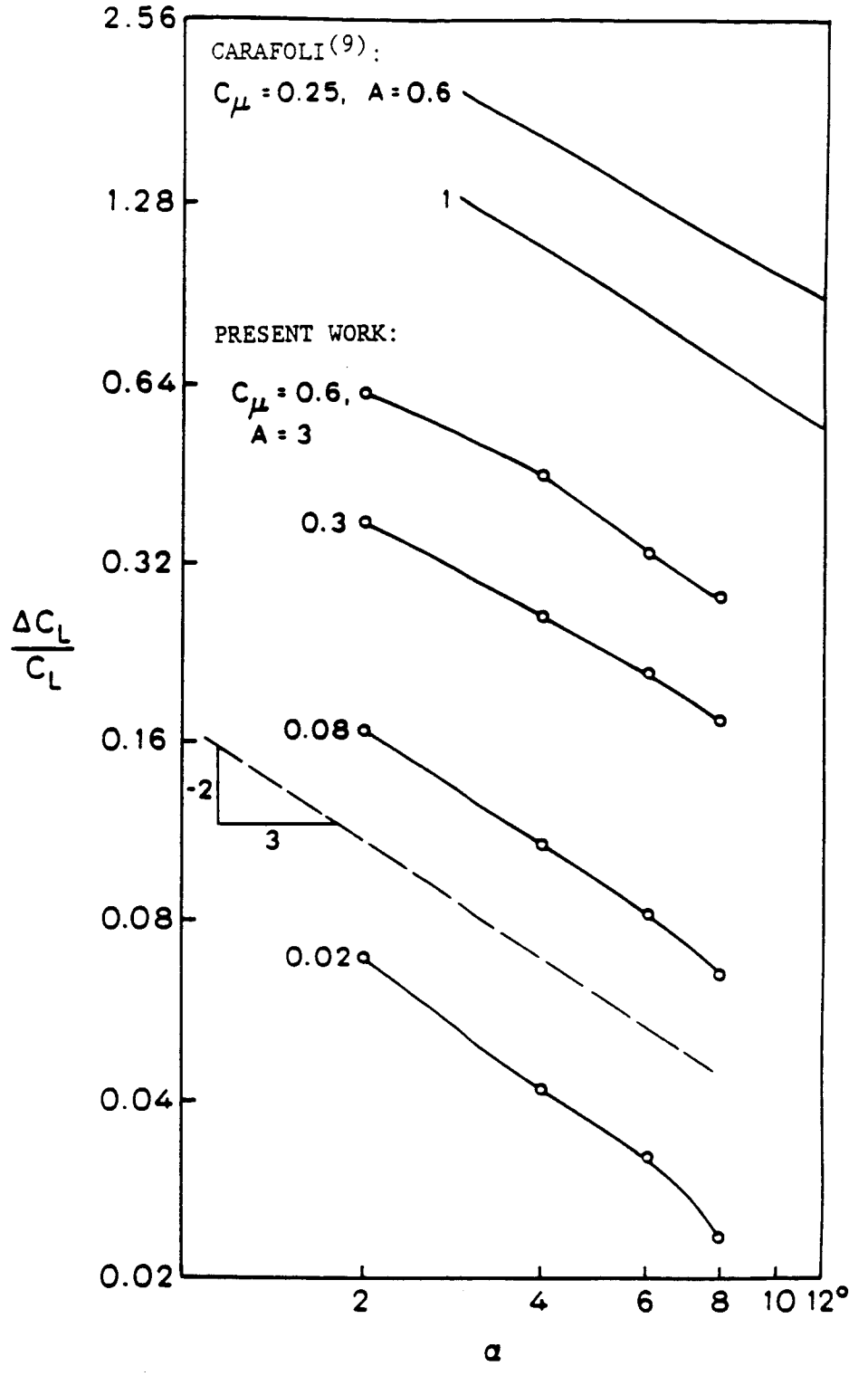

Fig. 40 Log-log plot of lift increment vs. angle of attack, straight blowing.

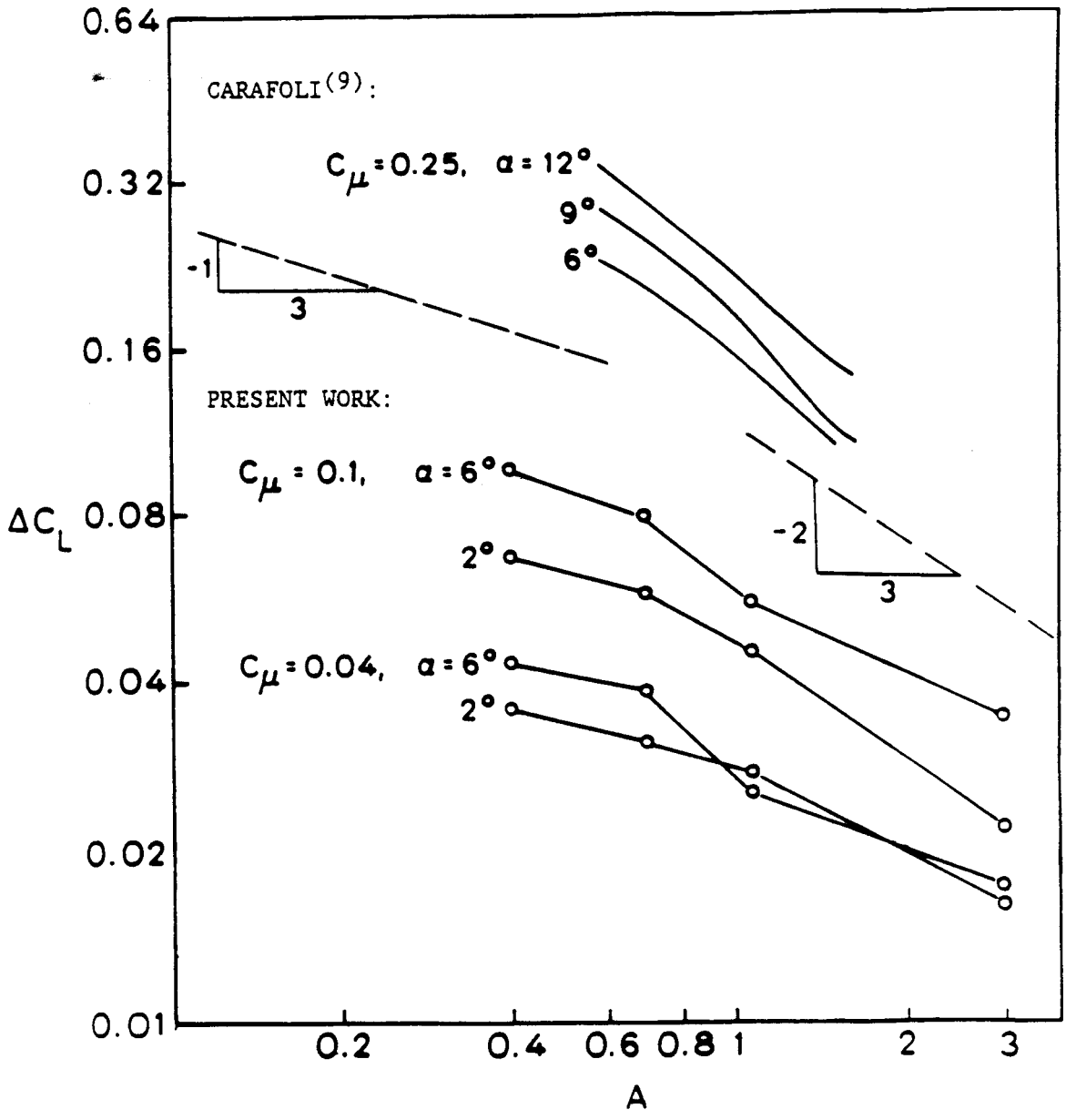

Fig. 41 Log-log plot of lift increment vs. aspect ratio, straight blowing.

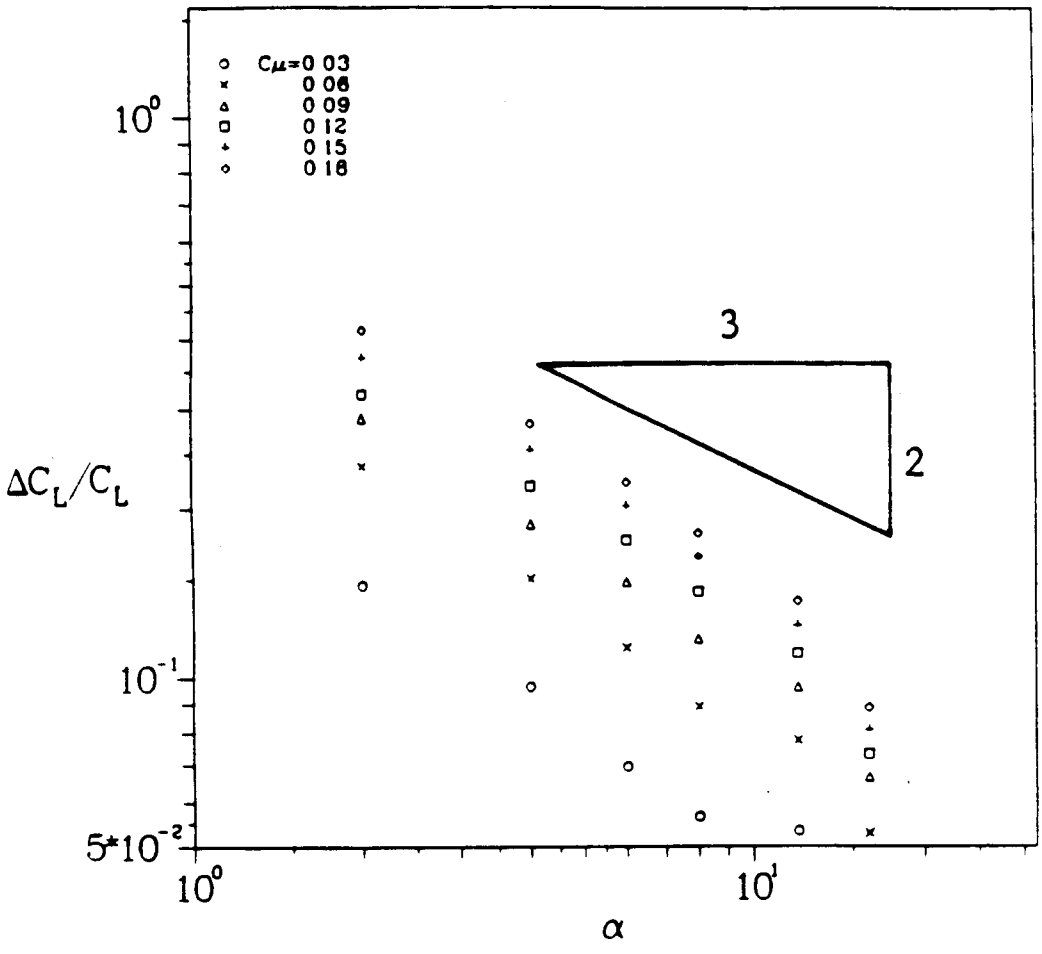

Fig. 42 Log-log plot, offset-up.

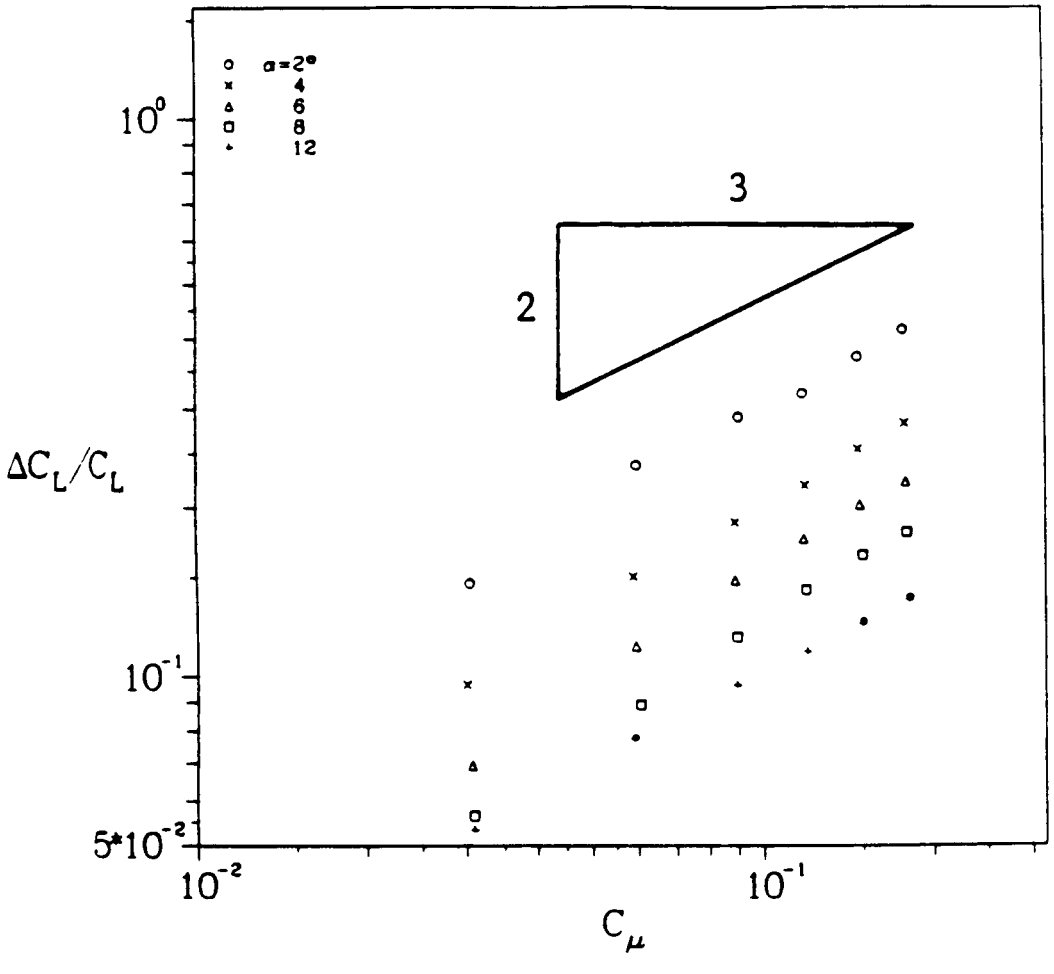

Fig. 43 Log-log plot, offset-up.

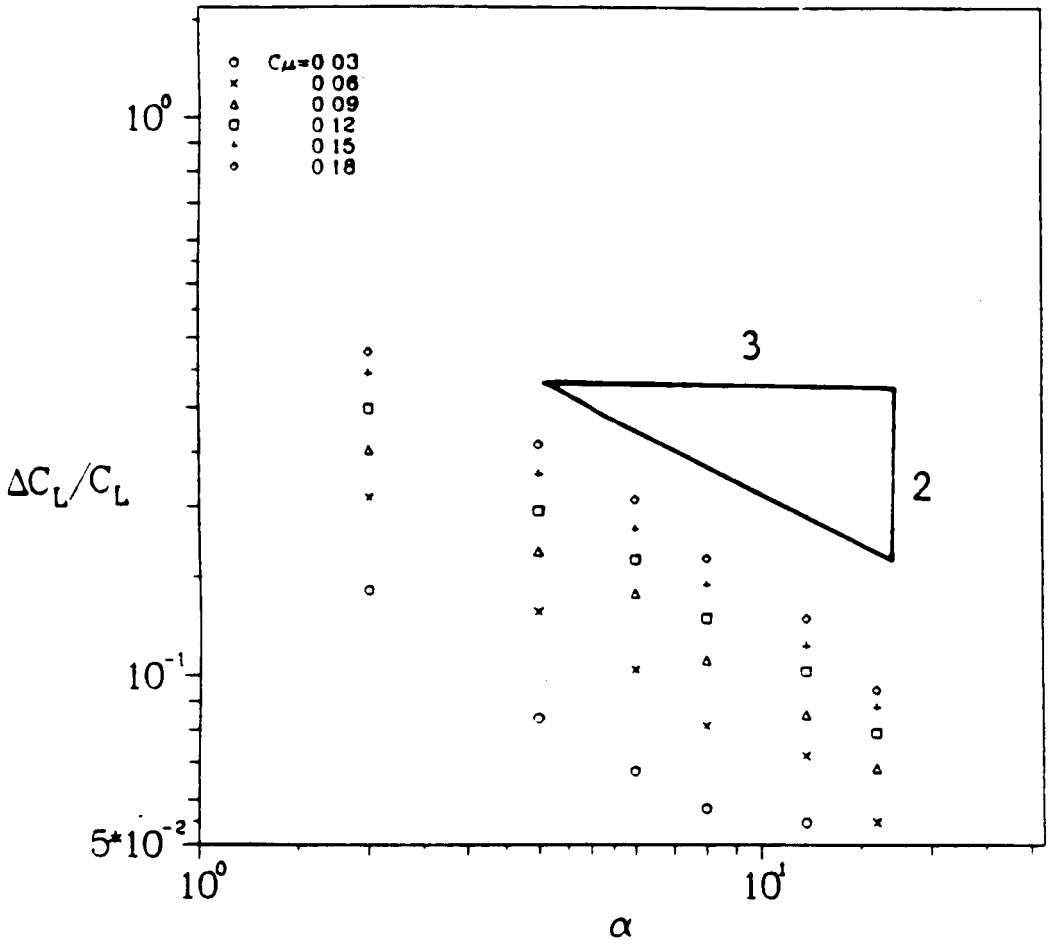

Fig. 44 Log-log plot, slanted-down.

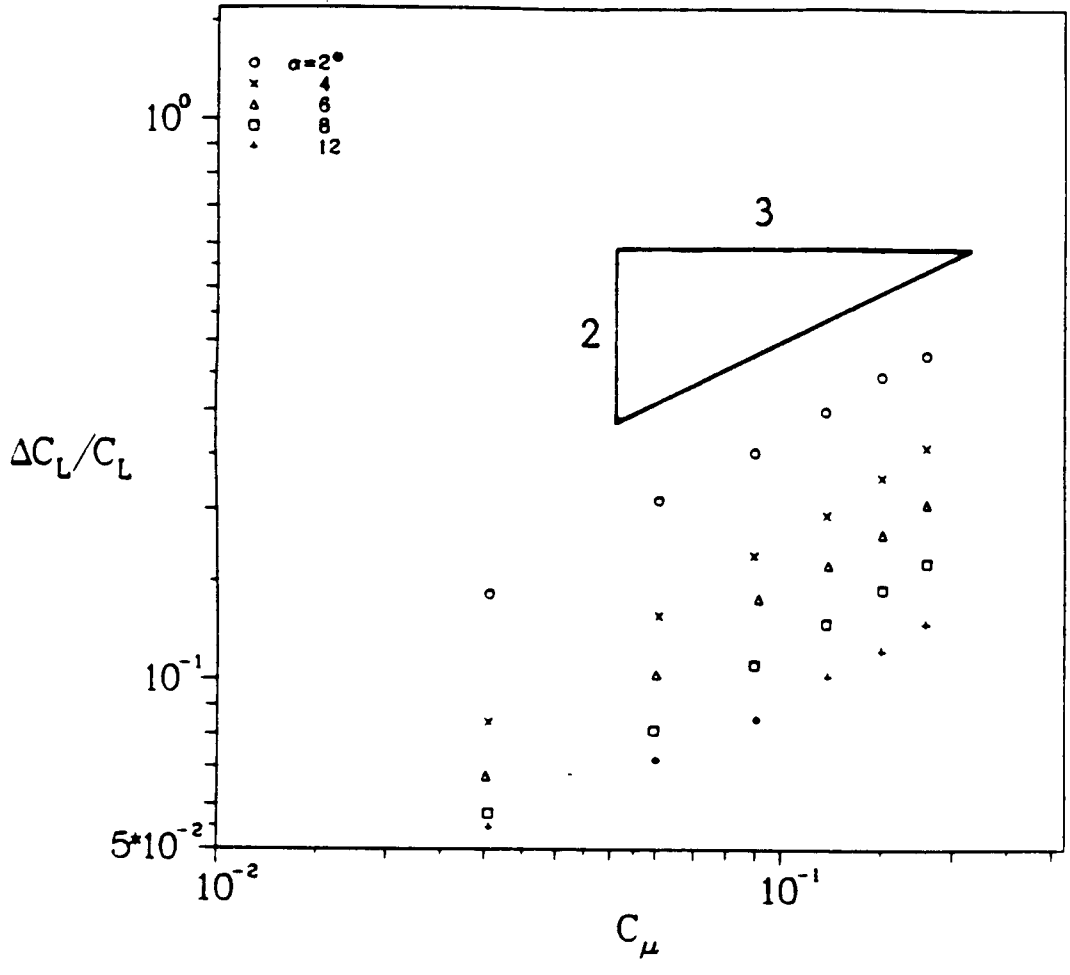

Fig. 45 Log-log plot, slanted-down.

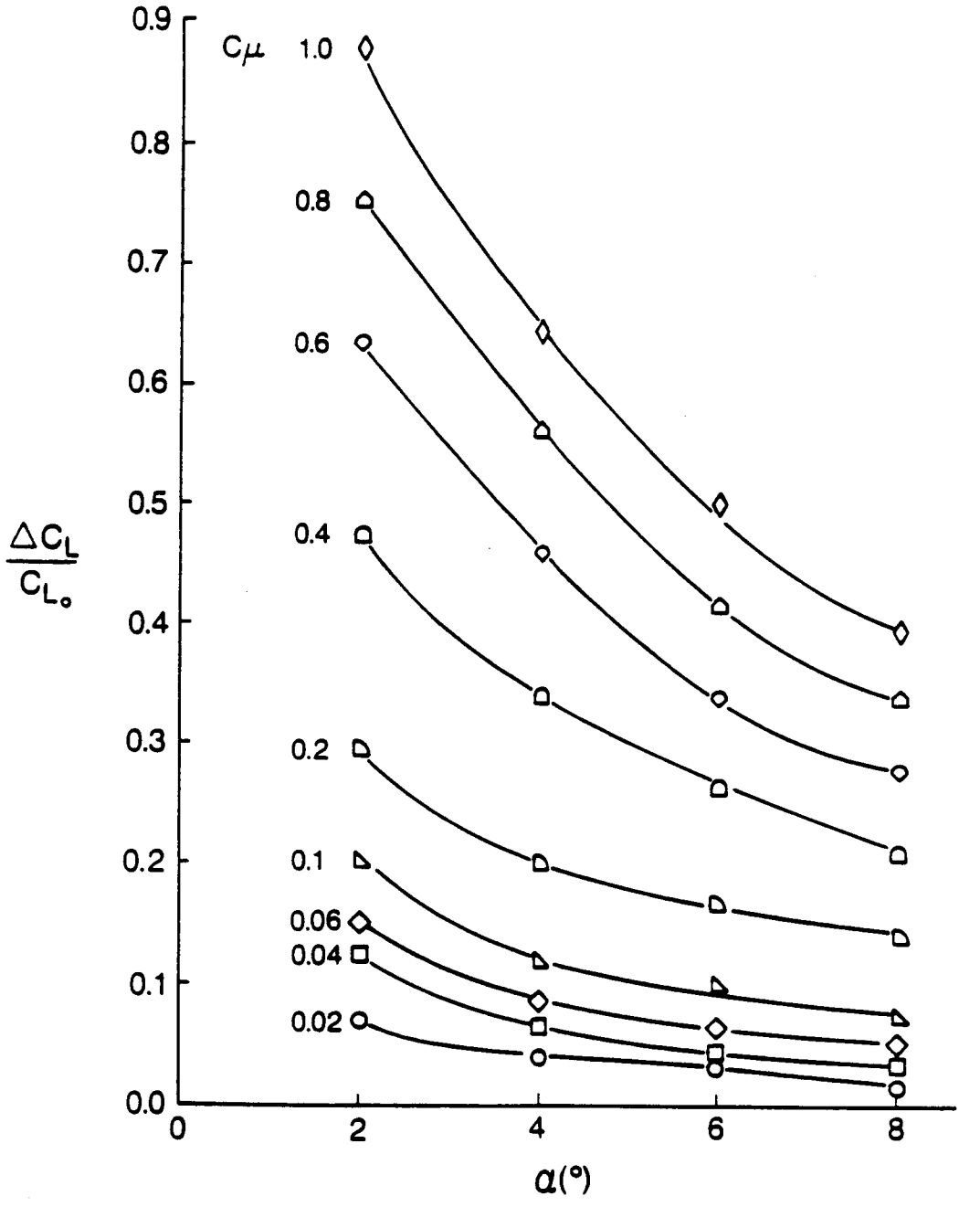

Fig. 46 Relative lift increment, straight blowing.

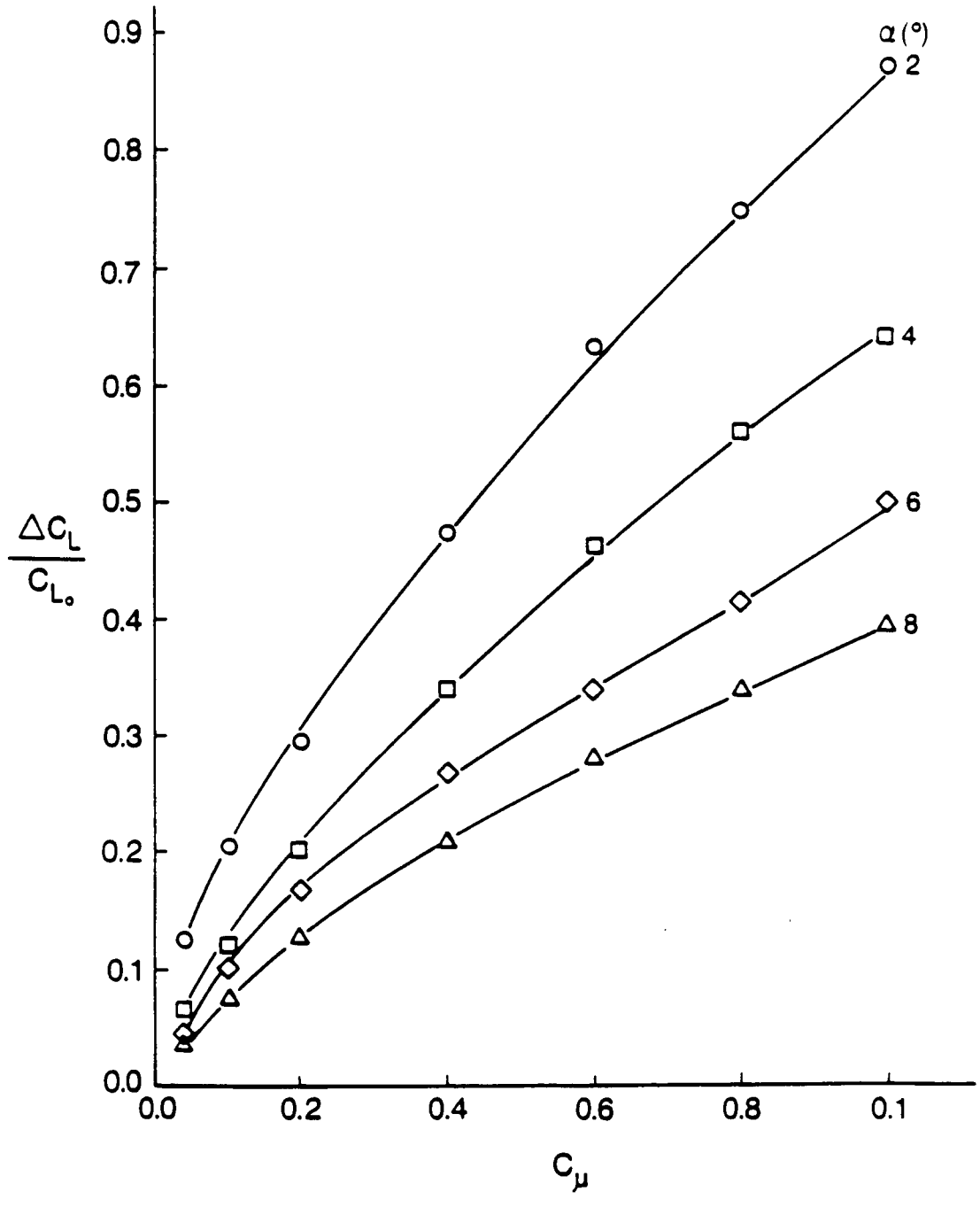

Fig. 47 Relative lift increment, straight blowing.

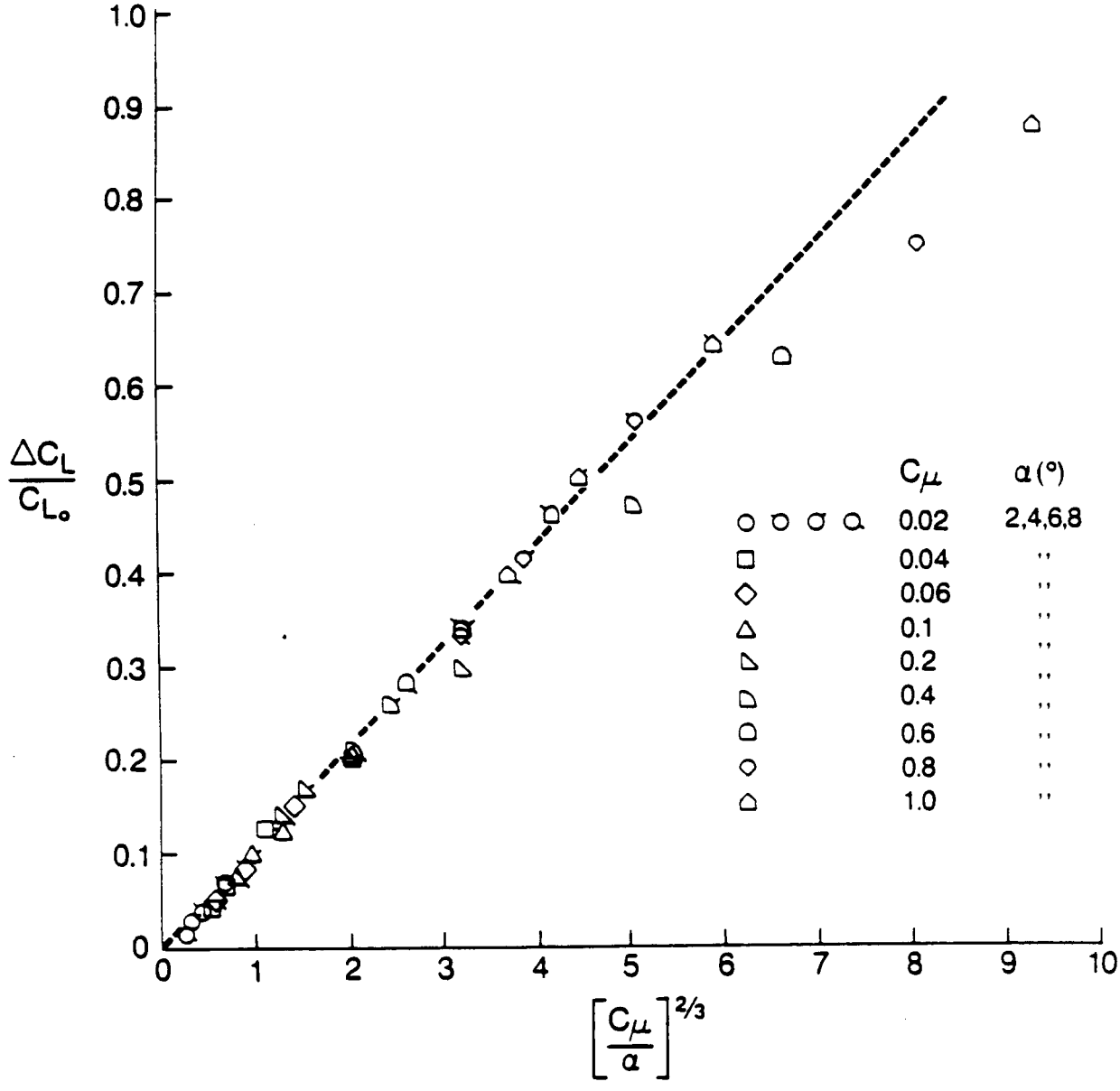

Fig. 48 Data collapse for A = 3.14.

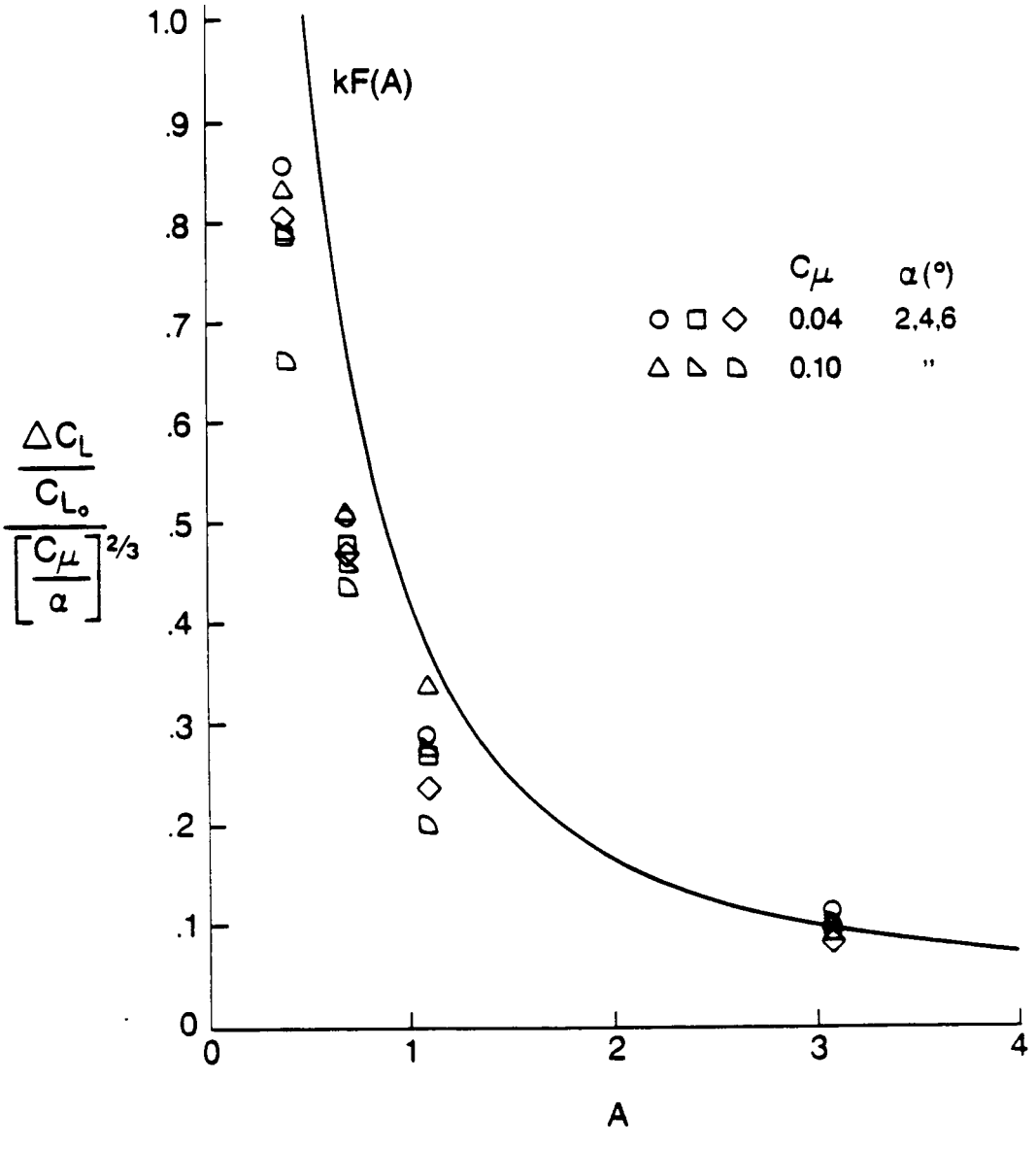

Fig. 49 Comparison between theory [Eq. (2.26)] and experiment, k = 0.3.

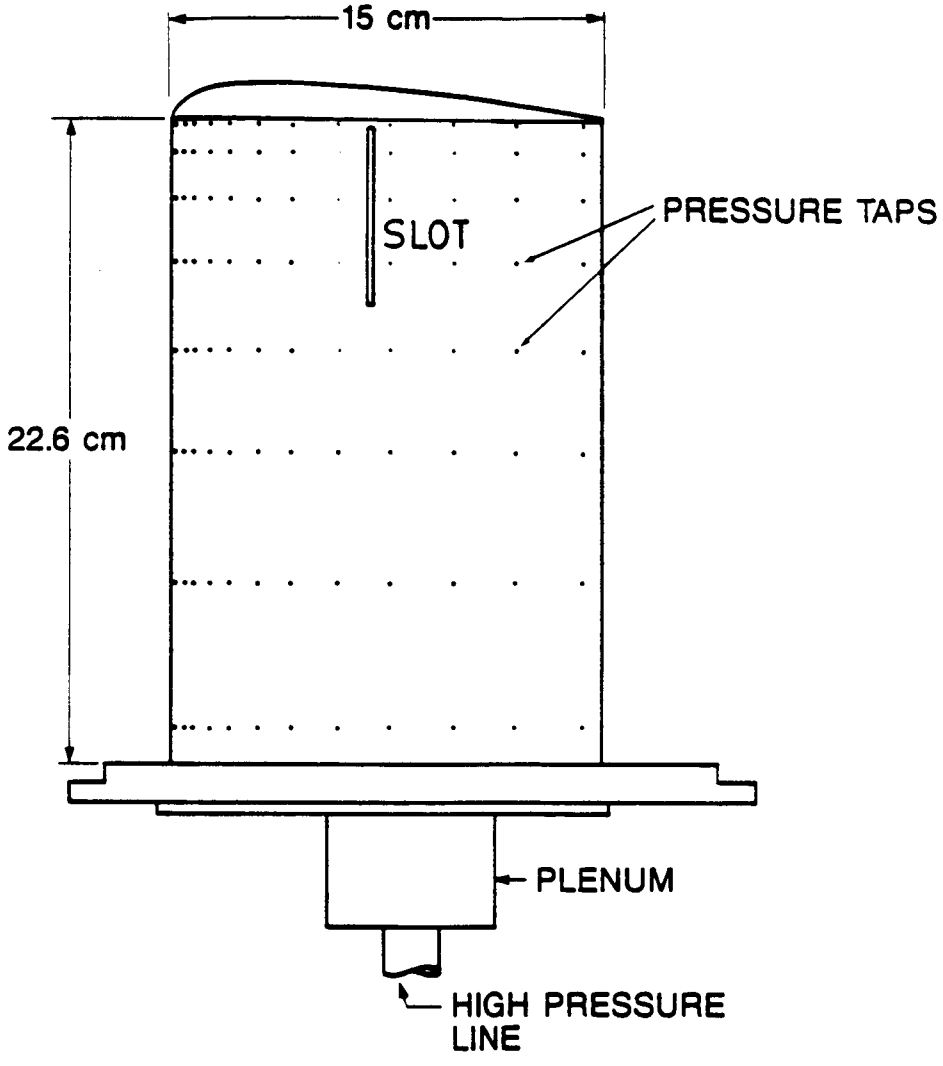

Fig. 50 Wind tunnel model for jet spoiler concept.

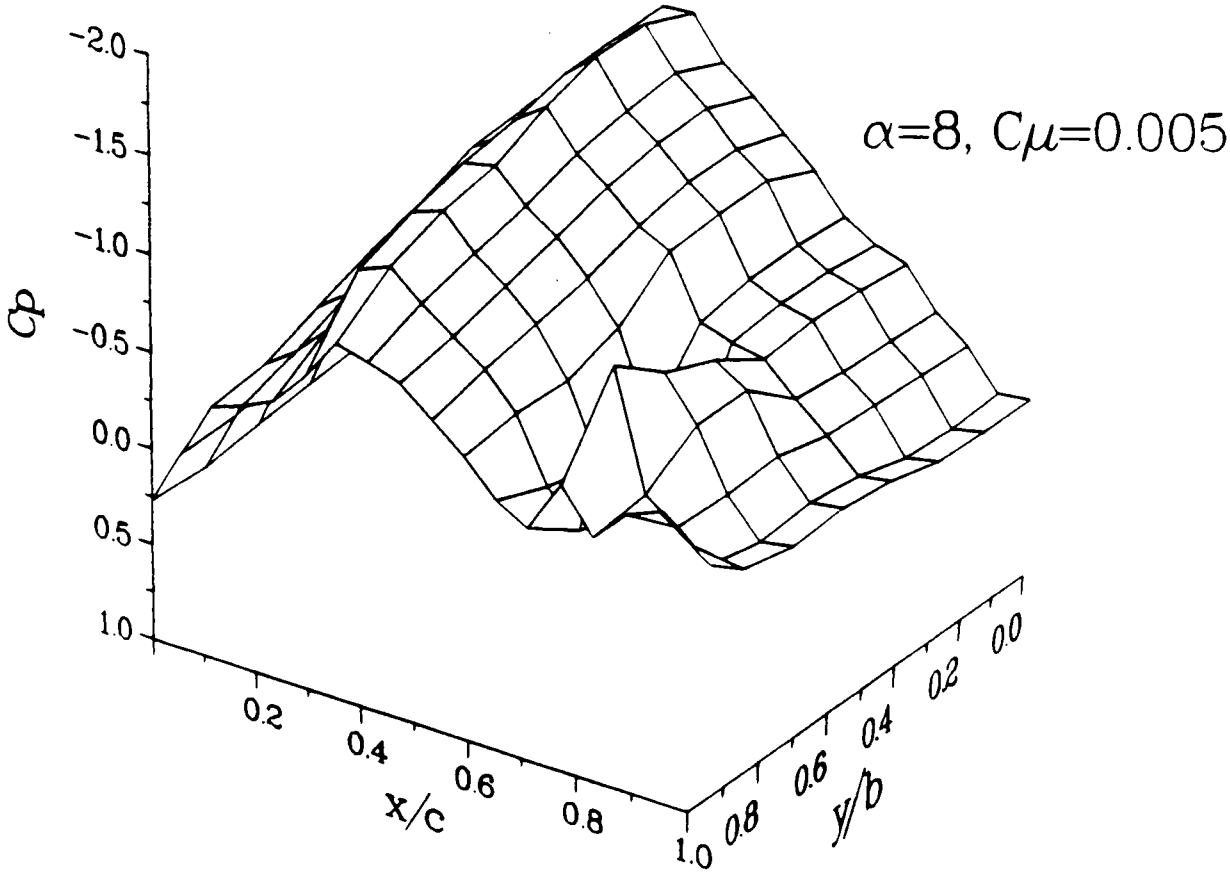

Fig. 51 Upper surface pressure distribution, one-sided.

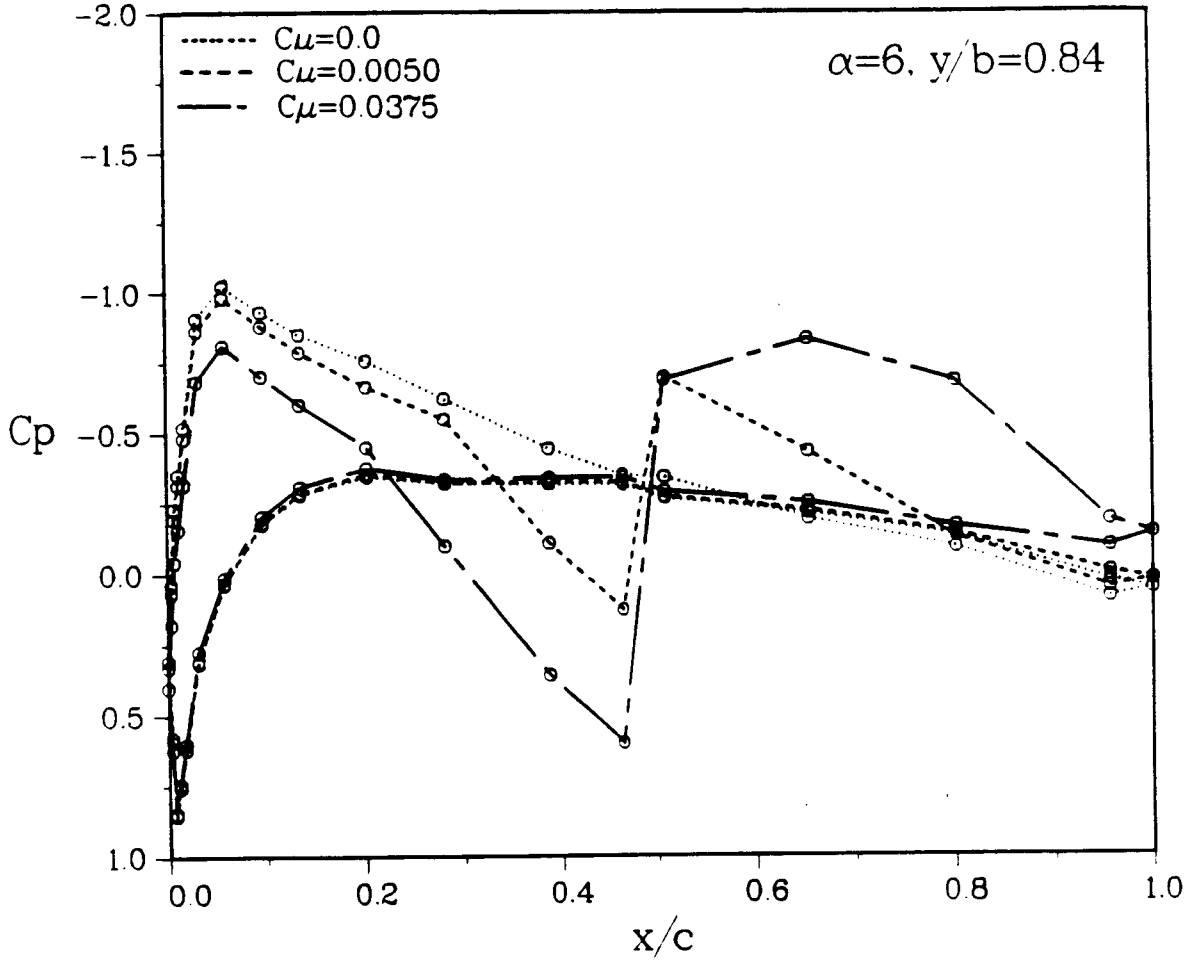

Fig. 52 Chordwise pressure distribution, one sided.

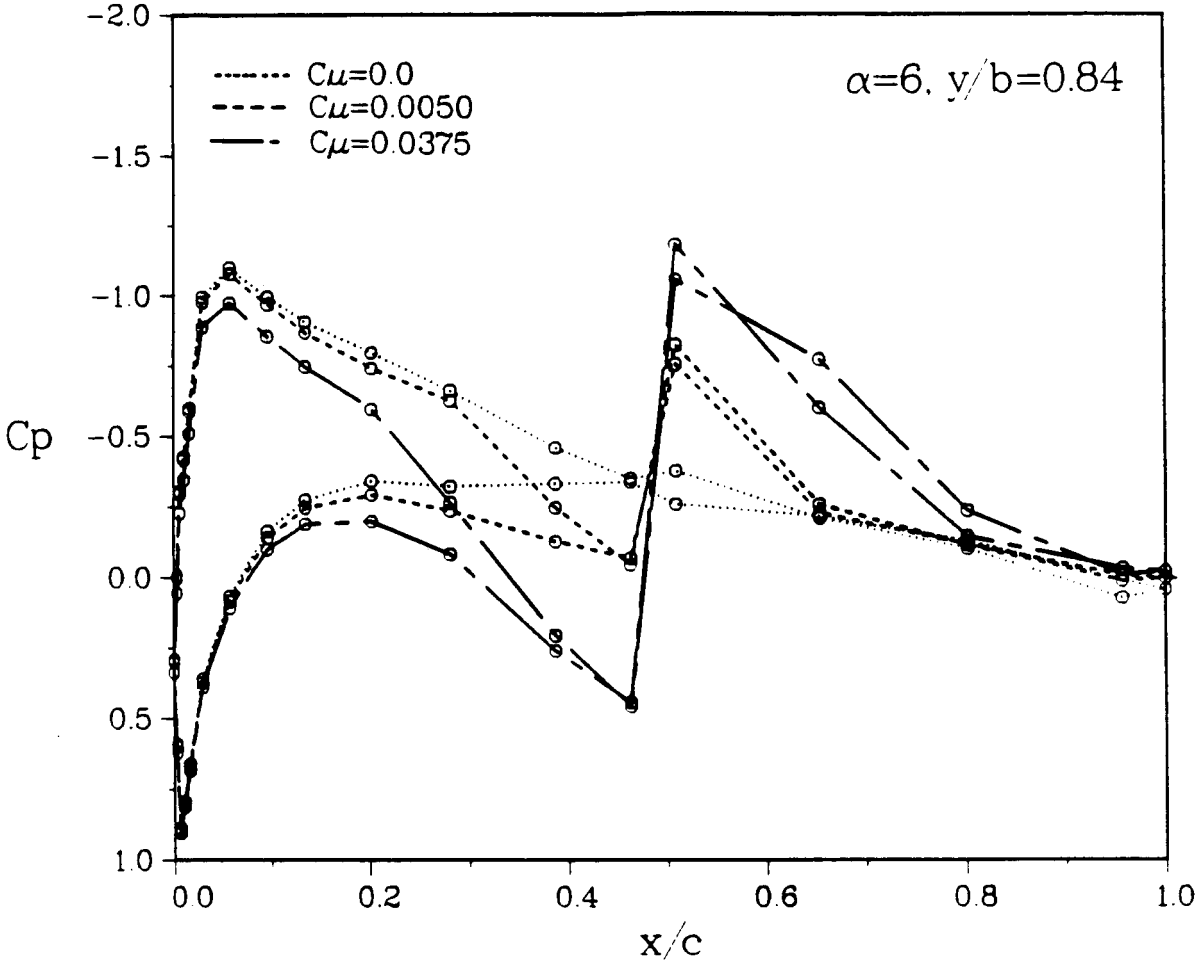

Fig. 53 Chordwise pressure distribution, two-sided.

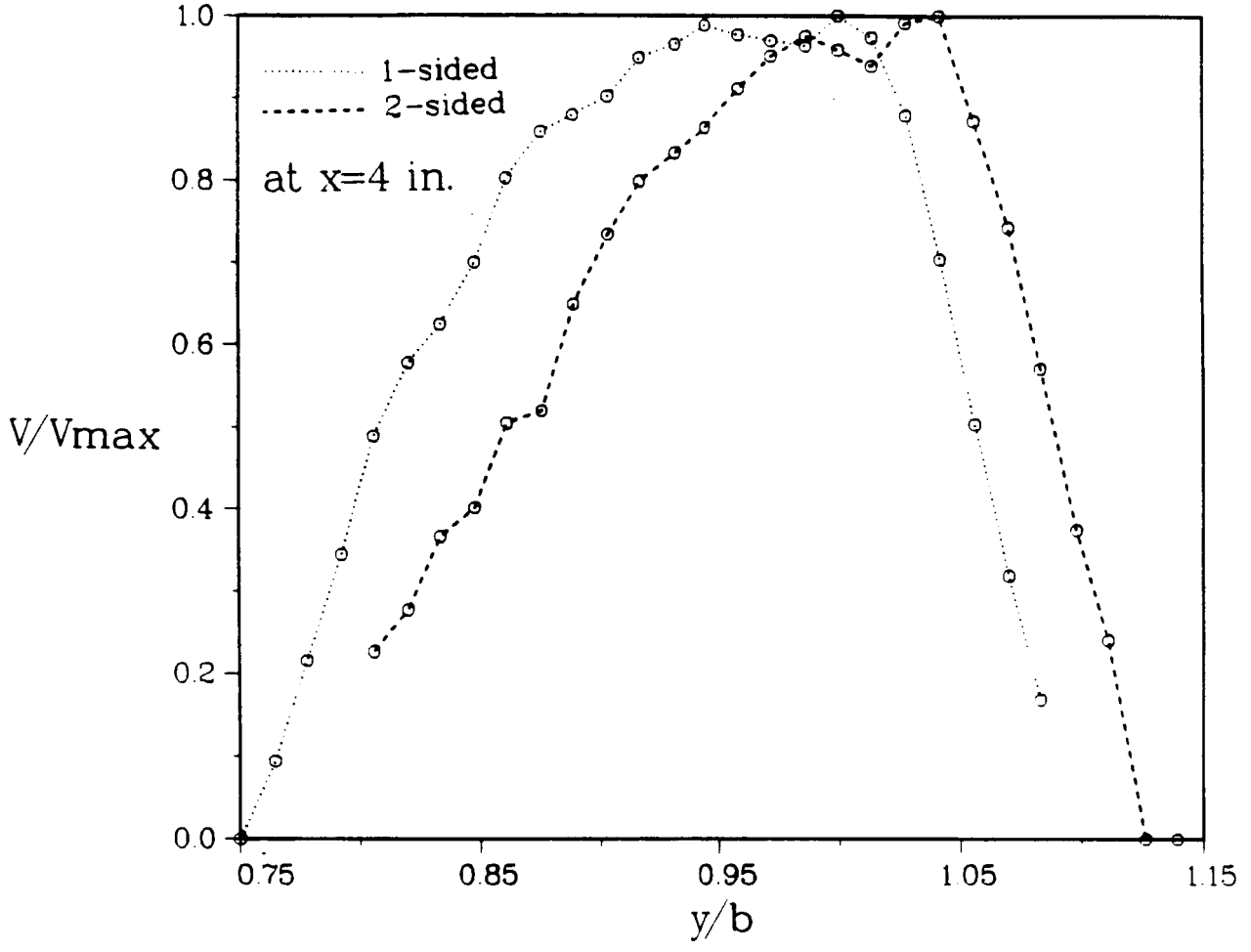

Fig. 54 Jet velocity survey at 4" from slot.

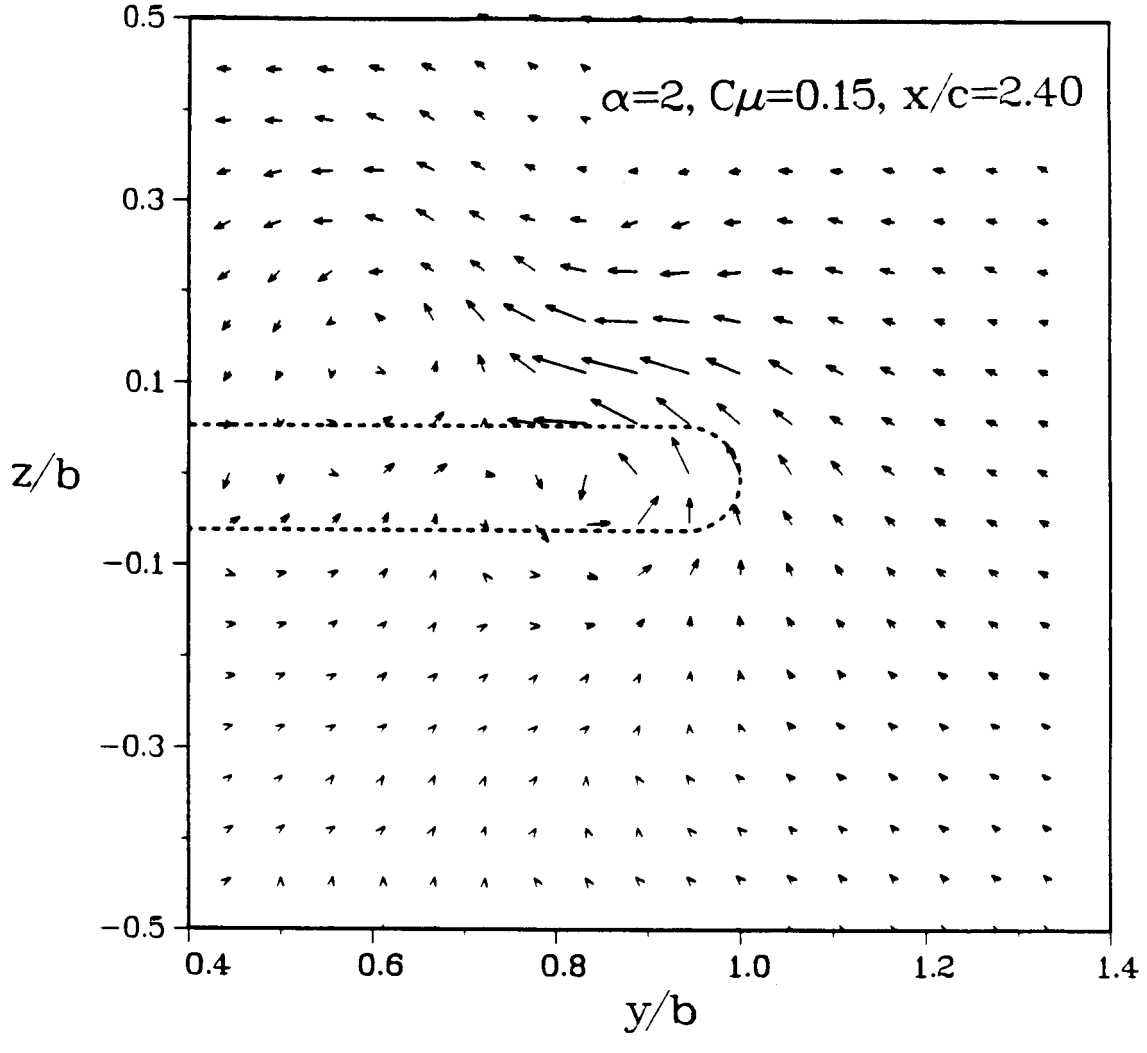

Fig. 55 Flow mapping, one-sided.

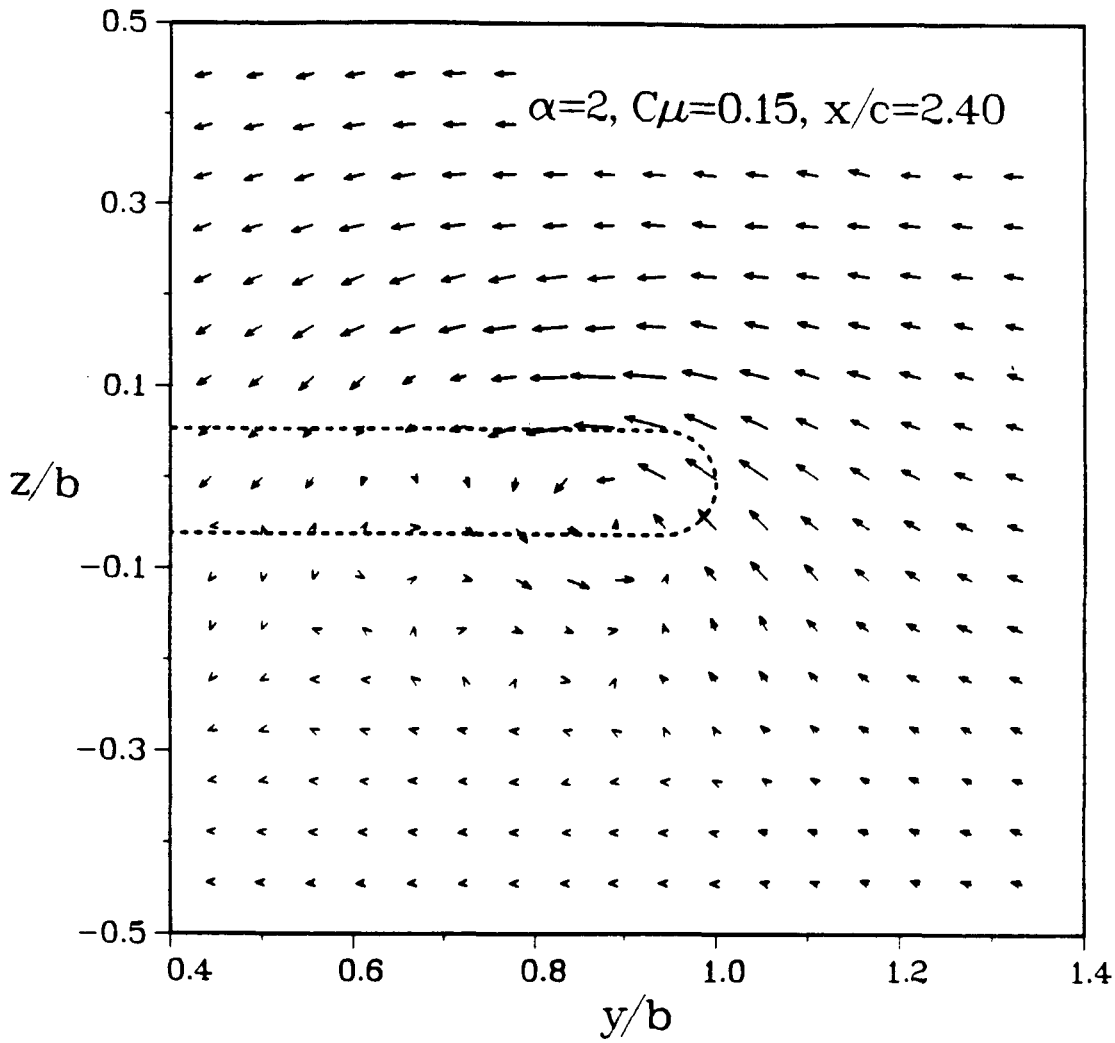

Fig. 56 Flow mapping, two-sided.

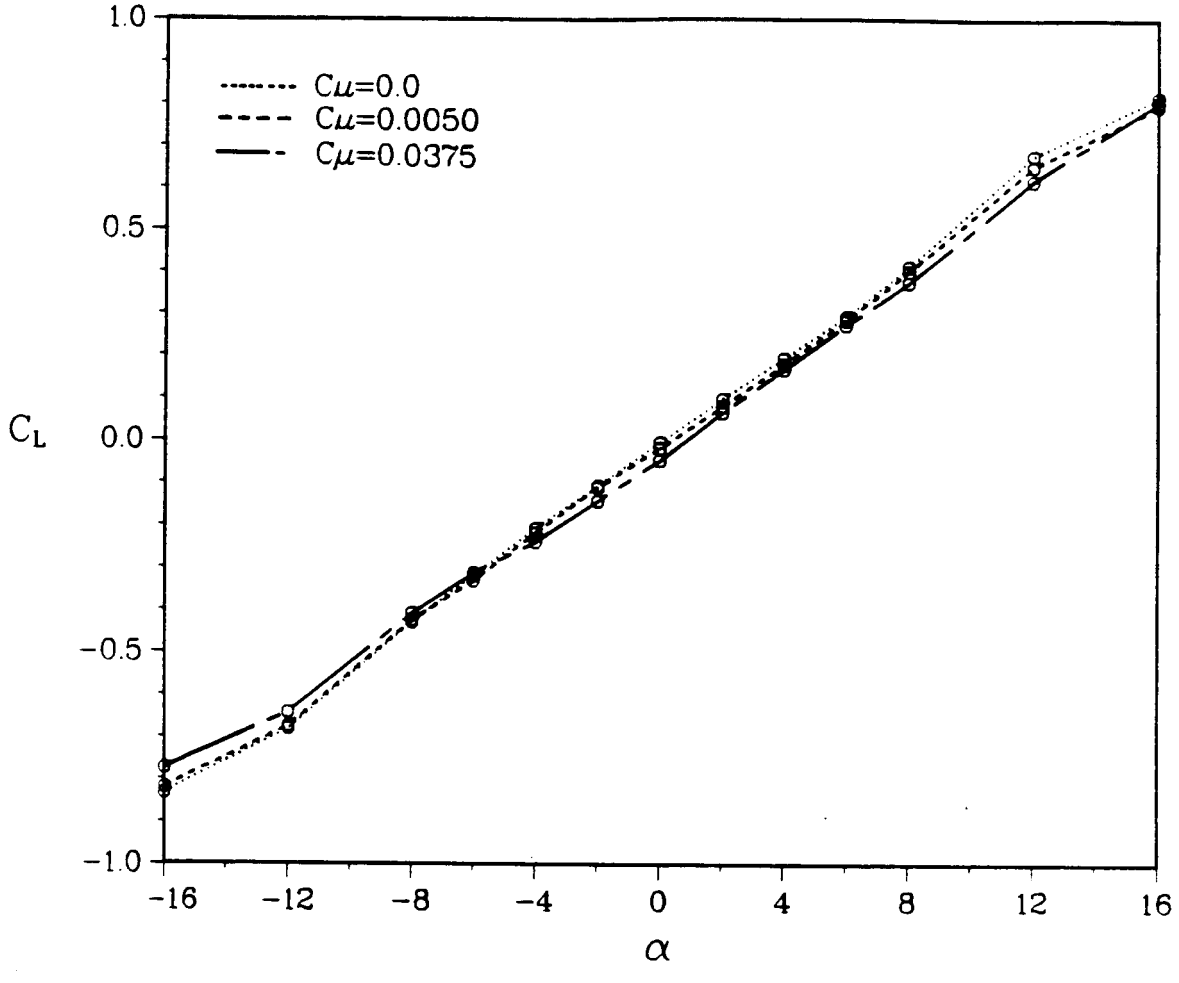

Fig. 57 Effect of blowing on lift coefficient, one-sided.

C-2

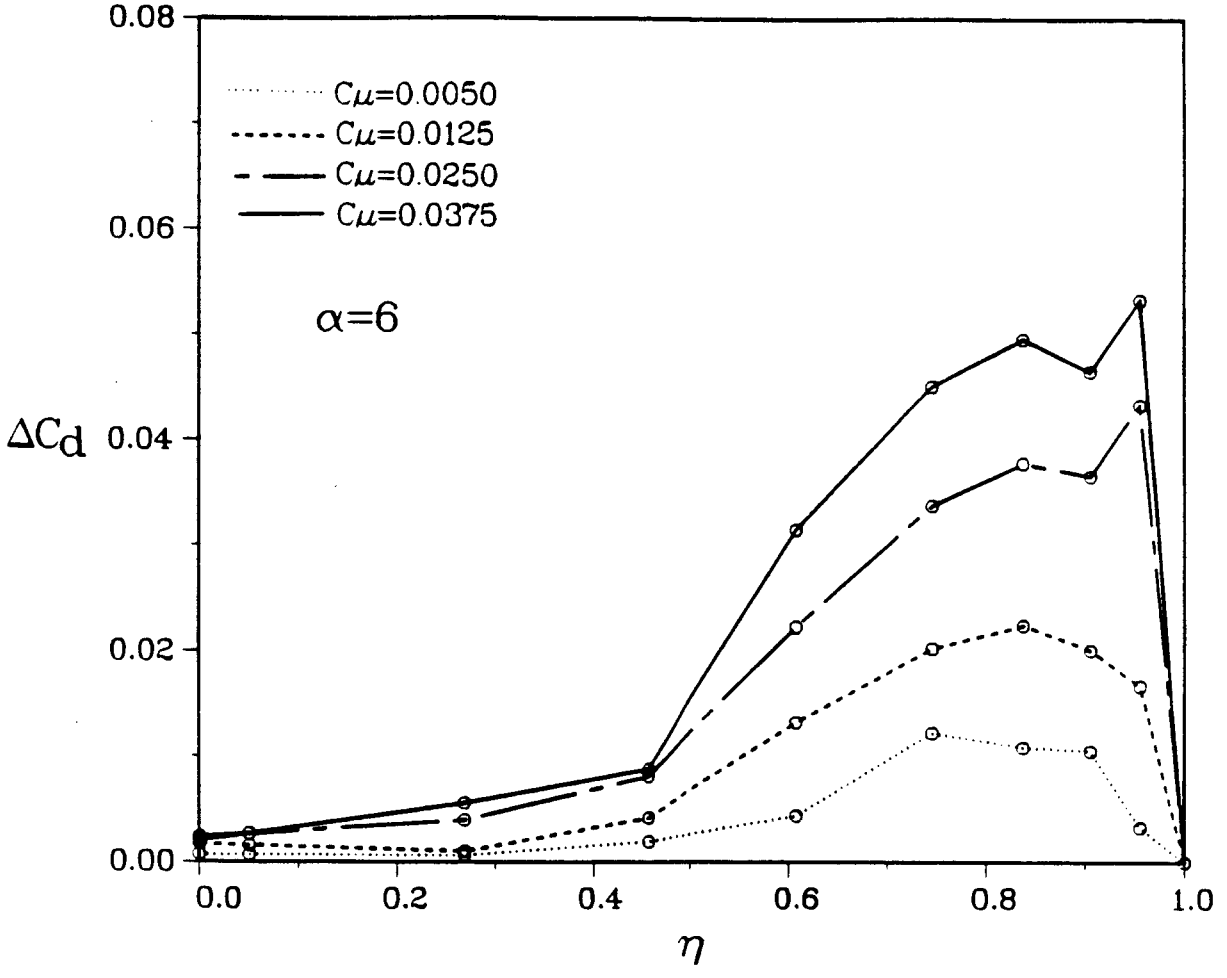

Fig. 58 Local drag increment, one-sided.

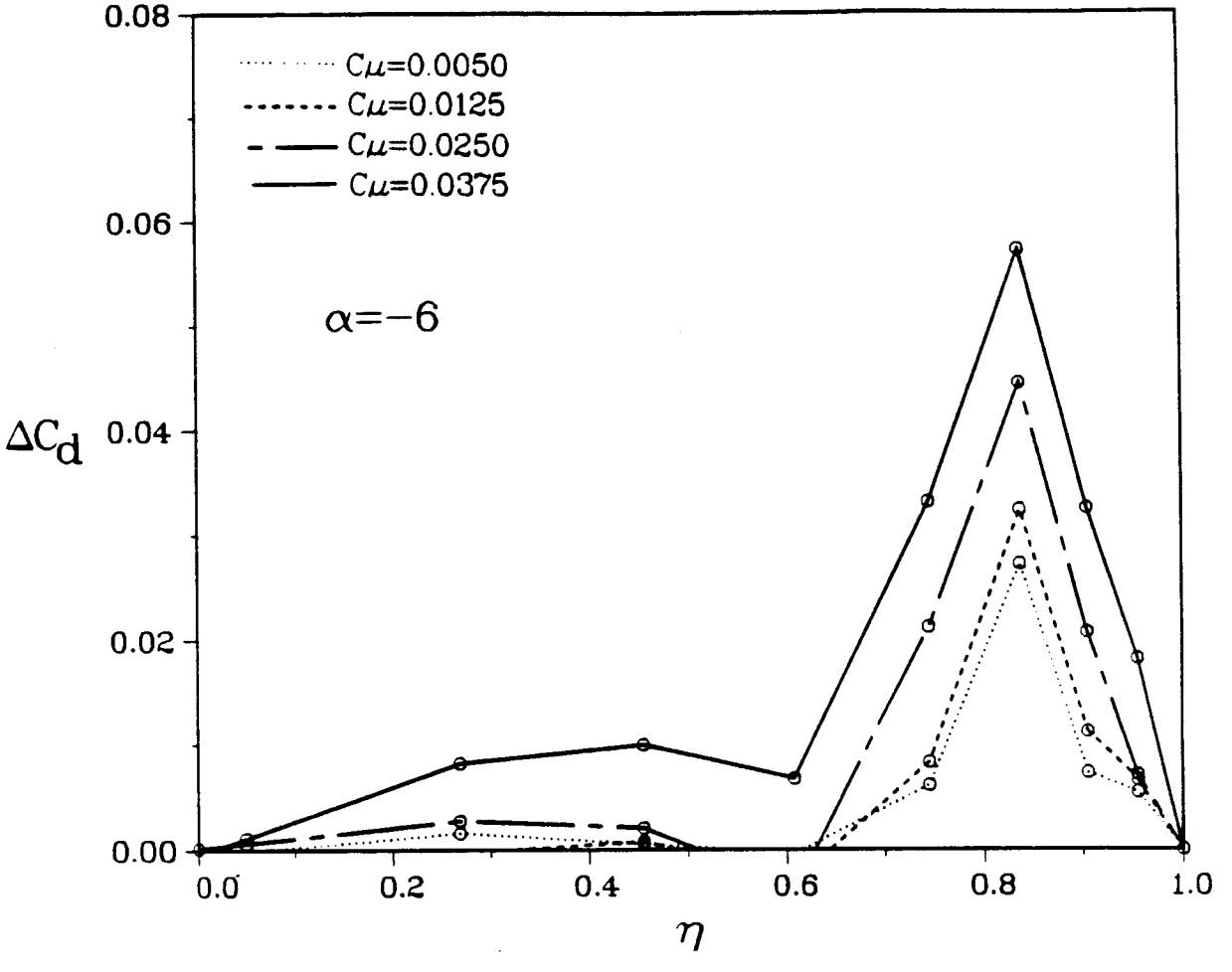

Fig. 59 Local drag increment, one sided.

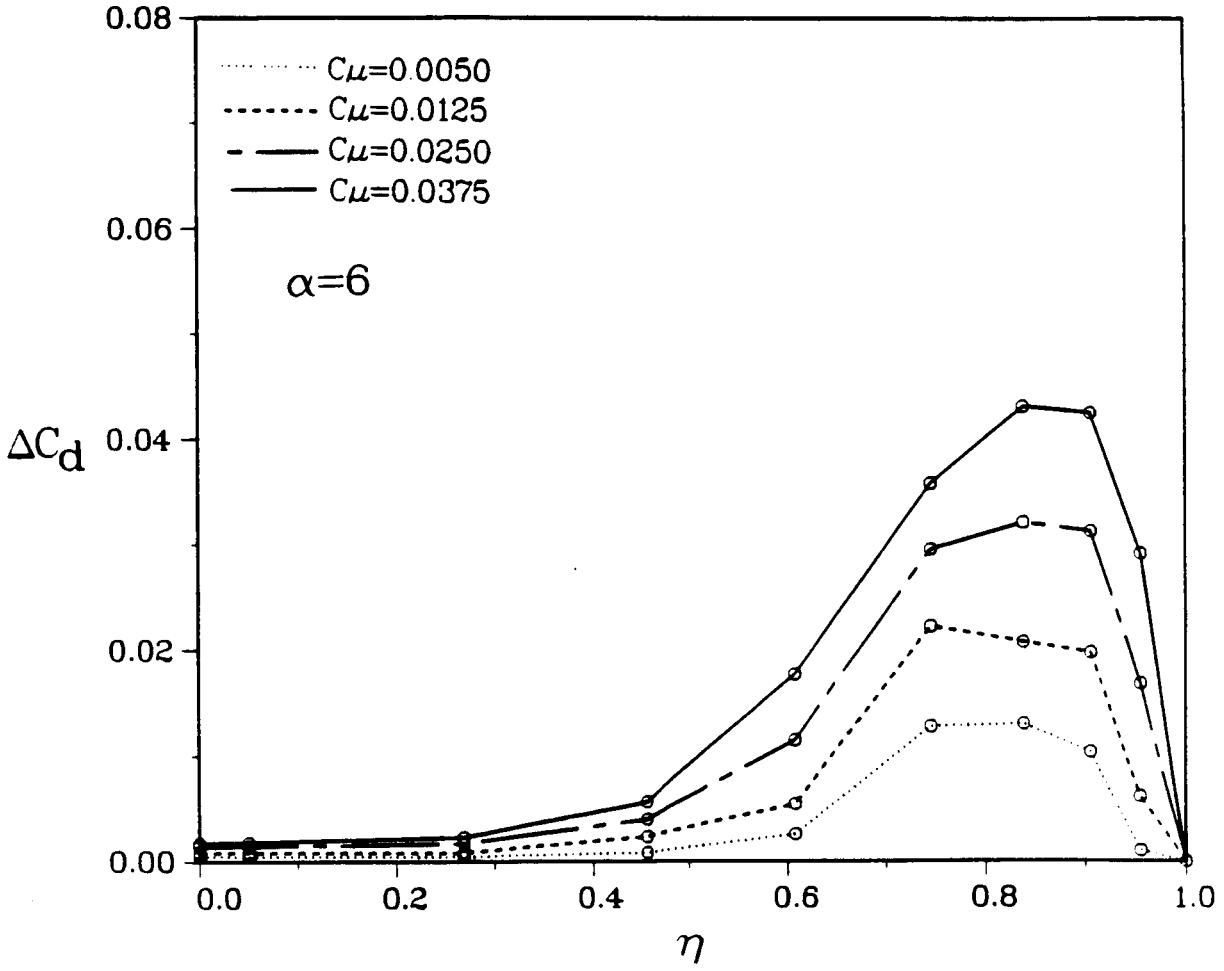

Fig. 60 Local drag increment, two-sided.

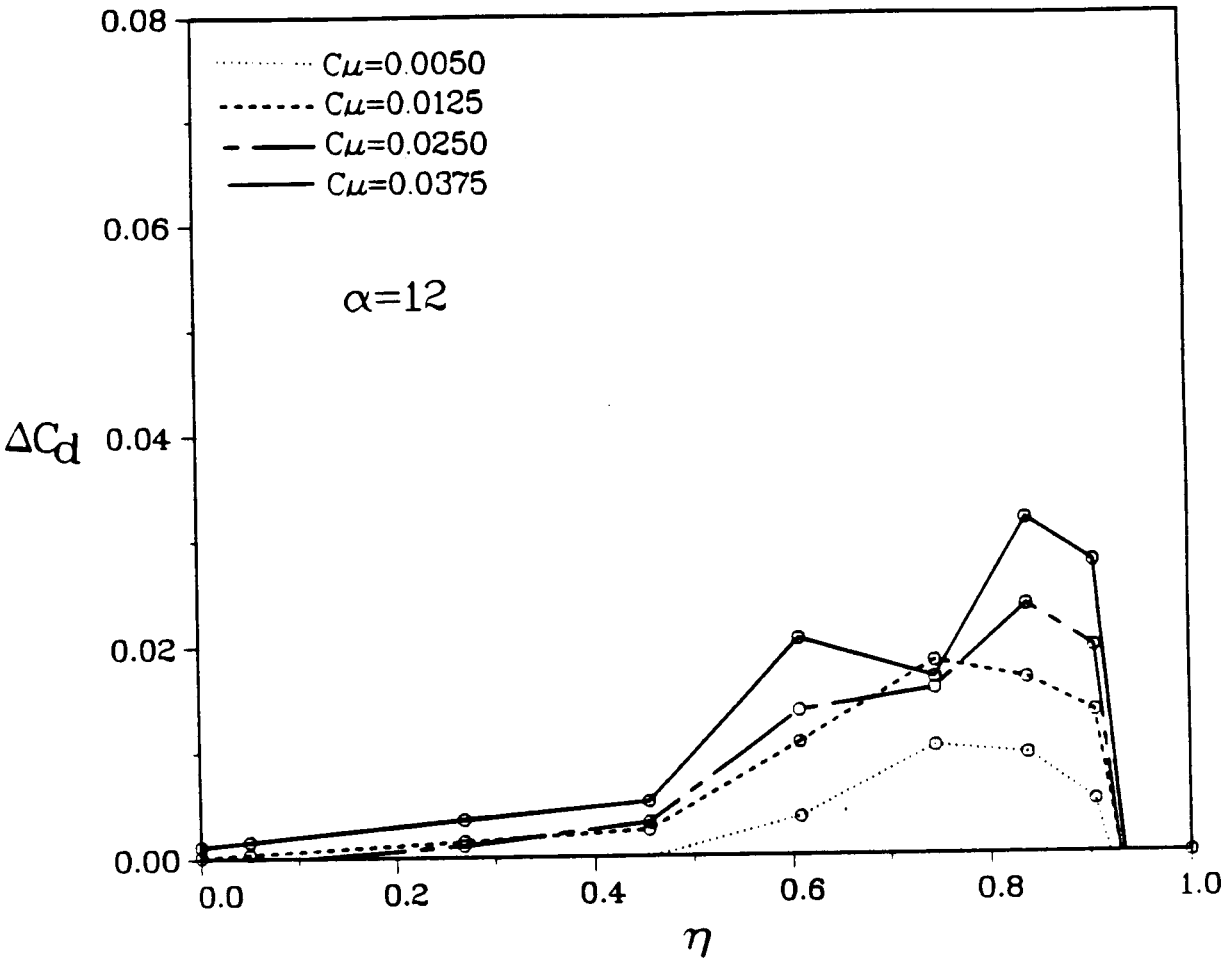

Fig. 61 Local drag increment, two-sided.

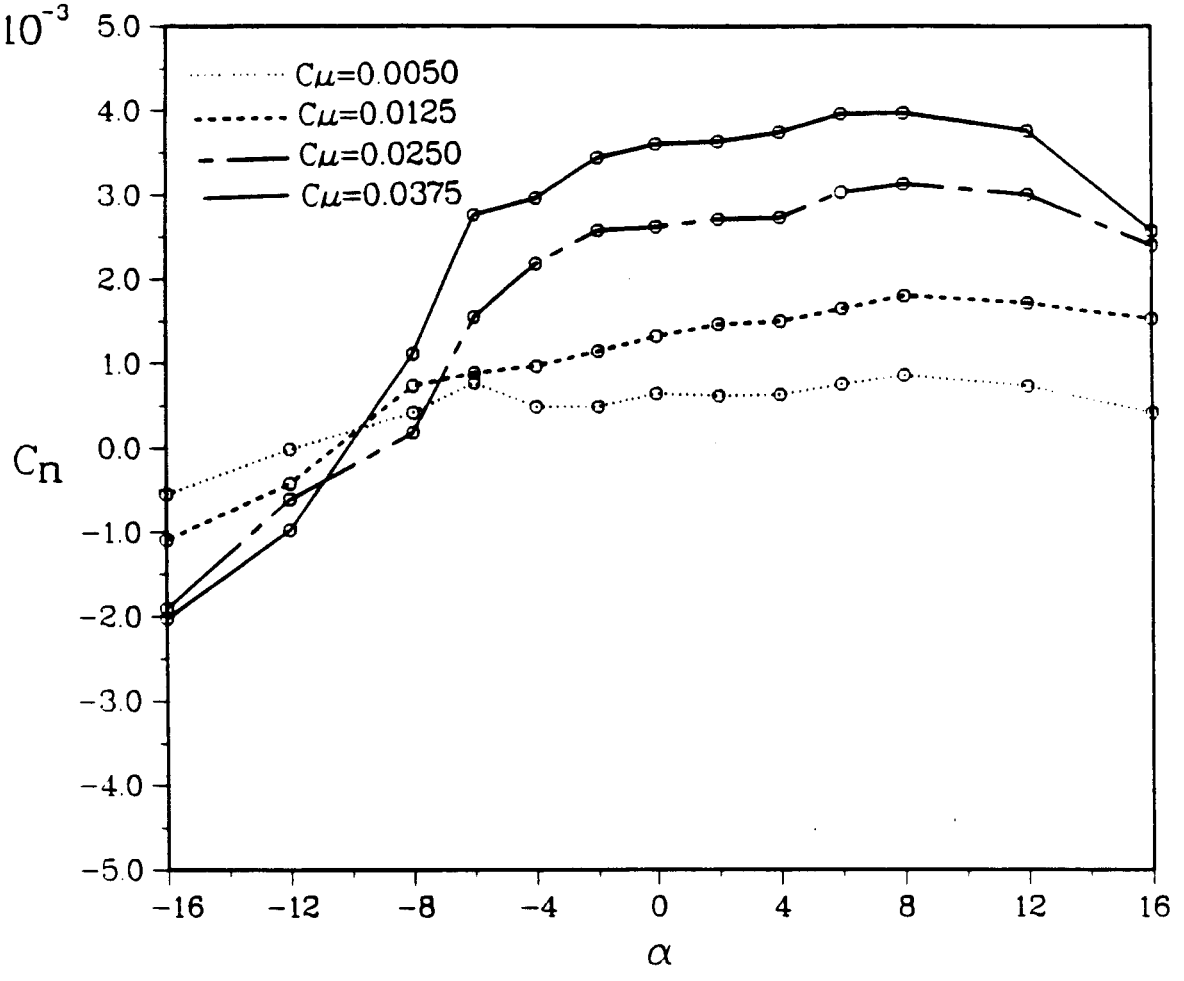

Fig. 62 Yawing moment coefficient, one-sided.

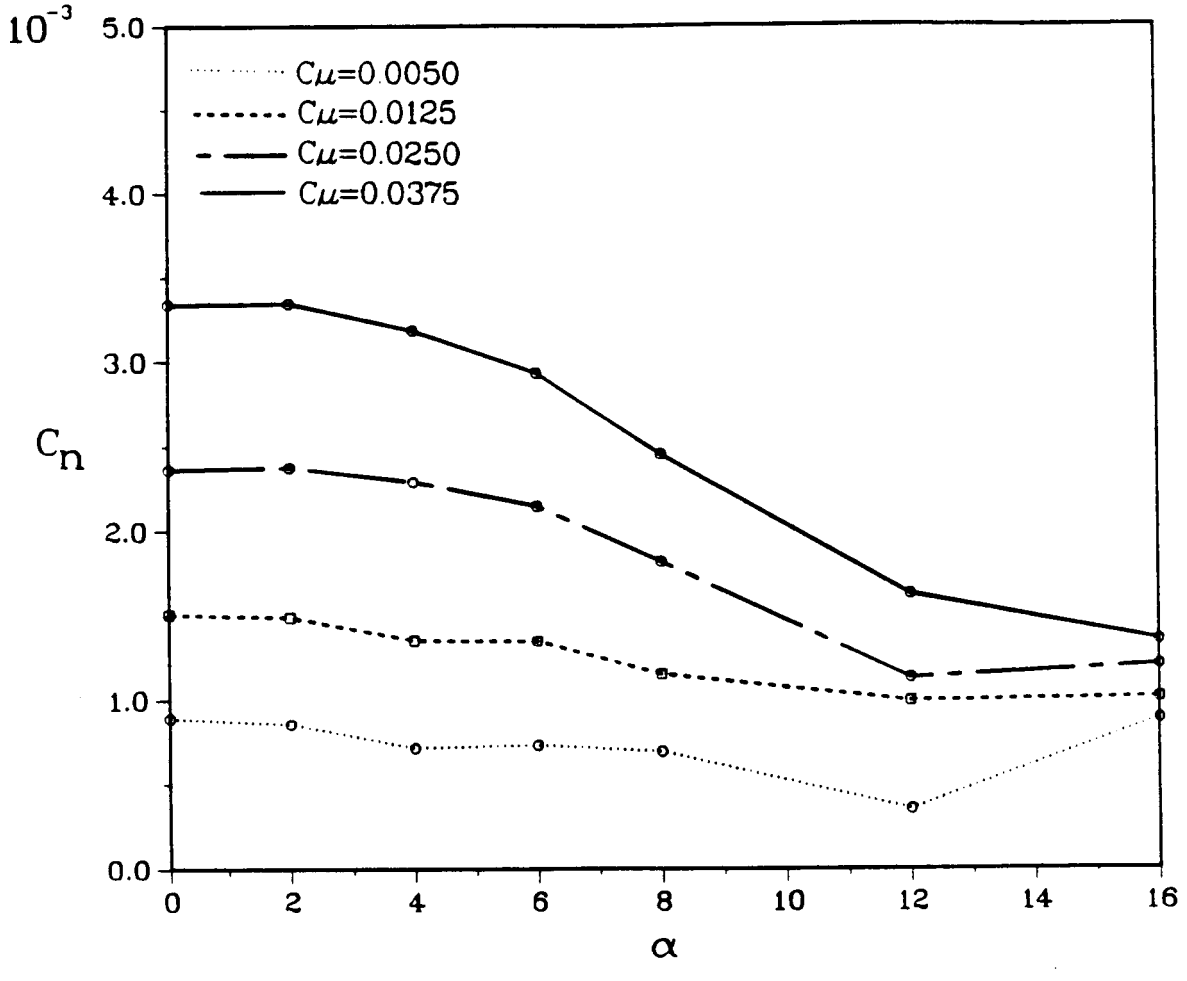

Fig. 63 Yawing moment coefficient, two-sided.

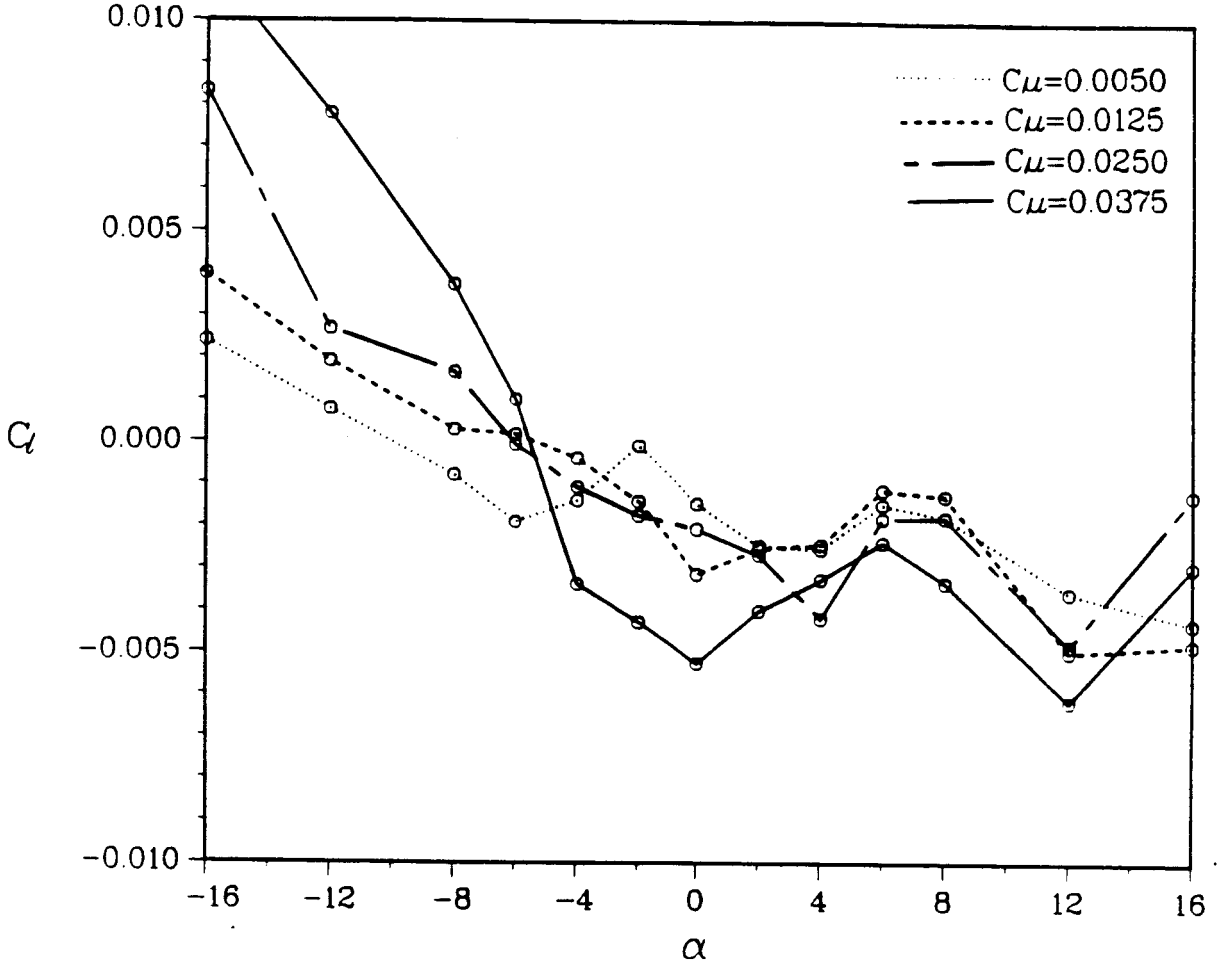

Fig. 64 Rolling moment coefficient, one-sided.

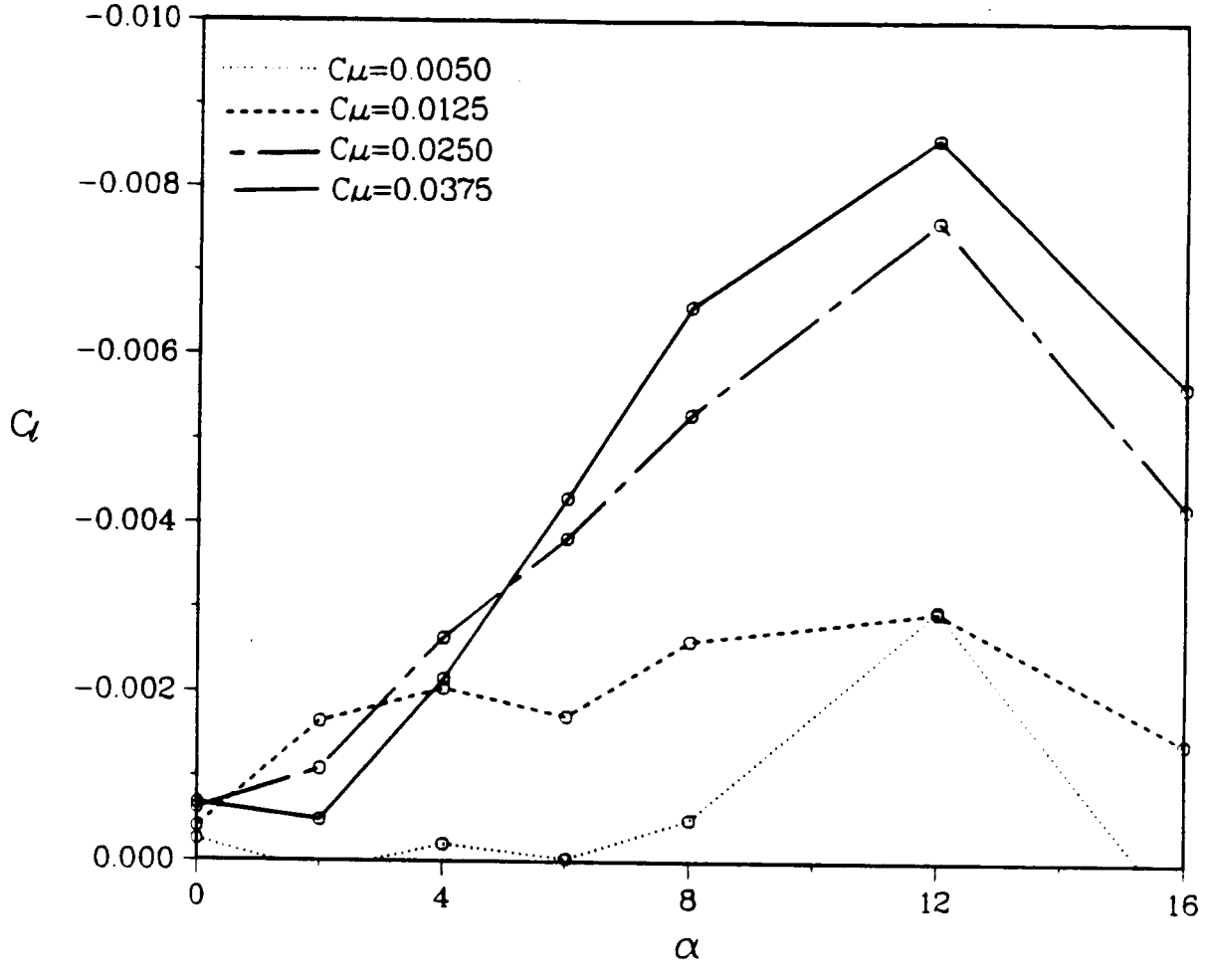

Fig. 65 Rolling moment coefficient, two-sided.

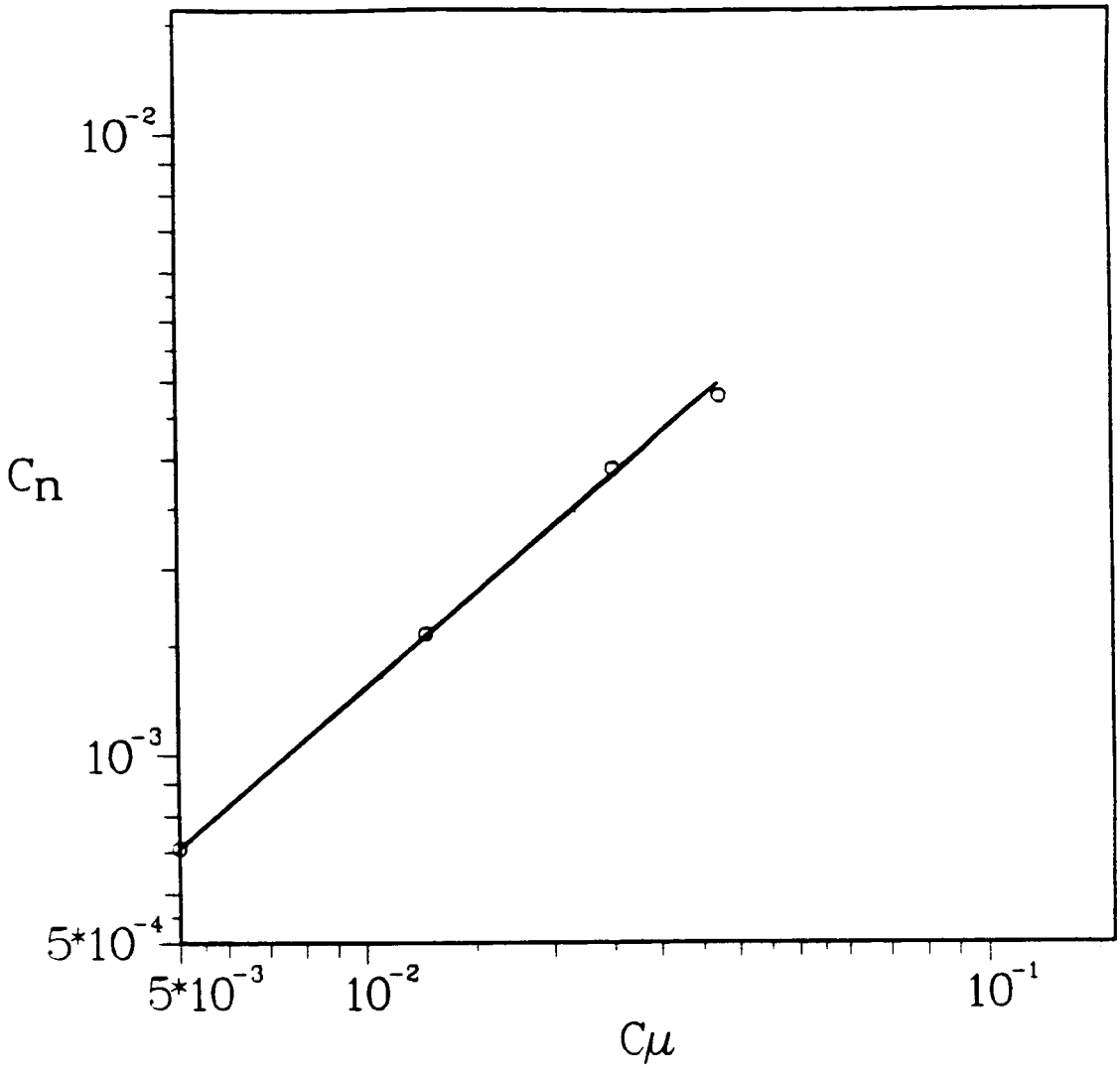

Fig. 66 Log-log plot of yawing moment coefficient vs. jet intensity.

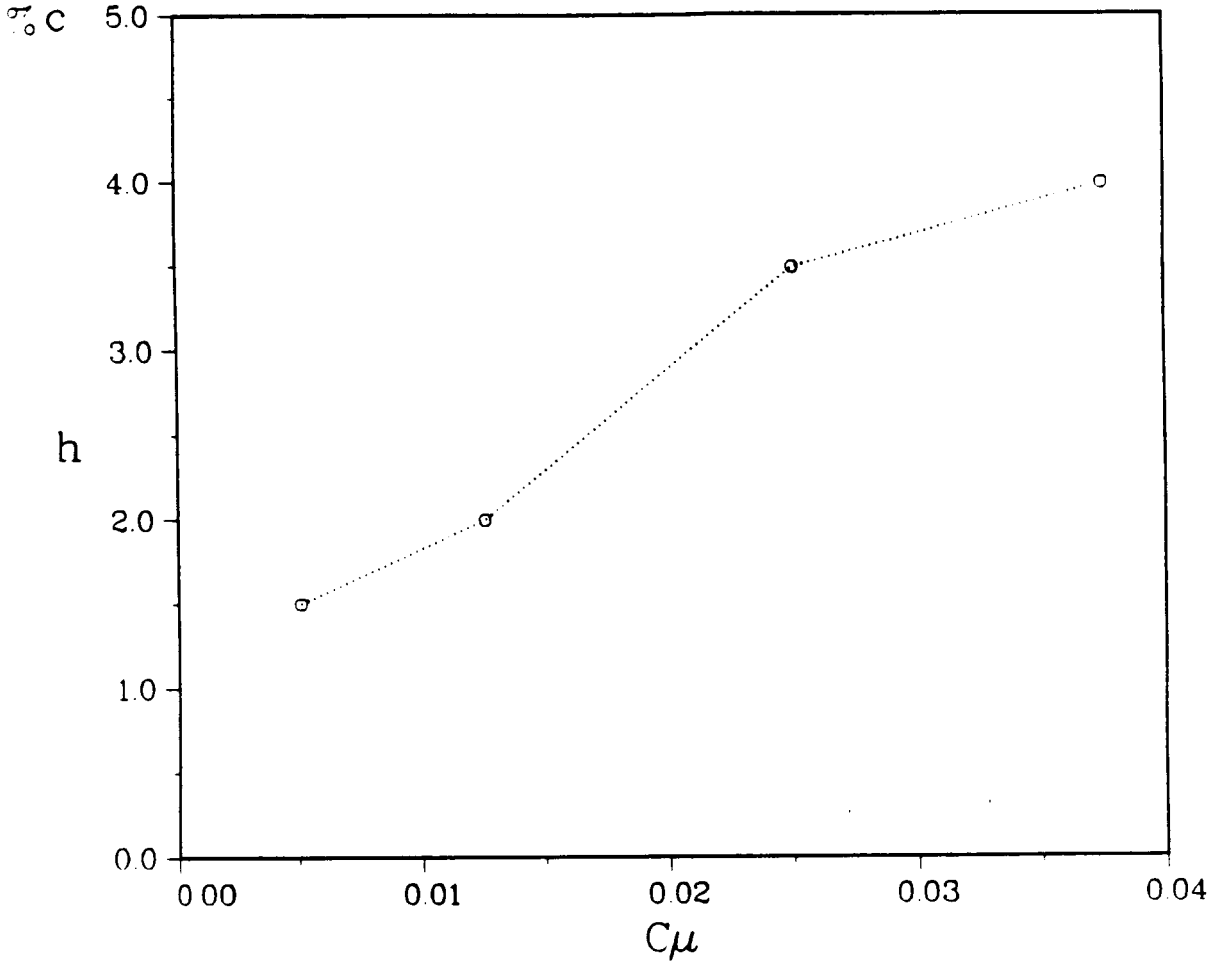

Fig. 67 Equivalent solid spoiler vertical projection.